NYO - 10204
MITNE - 16

THEORY AND USE OF SMALL SUBCRITICAL ASSEMBLIES FOR THE MEASUREMENT OF REACTOR PARAMETERS

by

J. Peak, I. Kaplan, T. J. Thompson

Contract AT (30-1) 2344

U. S. Atomic Energy Commission

April 9, 1962

Department of Nuclear Engineering
Massachusetts Institute of Technology
Cambridge, Massachusetts

MASSACHUSETTS INSTITUTE OF TECHNOLOGY
DEPARTMENT OF NUCLEAR ENGINEERING
Cambridge 39, Massachusetts

THEORY AND USE OF SMALL SUBCRITICAL ASSEMBLIES FOR THE MEASUREMENT OF REACTOR PARAMETERS

by

J. C. PEAK, I. KAPLAN, and T. J. THOMPSON

April 2, 1962

NYO - 10204
AEC Research and Development Report
UC - 34 Physics
(TID - 4500, 17th Edition)

Contract AT(30 - 1)2344
U.S. Atomic Energy Commission

DISTRIBUTION

NYO - 10204

AEC Research and Development Report

UC - 34 Physics

(TID - 4500, 17th Edition)

1. USAEC, New York Operations Office (D. Richtmann)
2. USAEC, Division of Reactor Development (P. Hemmig)
3. USAEC, New York Patents Office (H. Potter)
4. USAEC, New York Operations Office (S. Strauch)
5. USAEC, Division of Reactor Development, Reports and Statistics Branch
6. USAEC, Maritime Reactors Branch
7. USAEC, Civilian Reactors Branch
8. USAEC, Army Reactors Branch
9. USAEC, Naval Reactors Branch
10. Advisory Committee on Reactor Physics (E. R. Cohen)
11. ACRP (G. Dessauer)
12. ACRP (D. de Bloisblanc)
13. ACRP (M. Edlund)
14. ACRP (R. Ehrlich)
15. ACRP (I. Kaplan)
16. ACRP (H. Kouts)
17. ACRP (F. C. Maienschein)
18. ACRP (J. W. Morfitt)
19. ACRP (B. I. Spinrad)
20. ACRP (P. F. Zweifel)

21. ACRP (P. Gast)
22. ACRP (G. Hansen)
23. ACRP (S. Krasik)
24. ACRP (T. Merkle)
25. ACRP (T. M. Snyder)
26. ACRP (J. J. Taylor)
27. - 29. O. T. I. E., Oak Ridge, for Standard Distribution, UC - 34, TID - 4500 (17th Edition)
30. - 49. J. C. Peak
50. - 100. Internal Distribution

ABSTRACT

The use of small subcritical assemblies for the measurement of reactor parameters in the preliminary study of new types of reactors offers potential savings in time and money. A theoretical and experimental investigation was made to determine whether small assemblies could be so used.

Age-diffusion theory was applied to the general case of a cylindrical subcritical assembly with a thermal neutron source on one end. The solutions, obtained by the use of operational calculus, allow calculation of the thermal flux due to the source, the thermal flux due to neutrons born and moderated in the assembly, and the slowing down density at any particular age, for any point in the assembly. Solutions are given for two different source conditions.

Methods of correction for source and leakage effects in small assemblies were developed for measurements of lattice parameters. They can be applied by using any valid representation of the thermal neutron flux and the slowing down density in the vicinity of the experimental position. The corrections can be tested for consistency by comparison with the experimental values.

Three dimensionless parameters were shown to characterize the size of an assembly in terms of its neutron behavior. Three other measures were advanced by which a proposed experimental position in a subcritical assembly could be evaluated. Tables illustrating the use of these parameters and measures were presented for 128 possible subcritical assemblies.

Experimental measurements were made in nine small assemblies 16 inches in height and 20 inches in diameter. Slightly enriched uranium rods of 0.250 inch diameter served as fuel at three lattice spacings of 0.880, 1.128, and 1.340 inches. Mixtures of water and heavy water at concentrations of 99.8, 90.3, and 80.2 mole percent D_2O were used as moderator at each of the three lattice spacings.

The following experimental measurements were made in each assembly: (1) Axial and radial flux traverses with bare and cadmium covered gold foils. (2) The U^{238} cadmium ratio in a rod. (3) The U^{238}/U^{235} fission ratio in a rod. (4) Intracell flux traverses with bare and cadmium covered gold foils were made in six of the nine assemblies.

Comparisons between the theoretical and experimental flux traverses of the assembly showed good agreement, especially in view of the small size of the assembly.

The corrected measurements of the U^{238} cadmium ratios, and the U^{238}/U^{235} fission ratios showed good overall consistency.

Systematic deviations were found between the intracell flux traverses and the theoretical traverses computed by means of the Thermos code. They are thought to be due to the particular scattering kernel used.

The results are promising enough so that further theoretical and experimental research on small subcritical assemblies is justified.

This work was done in part at the M. I. T. Computation Center, Cambridge, Massachusetts.

ACKNOWLEDGMENTS

The success of an experimental program of the scope of the M. I. T. Lattice Project is due to the combined efforts of a number of individuals. The results of this particular report are primarily due to the work of the principal author, John Carl Peak, who has submitted substantially this same report in partial fulfillment of the requirements for the Ph. D. degree at M. I. T. He has been assisted by other students working on the project, as well as by those mentioned specifically below.

Mr. A. E. Profio has been responsible for much of the design and operation of the Lattice Facility as a whole. Direction of the over-all project is shared by A. E. Profio and two of the authors, Professors I. Kaplan and T. J. Thompson. Mr. Joseph Barch has given considerable assistance in setting up experiments.

Staffs of the M. I. T. Reactor, the Reactor Machine Shop, and the Radiation Protection Office have provided continual assistance and advice during the experimental part of this work. Mr. Francis Woodworth, Project Machinist of the Reactor, was of particular assistance with building the equipment, and Mr. Robert DiMartino of the Radiation Protection Office and the Shift Supervisors of the reactor provided help on every experiment.

The authors are indebted to Dr. Henry Honeck, of the Brookhaven National Laboratory, for providing copies of the Thermos code and considerable advice on its use. The other codes utilized in this work were developed with the advice of Dr. Kent Hansen of the Nuclear Engineering Department and the staff of the M. I. T. Computation Center. The authors are further indebted to Dr. David Wehmeyer, of the Atomic Energy Division, the Babcock and Wilcox Co., for making available the results of some machine computations which were used in this research.

All of the above individuals and groups were essential to the completion of this work.

TABLE OF CONTENTS

TABLE OF CONTENTS (continued)

TABLE OF CONTENTS (continued)

TABLE OF CONTENTS (continued)

LIST OF FIGURES

LIST OF FIGURES (continued)

LIST OF TABLES

CHAPTER 1.
INTRODUCTION

1.1 PREFACE

Subcritical assemblies or "exponential assemblies" have several advantages for the measurement of reactor parameters. They are smaller than critical assemblies and consequently require less material. They do not require elaborate control mechanisms and safety features and, since they usually operate at a much lower flux level, they do not require as much shielding as a critical experiment would. Finally, the ratio of moderator volume to fuel volume usually can be varied with small effort in an exponential assembly.

There are some inherent disadvantages in an exponential experiment. The higher leakage rate, as compared with that in a critical assembly, may necessitate corrections in some of the measurements. Source effects, which are totally absent in a critical experiment, may be troublesome in an exponential experiment. Furthermore, some kinds of experiments are difficult to do, such as measurements of control rod worth. Nevertheless, exponential lattices remain useful tools both for the testing of theory and for reactor design.

Very small subcritical assemblies have been used on several occasions, although most experimenters have preferred exponential assemblies that were not far from critical. Wikdahl and Åkerhielm (39) have shown that thermal disadvantage factors could be measured in a 90 cm by 28 cm by 28 cm assembly of one-inch natural uranium rods and heavy water placed in the thermal column of the Swedish reactor R-1. A more extensive series of measurements was made at the Brookhaven National Laboratory (22, 23) with slightly enriched uranium rods moderated with water. A "miniature lattice" of 16-inch long rods in a 12-inch diameter tank was used to determine the cell properties of the various assemblies. Measurements were made in

the various assemblies. Measurements were made of the thermal disadvantage factor, the ratio of U^{238} fissions to U^{235} fissions, the U^{238} cadmium ratio, and the U^{235} cadmium ratio in the rods. These quantities were shown to have the same values as were obtained in a much larger assembly constructed of the same materials.

Several interesting questions immediately arise when the use of small exponential assemblies is considered. They include:

1. Can a small exponential assembly be used to obtain information that can be applied to a full-scale reactor?

2. Can valid corrections be made for the leakage and source effects in a small assembly?

3. Where is the best place to make cell measurements inside a small assembly?

The theoretical development and research reported in the following pages were motivated by the above questions.

1.2 MEASUREMENTS IN MIXED MODERATOR LATTICES

An example of a reactor system for which exponential measurements are relatively expensive is one with a moderator mixture of water and heavy water. The use of such a moderator as a control feature of a reactor has been suggested by Edlund and Rhode (7). In their proposed "Spectral Shift" reactor the heavy water moderator is to be mixed with increasing amounts of water throughout the core lifetime. The reactivity will then be controlled primarily through resonance absorption in the fuel rather than with control rods. The addition of H_2O will, of course, have secondary effects on the thermal utilization and the non-escape probabilities. This proposed reactor system offers the potential of very high burnups and high conversion ratios, and consequent lower fuel charges.

The theoretical problems of mixtures of water and heavy water are also interesting, especially in the thermal energy region where chemical binding phenomena are important. Finally, from the standpoint of the cost of experimentation, the mixing of pure heavy water with ordinary water leads to a considerable extra expense. For this

reason, it is desirable to make such experiments in as small an assembly as possible.

Only a few measurements of cell parameters in lattices moderated with mixtures of water and heavy water have been made until recently. Finn and Wade (9) made three intracell flux distribution measurements as part of an effort to find the effect of water contamination on a natural uranium, heavy water lattice. The fuel rods were one inch in diameter and the volume ratio of moderator to fuel was 12.3. They obtained values of the disadvantage factor for 99.8, 98.4, and 91.8 mole per cent D_2O in the moderator, and found the measured disadvantage factors to agree with P_3 calculations. They also reported a series of buckling measurements over the same range of moderator purity and a fair range of volume ratios. A series of measurements has been made by the Babcock and Wilcox Company. These experiments, reported by Snidow and others (35), were made in critical assemblies of 0.444-inch rods of UO_2 enriched to 4 per cent U^{235}; the ratio of moderator volume to fuel volume was 1.0. Six experiments covering a range of D_2O concentrations from zero to 76.7 mole per cent, some with boron poisoning, were made. Lattice bucklings were measured, as well as the thermal disadvantage factors and the cadmium ratios of U^{235} and U^{238} in the rods. The parameter ranges selected for experimentation correspond to those of interest from the standpoint of reactor design. Wittkopf and Roach (40) have made a theoretical analysis of these data by means of machine calculations and have obtained reasonably good agreement between theory and experiment.

Neutron age measurements have been made in mixtures of water and heavy water by Wade (36) at the Savannah River Laboratory. These measurements have been used by Goldstein (11) for comparison with various theoretical treatments; his review paper also included the results of calculations by Coveyou and Sullivan and by H. D. Brown on mixtures of water and heavy water. Wade's measurements have been used recently by Joanou, Goodjohn, and Wikner (19) for comparison with a moments calculation, and by Wittkopf and Roach (40) for

comparison with a Greuling-Goertzel slowing down calculation. Finally, neutron age measurements have been made in thorium oxide lattices moderated with mixtures of water and heavy water by Roberts and Pettus (27, 30). All of the theoretical treatments cited showed reasonably good agreement with the data, particularly that of Joanou, Goodjohn, and Wikner, and that of Wittkopf and Roach.

1.3 SCOPE OF THE EXPERIMENTAL WORK

The availability of a set of quarter-inch diameter rods containing uranium enriched to 1.143 per cent U^{235} made possible a series of experiments with mixtures of water and heavy water as moderator. These rods had been used previously in experiments with miniature lattices at the Brookhaven National Laboratory. Calculations of the resonance escape probability and the thermal utilization for lattices containing these slightly enriched rods showed the most variation in the upper values of heavy water concentration and at relatively large moderator-to-fuel volume ratios. Consequently, cell parameter measurements were made in three different lattices with rod spacings corresponding to moderator-to-uranium volume ratios of 30.0, 20.8, and 12.0, respectively. At each spacing, three mixtures of water and heavy water were used, consisting of 99.8, 90.27, and 80.23 mole per cent D_2O, respectively.

Measurements were made, in each of the nine lattices, of the ratio of fissions in U^{238} to fissions in U^{235}, and of the cadmium ratio of U^{238} in the rods. Intracell flux traverses were made with gold foils in the lattices with 90.27 and 80.23 mole per cent D_2O. Finally, axial and radial flux traverses were made across the entire assembly in each lattice.

The experiments were made in the Small Exponential Assembly, an experimental apparatus fabricated at M.I.T. by J. Bratten (3). It was modified somewhat for these experiments, and consisted of an aluminum tank in the form of a right circular cylinder 21 inches in height and 20 inches in diameter, together with appropriate grid plates for the fuel rods. The assembly was equipped with lines and

valves for filling from heavy water drums, and held about 100 liters of moderator. It was also equipped with removable fast and slow neutron shielding and a wheeled stand. The neutron beam port of the Medical Therapy Facility at the M. I. T. Reactor was used as a neutron source for the assembly.

1.4 SCOPE OF THE THEORETICAL DEVELOPMENT

An exponential assembly is distinguished from a critical assembly of the same material in that it has a higher neutron leakage rate. The leakage rate prevents the chain reaction from sustaining itself and consequently a neutron source is required. The Lattice Facility and the Small Exponential Assembly at M. I. T. are typical of many such facilities in that each is a right circular cylinder, has little reflection at the boundaries, and has a large thermal neutron source at one end.

The theory of the exponential assembly has been limited in the past largely to determining what reactor quantities may be inferred from such experiments, and to determining harmonic, source, and end corrections for the data. One exception is the work of Barnes and others (1) at the Argonne National Laboratory in connection with some exponential experiments performed there on natural uranium lattices in heavy water. By using two group diffusion theory they obtained a solution for the general problem of a cylindrical assembly fed with thermal neutrons from a graphite pedestal. They also gave an expression for determining the height above the pedestal where the ratio of the fast to slow neutrons would be found to be constant.

Since both the Lattice Facility and the Small Exponential Assembly had somewhat different boundary conditions at the source end than the case considered by Barnes et al, a general treatment of the exponential assembly with non-reflecting boundary conditions was carried through with age-diffusion theory. The solution yielded, at any point in the assembly, the thermal flux due to source neutrons, the thermal flux due to neutrons born and moderated in the assembly, and the slowing down density at any particular value of the Fermi age.

A machine code for the IBM 709 was written to compute these various quantities. Extensive use of the machine code was made to determine the corrections to apply to the cell parameters measured in the Small Exponential Assembly. Furthermore, tables were prepared, giving values of the flux quality and magnitude and the extent of the useful experimental region in 128 possible exponential assemblies.

1.5 USE OF THE "THERMOS" MACHINE CODE

To compare the intracell flux traverses with the best available theory and to compute average values of certain parameters for the lattices, extensive use was made of the Thermos machine code for the IBM 709 developed by Honeck (17). The Thermos code computes the scalar thermal neutron spectrum as a function of position in a lattice cell.

CHAPTER 2.
THEORY OF A SMALL EXPONENTIAL ASSEMBLY

2.1 INTRODUCTION

The purpose of this section is to present the theory of a small exponential assembly, and to obtain appropriate corrections to be applied to measurements made in it. Complete solutions of the age-diffusion equations are found for two different source conditions by the methods of operational calculus.

The age-diffusion equations are transformed in the spatial variables by means of finite Fourier transformations. They are then solved in terms of the age variable. The result, for each source condition, yields the solution by application of the inversion formulas for the Fourier transformations. Experimental verification of the formulas is considered.

Correction factors for data measured in small assemblies are obtained. Finally, the general solutions are applied to large exponential assemblies in order to find the flux quality and magnitude.

2.2 GENERAL SOLUTION FOR A PLANE THERMAL NEUTRON SOURCE

The following solution is for a homogeneous, subcritical assembly in the form of a right circular cylinder. A plane thermal neutron source is incident upon one end. The coordinate system is shown in Figure 2-1.

If the source neutrons are assumed to belong to one thermal energy group the diffusion equation for the source group is

$$D_s \nabla^2 \phi_s(r, z) - \Sigma_a^s \phi_s(r, z) = 0 \quad , \qquad (2.2\text{-}1)$$

where Σ_a^s is the macroscopic absorption cross section for source neutrons and D_s is the thermal diffusion constant.

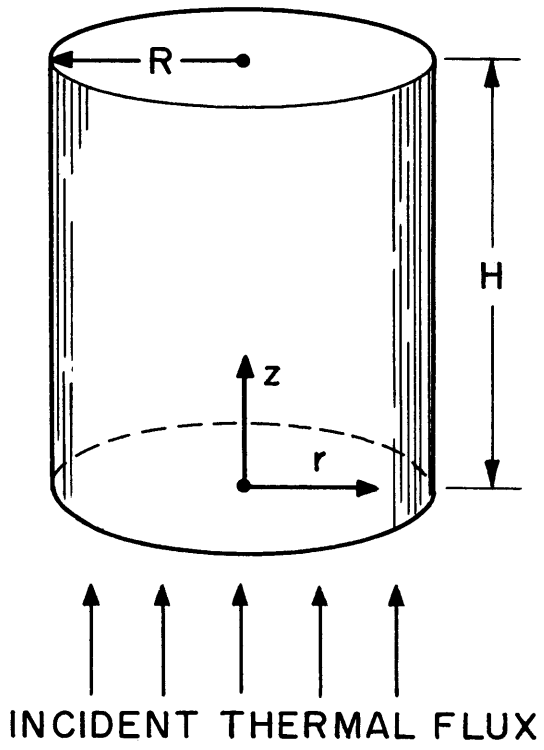

FIG. 2 -1 EXPONENTIAL
ASSEMBLY GEOMETRY

The boundary conditions are:

a. The thermal source neutron flux vanishes at the extrapolated boundaries, so that

$$\phi_s(r, z) = 0 \quad \text{at } r = R, \text{ and } z = H, \tag{2.2-2}$$

where R and H are the extrapolated radius and height of the assembly, respectively.

b. The incoming thermal neutron current at the source end, F(r), is related to thermal flux by

$$F(r) = -D_s\left[\frac{\partial \phi_s(r, z)}{\partial z}\right] \qquad \text{at } z = 0 \ . \tag{2.2-3}$$

If the incident current is a plane source independent of r, it may be expressed as

$$F(r) = F \quad \text{(a constant)} \ . \tag{2.2-4}$$

A finite Hankel transformation can be used to solve equation (2.2-1). This transformation is defined (34) in the following way. If

$$\bar{f}(\psi_i) = \int_0^R rf(r)\, J_o(\psi_i r)\, dr \ , \tag{2.2-5}$$

where

$$J_o(\psi_i R) = 0 \ , \tag{2.2-6}$$

then

$$f(r) = \frac{2}{R^2} \sum_{i=1}^{\infty} \bar{f}(\psi_i)\, \frac{J_o(\psi_i r)}{[J_1(\psi_i R)]^2} \ , \tag{2.2-7}$$

where the bar is an operational notation indicating the transform of the function f(r); J_o and J_1 refer to the Bessel function of the first kind, of order 0 and 1, respectively. The transformation fits the coordinate system of Figure 2-1.

The Laplacian operator ∇^2 has the following expansion in circular cylindrical coordinates with no angular dependence:

$$\nabla^2 f = \frac{\partial^2 f}{\partial r^2} + \frac{1}{r}\left[\frac{\partial f}{\partial r}\right] + \frac{\partial^2 f}{\partial z^2} \ . \tag{2.2-8}$$

The Hankel transform of $\nabla^2 f$ is

$$\int_0^R r[\nabla^2 f(r, z)]\ J_o(\psi_i r)\ dr$$

$$= R\psi_i f(R, z)\ J_1(\psi_i r) - \psi_i^2 \bar{f}(\psi_i, z) + \frac{\partial^2 \bar{f}(\psi_i, z)}{\partial z^2} \quad . \qquad (2.2\text{-}9)$$

In the Hankel transformation of equation (2.2-1), the term $\nabla^2 \phi_s(r, z)$ is transformed as in equation (2.2-9); but

$$\phi_s(R, z) = 0 \qquad (2.2\text{-}2)$$

because of the boundary conditions. Thus the first term on the right side of equation (2.2-9) is zero.

The transformation of equation (2.2-1) yields

$$D_s\left[-\psi_i^2 \bar{\phi}_s(\psi_i, z) + \frac{\partial^2 \bar{\phi}_s(\psi_i, z)}{\partial z^2}\right] - \Sigma_a^s \bar{\phi}_s(\psi_i, z) = 0 \quad . \qquad (2.2\text{-}10)$$

Rearrangement of this equation gives

$$\frac{\partial^2 \bar{\phi}_s(\psi_i, z)}{\partial z^2} = \left[\frac{\Sigma_a^s}{D_s} + \psi_i^2\right] \bar{\phi}_s(\psi_i, z) \quad . \qquad (2.2\text{-}11)$$

The introduction of the quantity

$$\beta_i^2 = \frac{\Sigma_a^s}{D_s} + \psi_i^2 \qquad (2.2\text{-}12)$$

reduces equation (2.2-11) to

$$\frac{\partial^2 \bar{\phi}_s(\psi_i, z)}{\partial z^2} = \beta_i^2 \bar{\phi}_s(\psi_i, z) \quad . \qquad (2.2\text{-}13)$$

Equation (2.2-13) is a simple differential equation in the variable z, for the transformed function $\bar{\phi}_s$. It can be solved to fit the transformed boundary conditions

$$\bar{\phi}_s(\psi_i, H) = 0 \qquad (2.2\text{-}14)$$

and,

$$\bar{F} = -D_s\left[\frac{\partial \bar{\phi}_s(\psi_i, z)}{\partial z}\right] \qquad (2.2\text{-}15)$$

at $z = 0$.

The solution of equation (2.2-13) which satisfies equations (2.2-14) and (2.2-15) is

$$\bar{\phi}_s(\psi_i, z) = \left[\frac{\bar{F}}{D_s\beta_i}\right]\left[\frac{\sinh(\beta_i[H-z])}{\cosh(\beta_i H)}\right] . \qquad (2.2\text{-}16)$$

Since F, as a plane source, is a constant in the variable r, the transform of F is

$$\bar{F}(\psi_i) = F\int_0^R rJ_o(\psi_i r)\,dr , \qquad (2.2\text{-}17)$$

or,

$$\bar{F}(\psi_i) = \frac{FRJ_1(\psi_i R)}{\psi_i} . \qquad (2.2\text{-}18)$$

Substituting equation (2.2-18) into equation (2.2-16) gives

$$\bar{\phi}_s(\psi_i, z) = \left[\frac{FR}{\psi_i\beta_i D_s}\right][J_1(\psi_i R)]\left[\frac{\sinh(\beta_i[H-z])}{\cosh(\beta_i H)}\right] . \qquad (2.2\text{-}19)$$

The solution now can be found by inverting equation (2.2-19), by means of the inversion formula, (2.2-7). The result is

$$\phi_s(r, z) = \frac{2F}{D_s R}\sum_{i=1}^{\infty}\left[\frac{1}{\psi_i\beta_i}\right]\left[\frac{J_o(\psi_i r)}{J_1(\psi_i R)}\right]\left[\frac{\sinh(\beta_i[H-z])}{\cosh(\beta_i H)}\right] . \qquad (2.2\text{-}20)$$

Equation (2.2-20) is the general solution, in the plane source case, for the thermal flux at any point in the assembly due solely to source neutrons. These neutrons cause fissions, however, and give rise to fission energy neutrons. Some of the fission energy neutrons escape while the rest are captured or moderated to thermal energies. The expressions for the slowing down density and the thermal flux due to these lattice born and moderated neutrons will be considered next.

The total thermal flux at any point in the assembly will then be the sum, at that point, of the source neutron flux and the lattice born and moderated neutron flux.

The diffusion equation for the lattice born thermal neutrons is,

$$D_e \nabla^2 \phi_e(r, z) - \Sigma_a^e \phi_e(r, z) + p_o q(\tau_o, r, z) = 0 \qquad (2.2\text{-}21)$$

where a superscript or subscript e indicates quantities pertaining to the lattice born and moderated neutrons. The Fermi age of the neutrons to the thermal energy group is represented by τ_o and the resonance escape probability to thermal energies is denoted by p_o. The slowing down density, q, is for a system with no resonance absorption, since these absorptions are taken into account in the value of p_o.

The Fermi age equation for the slowing down density is

$$\nabla^2 q(\tau, r, z) = \frac{\partial q(\tau, r, z)}{\partial \tau} \ . \qquad (2.2\text{-}22)$$

The boundary conditions for the two equations are:

a. Both $\phi_e(r, z)$ and $q(\tau, r, z)$ are zero at the same extrapolated boundaries $z = 0$, $z = H$, and $r = R$. These conditions assume no reflection at any boundary and would not be applicable to an assembly mounted on a thick graphite pedestal. They do correspond to the experimental condition for the Lattice Facility and the Small Exponential Assembly at M. I. T.

b. The second boundary condition, which links equations (2.2-20), (2.2-21), and (2.2-22), is

$$q(\tau, r, z) = \frac{k_\infty}{p_o}\left[\Sigma_a^e \phi_e(r, z) + \Sigma_a^s \phi_s(r, z)\right] \qquad (2.2\text{-}23)$$

at

$$\tau = 0 \ .$$

The Hankel transforms of equations (2.2-21) and (2.2-22) are, respectively,

$$-\psi_i^2 \bar{\phi}_e(\psi_i, z) + \frac{\partial^2 \bar{\phi}_e(\psi_i, z)}{\partial z^2} - \frac{\Sigma_a^e \bar{\phi}_e(\psi_i, z)}{D_e} + \frac{p_o \bar{q}(\tau_o, \psi_i, z)}{D_e} = 0 \ , \qquad (2.2\text{-}24)$$

and

$$-\psi_i^2 \bar{q}(\tau, \psi_i, z) + \frac{\partial^2 \bar{q}(\tau, \psi_i, z)}{\partial z^2} = \frac{\partial \bar{q}(\tau, \psi_i, z)}{\partial \tau} \quad . \tag{2.2-25}$$

These equations may be transformed again on the z variable by using a finite Fourier sine transformation. This transformation is defined in the following way.

If

$$\bar{f}(n) = \int_0^H f(z) \sin\left(\frac{n\pi z}{H}\right) dz \quad , \tag{2.2-26}$$

then

$$f(z) = \frac{2}{H} \sum_{n=1}^{\infty} \bar{f}(n) \sin\left(\frac{n\pi z}{H}\right) \quad . \tag{2.2-27}$$

The finite sine transformation of the second derivative is,

$$\int_0^H \left[\frac{\partial^2 f(z)}{\partial z^2}\right] \sin\left(\frac{n\pi z}{H}\right) dz = -\frac{n^2\pi^2 \bar{f}(n)}{H^2} \quad . \tag{2.2-28}$$

Application of the finite Fourier sine transformation to equations (2.2-24) and (2.2-25) yields, respectively,

$$\left[-\psi_i^2 - \frac{n^2\pi^2}{H^2} - \frac{\Sigma_a^e}{D_e}\right] \bar{\bar{\phi}}_e(\psi_i, n) + \left[\frac{p_o}{D_e}\right] \bar{\bar{q}}(\tau_o, \psi_i, n) = 0 \quad , \tag{2.2-29}$$

and

$$\left[-\psi_i^2 - \frac{n^2\pi^2}{H^2}\right] \bar{\bar{q}}(\tau, \psi_i, n) - \frac{\partial \bar{\bar{q}}(\tau, \psi_i, n)}{\partial \tau} = 0 \quad , \tag{2.2-30}$$

where the double bar indicates the doubly transformed function.

Equation (2.2-30) can be solved in terms of the age variable τ,

$$\bar{\bar{q}} = C\left[\exp(-B_{i,n}^2 \tau)\right] , \tag{2.2-31}$$

where C is a constant to be determined and

$$B_{i,n}^2 = \psi_i^2 + \frac{n^2\pi^2}{H^2} \quad . \tag{2.2-32}$$

$B^2_{i,n}$ is the buckling of each mode in the double expansion; when

$$i = n = 1$$

it reduces to the well known expression

$$B^2_{1,1} = \left[\frac{2.405}{R}\right]^2 + \left[\frac{\pi}{H}\right]^2 \quad . \tag{2.2-33}$$

The constant C in equation (2.2-31) may be determined from the boundary condition for $\tau = 0$. The double transformation of this boundary condition, as expressed in (2.2-23), is

$$\bar{\bar{q}}(0, \psi_i, n) = \frac{k_\infty}{p_o}\left[\Sigma^e_a \bar{\bar{\phi}}_e(\psi_i, n) + \Sigma^s_a \bar{\bar{\phi}}_s(\psi_i, n)\right] \quad . \tag{2.2-34}$$

The constant C is equal to the right side of equation (2.2-34) since, from equation (2.2-31),

$$\bar{\bar{q}}(0, \psi_i, n) = C[\exp(0)] = C \quad . \tag{2.2-35}$$

Thus,

$$\bar{\bar{q}}(\tau, \psi_i, n)$$

$$= \frac{k_\infty}{p_o}\left[\Sigma^e_a \bar{\bar{\phi}}_e(\psi_i, n) + \Sigma^s_a \bar{\bar{\phi}}_s(\psi_i, n)\right]\left[\exp(-B^2_{i,n}\tau)\right] \quad . \tag{2.2-36}$$

Equation (2.2-36) can be substituted into equation (2.2-29) to yield

$$\bar{\bar{\phi}}_e(\psi_i, n)$$

$$= \frac{k_\infty \Sigma^s_a \bar{\bar{\phi}}_s(\psi_i, n)\left[\exp(-B^2_{i,n}\tau_o)\right]}{D_e\left[\psi_i^2 + \frac{n^2\pi^2}{H^2} + \frac{\Sigma^e_a}{D_e} - \frac{k_\infty \Sigma^e_a}{D_e}\left[\exp(-B^2_{i,n}\tau_o)\right]\right]} \quad . \tag{2.2-37}$$

The thermal neutron diffusion length, defined as,

$$L^2_e = \frac{D_e}{\Sigma^e_a} \tag{2.2-38}$$

together with equation (2.2-32), may be used to rearrange equation

(2.2-37) to the following form:

$$\Sigma_a^e \bar{\bar{\phi}}_e(\psi_i, n) = \Sigma_a^s \bar{\bar{\phi}}_s(\psi_i, n)\left[\frac{1}{\frac{1 + L_e^2 B_{i,n}^2}{k_\infty\left[\exp(-B_{i,n}^2 \tau_o)\right]} - 1}\right] . \quad (2.2\text{-}39)$$

Defining the finite multiplication factor for each mode as

$$k_{i,n} = \frac{k_\infty\left[\exp(-B_{i,n}^2 \tau_o)\right]}{1 + L_e^2 B_{i,n}^2} , \quad (2.2\text{-}40)$$

yields the result,

$$\Sigma_a^e \bar{\bar{\phi}}_e(\psi_i, n) = \Sigma_a^s \bar{\bar{\phi}}_s(\psi_i, n)\left[\frac{1}{\frac{1}{k_{i,n}} - 1}\right] . \quad (2.2\text{-}41)$$

The bracketed quantity in equation (2.2-41) is the sum of the infinite series,

$$k_{i,n} + k_{i,n}^2 + k_{i,n}^3 \cdots ,$$

since $k_{i,n}$ is less than 1.0 in an exponential assembly.

The expression for $\bar{\bar{\phi}}_s(\psi_i, n)$ can be obtained by making a sine transformation of equation (2.2-19). The sine transformation of the hyperbolic sine function is

$$\int_0^H [\sinh(\beta_i[H-z])] \sin\left(\frac{n\pi z}{H}\right) dz = \frac{n\pi H}{n^2\pi^2 + \beta_i^2 H^2}[\sinh(\beta_i H)] . \quad (2.2\text{-}42)$$

Thus, the sine transformation of equation (2.2-19) is

$$\bar{\bar{\phi}}_s(\psi_i, n) = \frac{FR}{\psi_i D_s \beta_i}[J_1(\psi_i R)]\left[\frac{n\pi H}{n^2\pi^2 + \beta_i^2 H^2}\right]\left[\frac{\sinh(\beta_i H)}{\cosh(\beta_i H)}\right] . \quad (2.2\text{-}43)$$

If equation (2.2-43) is used, equation (2.2-41) can be written as,

$$\bar{\bar{\phi}}_e(\psi_i, n) = \frac{\Sigma_a^s}{\Sigma_a^e}\left[\frac{1}{\frac{1}{k_{i,n}} - 1}\right]\left[\frac{FRJ_1(\psi_i R)}{\psi_i D_s \beta_i}\right]\left[\frac{n\pi H[\tanh(\beta_i H)]}{n^2\pi^2 + \beta_i^2 H^2}\right] . \quad (2.2\text{-}44)$$

This equation may now be inverted twice, by using the inversion formulas (2. 2-7) and (2. 2-27), to yield the answer,

$$\phi_e(r, z) = \frac{\Sigma_a^s}{\Sigma_a^e}\left[\frac{4F}{RD_s}\right]\sum_{i=1}^{\infty}\sum_{n=1}^{\infty}\left[\frac{1}{\frac{1}{k_{i,n}} - 1}\right]\left[\frac{1}{\beta_i\psi_i}\right]$$

$$\times\left[\frac{n\pi}{n^2\pi^2 + \beta_i^2H^2}\right]\left[\frac{\tanh(\beta_iH)}{J_1(\psi_iR)}\right] J_o(\psi_ir)\sin\left(\frac{n\pi z}{H}\right) . \quad (2.\ 2\text{-}45)$$

Equation (2. 2-45) is the general solution in the plane source case for the thermal flux at any point in the assembly due solely to neutrons born and moderated in the assembly.

The double transform of the slowing down density can be obtained by substituting equation (2. 2-39) into equation (2. 2-36). The result is

$$\bar{\bar{q}}(\tau, \psi_i, n) = \frac{k_\infty}{p_o}\left[\frac{1}{\frac{1}{k_{i,n}} - 1}\right]\Sigma_a^s\bar{\bar{\phi}}_s(\psi_i, n)\left[\exp\left(-B_{i,n}^2\tau_o\right)\right] . \quad (2.\ 2\text{-}46)$$

Equation (2. 2-43) can be substituted into this expression and the result inverted twice to yield the solution for the slowing down density,

$$q(\tau, r, z) = \frac{k_\infty\Sigma_a^s}{p_o}\left[\frac{4F}{RD_s}\right]\sum_{i=1}^{\infty}\sum_{n=1}^{\infty}\left[\frac{1}{1-k_{i,n}}\right]\left[\frac{1}{\beta_i\psi_i}\right]\left[\frac{n\pi}{n^2\pi^2 + \beta_i^2H^2}\right]$$

$$\times\left[\frac{\tanh(\beta_iH)}{J_1(\psi_iR)}\right]\left[\exp\left(-B_{i,n}^2\tau\right)\right] J_o(\psi_ir)\sin\left(\frac{n\pi z}{H}\right) . \quad (2.\ 2\text{-}47)$$

Equation (2. 2-47) is the general solution in the plane source case for the slowing down density at any point in the assembly.

2.3 GENERAL SOLUTION FOR A J_o-SHAPED THERMAL NEUTRON SOURCE

When the intensity of the neutron current at the source end is defined by

$$F(r) = FJ_o(2.405r/R), \qquad \text{at } z = 0 ,$$

or

$$F(r) = FJ_o(\psi_1 r) , \tag{2.3-1}$$

the solution of the exponential problem is straightforward. The procedure is identical to the previous solution for a plane source through equation (2.2-16). The Hankel transformation of F(r) for a J_o-shaped source is

$$\int_0^R r[FJ_o(\psi_1 r)]\, J_o(\psi_i r)\, dr = \frac{FR^2}{2}[J_1(\psi_1 R)]^2 , \quad (i=1) ,$$
$$= 0 , \quad (i\neq 1) . \tag{2.3-2}$$

When equation (2.3-2) is substituted into (2.2-16) and the result is inverted, the general solution for the thermal neutron flux due solely to the J_o-shaped source is

$$\phi_s(r, z) = \frac{F}{D_s\beta_1}\left[\frac{\sinh(\beta_1[H-z])}{\cosh(\beta_1 H)}\right] J_o(\psi_1 r) . \tag{2.3-3}$$

The solution procedure for the thermal flux of neutrons born and moderated in the assembly is identical to that for the plane source case through equation (2.2-41). The double transformation of (2.2-3) yields

$$\bar{\bar{\phi}}_s(\psi_i, n) = \frac{FR^2}{2}\left[\frac{1}{D_s\beta_1}\right]\left[\frac{n\pi H}{n^2\pi^2+\beta_1^2H^2}\right]\left[\frac{\sinh(\beta_1 H)}{\cosh(\beta_1 H)}\right] J_1(\psi_1 R) , \quad (i=1) ,$$
$$= 0 , \quad (i\neq 1) . \tag{2.3-4}$$

Substitution of equation (2.3-4) into equation (2.2-41) and double inversion of the result gives

$$\phi_e(r, z) = \frac{\Sigma_a^s}{\Sigma_a^e}\left[\frac{2F}{D_s\beta_1}\right][\tanh(\beta_1 H)] \sum_{n=1}^{\infty}\left[\frac{1}{\frac{1}{k_{1,n}} - 1}\right]$$

$$\times\left[\frac{n\pi}{n^2\pi^2 + \beta_1^2 H^2}\right] J_o(\psi_1 r) \sin\left(\frac{n\pi z}{H}\right) . \qquad (2.3\text{-}5)$$

Equation (2.3-5) is the general solution for the thermal neutron flux due solely to neutrons born and moderated in the assembly in the case of a J_o-shaped source.

The solution for the slowing down density is identical to the plane source procedure through equation (2.2-46). Substitution of equation (2.3-4) into equation (2.2-46) and double inversion of the result gives

$$q(\tau, r, z) = \frac{k_\infty \Sigma_a^s}{p_o}\left[\frac{2F}{D_s\beta_1}\right][\tanh(\beta_1 H)] \sum_{n=1}^{\infty}\left[\frac{1}{1 - k_{1,n}}\right]$$

$$\times\left[\frac{n\pi}{n^2\pi^2 + \beta_1^2 H^2}\right]\left[\exp(-B_{1,n}^2\tau)\right] J_o(\psi_1 r) \sin\left(\frac{n\pi z}{H}\right) .$$

(2.3-6)

Equation (2.3-6) is the general solution for the slowing down density in the case of a J_o-shaped thermal neutron source.

The equations for this case can also be obtained directly from the equations for the plane source case. The plane source expansion in a Hankel series contains the fundamental J_o mode as the first member of the series. Multiplying equations (2.2-20), (2.2-45), and (2.2-47) by the normalization factor,

$$\frac{R\psi_1}{2}[J_1(\psi_1 R)] ,$$

and dropping all but the first member of the Hankel series will yield equations (2.3-3), (2.3-5), and (2.3-6), respectively. The normalization factor is obtained by dividing equation (2.3-2) by equation (2.2-18).

2.4 EXPERIMENTAL VERIFICATION OF THE THEORY

The equations derived in sections 2.2 and 2.3 can be tested experimentally by making flux traverses with foils. The thermal neutron activation of a very thin 1/v detecting foil such as indium or gold would be proportional to the sum of the densities of the source neutrons and the lattice born neutrons. The resonance activation of the same foil would be proportional to the slowing down flux at the resonance activation energy. Thus, flux traverses made with bare and cadmium covered foils along the central axis of the assembly can be compared with the theory. The thermal flux is assumed to be a Maxwellian distribution, M(E), and is joined to the slowing down 1/E flux at 0.12 ev. The value of 0.12 ev corresponds to the commonly used joining point of 5 kT. The subcadmium 1/v activation of the foil is caused primarily by the thermal flux, with a small contribution from the 1/E flux between 0.12 ev and the cadmium cut-off. The epicadmium activation is caused by the resonance absorption of the foil and by the epicadmium 1/v absorption. A cadmium cut-off energy of 0.40 ev was chosen for 0.020 cadmium covers (38). The effective subcadmium absorption cross section, per unit thermal flux, of a foil in the traverse is

$$\sigma_{sub} = \int_0^{0.12} M(E)\, \sigma_{1/v}(E)\, dE + \int_{0.12}^{0.40} \left[\frac{\phi(E)}{\phi_t}\right] \sigma_{1/v}(E)\, dE \quad . \tag{2.4-1}$$

On using the relation for the energy region below the U^{238} resonances,

$$\phi(E) = \frac{p_o q}{\xi \Sigma_s E} \quad , \tag{2.4-2}$$

equation (2.4-1) may be written as

$$\sigma_{sub} = 0.886\, \sigma_o + \left[\frac{p_o q}{\phi_t \xi \Sigma_s}\right] [0.414\, \sigma_o] \quad , \tag{2.4-3}$$

where σ_o is the absorption cross section for 2200 m/sec neutrons, and

$$\phi_t = \phi_e + \phi_s \qquad \text{(the total thermal flux)} \ . \tag{2.4-4}$$

The effective epicadmium absorption cross section, per unit thermal flux, is

$$\sigma_{epi} = \int_0^{\infty} \left[\frac{\phi(E)}{\phi_t}\right] \sigma_{res}(E)\, dE + \int_{0.40}^{\infty} \left[\frac{\phi(E)}{\phi_t}\right] \sigma_{i/v}(E)\, dE$$

$$= \frac{p_o q}{\phi_t \xi \Sigma_s} [ERI + 0.500\sigma_o] \ , \tag{2.4-5}$$

where ERI denotes the effective resonance integral of the foil.

The cadmium ratio, R_f, of a foil at a point (r, z) in the assembly is then

$$R_f = \frac{\sigma_{sub} + \sigma_{epi}}{\sigma_{epi}} \ . \tag{2.4-6}$$

Substitution of equations (2.4-3) and (2.4-5) into equation (2.4-6) gives

$$\frac{p_o q(\tau_r, r, z)}{\phi_t(r, z)\ \xi \Sigma_s} = \frac{0.886}{[R_f(r, z) - 1]\left[\frac{ERI}{\sigma_o} + 0.500\right] - 0.414} \ , \tag{2.4-7}$$

where τ_r denotes the age at the resonance energy. If the value of $p_o q/\phi_t \xi \Sigma_s$ changes appreciably from the resonance energy to the epithermal subcadmium energy range, the above relationship will be in error, to an extent depending upon the relative values of the ERI and σ_o.

Equation (2.4-7) can be used for a direct comparison of the theory with experimental traverses of gold or indium foils. Only the experimentally determined cadmium ratio for a point of the traverse and the value of ERI/σ_o are needed to find the experimental value of $p_o q/\phi_t \xi \Sigma_s$ for the point. The theoretical value of $p_o q/\phi_t \xi \Sigma_s$ for the same point can be calculated by using the equations obtained in sections 2.2 or 2.3 together with an

appropriate value of $\xi\Sigma_s$.

The measured values of $p_o q$ and ϕ_t for each point of a traverse also can be compared separately to the corresponding theoretical values. The measured activity of a foil, after an irradiation for a time interval T, and following a delay of time length t before counting, is

$$\frac{\text{activity}}{\text{milligram}} = N\phi_t\chi\sigma[\exp(-\lambda t)][1-\exp(-\lambda T)] \quad , \qquad (2.4\text{-}8)$$

where χ is the counter efficiency and N is the number of foil atoms per milligram. If

$$a = N\chi\sigma_o[\exp(-\lambda t)][1-\exp(-\lambda T)] \quad , \qquad (2.4\text{-}9)$$

then

$$\phi_t(r, z) = \frac{\text{subcadmium activation per milligram}}{a\left[0.886 + 0.414\left[\dfrac{p_o q(\tau_r, r, z)}{\phi_t \xi\Sigma_s}\right]\right]} \quad , \qquad (2.4\text{-}10)$$

where the quantity $p_o q/\phi_t\xi\Sigma_s$ is determined from equation (2.4-7) and the experimental value of the cadmium ratio. Similarly,

$$p_o q(\tau_r, r, z) = \frac{\xi\Sigma_s[\text{epicadmium activation per milligram}]}{a\left[\dfrac{ERI}{\sigma_o} + 0.500\right]} \quad . \qquad (2.4\text{-}11)$$

Thus, $\phi_t(r, z)$ and $p_o q(\tau_r, r, z)$ can be compared to theory separately by using the measured activities at (r, z). Such a comparison was made for flux traverses measured in the Small Exponential Facility.

2.5 CORRECTION OF CADMIUM RATIO MEASUREMENTS TO CRITICAL ASSEMBLY VALUES

Leakage and source effects can affect a cadmium ratio measurement made in an exponential assembly. In correcting such a measurement, the bare critical assembly made of the same materials is a convenient reference standard.

According to age-diffusion theory, in a bare homogeneous

critical assembly the slowing down density is everywhere proportional to the thermal neutron flux. The relationship between the thermal flux and the slowing down density at a foil resonance below the U^{238} resonances is

$$p_o q(\tau_r) = k_\infty \Sigma_a \phi \left[\exp(-B_m^2 \tau_r)\right] \quad . \tag{2.5-1}$$

Equation (2.4-6) for a cadmium ratio measurement can be written as

$$R_f - 1 = \frac{0.886 + 0.414\left[\dfrac{p_o q}{\phi_t \xi \Sigma_s}\right]}{\dfrac{p_o q}{\phi_t \xi \Sigma_s}\left[\dfrac{ERI}{\sigma_o} + 0.500\right]} \quad . \tag{2.5-2}$$

The relationship between a cadmium ratio measurement made in a critical assembly and one made in an exponential assembly composed of the same materials is then

$$\frac{R_f^* - 1}{R_f(r,z) - 1} = \frac{0.886 + 0.414\left[\dfrac{p_o q^*(\tau_r)}{\phi^* \xi \Sigma_s}\right]}{\left[\dfrac{p_o q^*(\tau_r)}{\phi^* \xi \Sigma_s}\right]\left[\dfrac{ERI}{\sigma_o} + 0.500\right]} \Bigg/ \frac{0.886 + 0.414\left[\dfrac{p_o q(\tau_r, r, z)}{\phi_t(r,z) \xi \Sigma_s}\right]}{\left[\dfrac{p_o q(\tau_r, r, z)}{\phi_t(r,z)\, \xi \Sigma_s}\right]\left[\dfrac{ERI}{\sigma_o} + 0.500\right]} \quad , \tag{2.5-3}$$

where the asterisk denotes the critical assembly values. This equation may be written as

$$R_f^* - 1 = \left[\frac{0.886 + 0.414\left[\frac{p_o q^*(\tau_r)}{\phi^* \xi \Sigma_s}\right]}{0.886 + 0.414\left[\frac{p_o q(\tau_r, r, z)}{\phi_t(r, z)\, \xi \Sigma_s}\right]}\right]\left[\frac{\frac{p_o q(\tau_r, r, z)}{\phi_t(r, z)}}{\frac{p_o q^*(\tau_r)}{\phi^*}}\right][R_f(r, z) - 1] \quad . \tag{2.5-4}$$

Equation (2.5-4) is the desired relation for correcting a cadmium ratio measurement made at point (r, z) in an exponential assembly to the critical assembly value. The equations of sections 2.2 or 2.3 together with equation (2.5-1) can be used to calculate the values of $q^*(\tau_r)$, ϕ^*, $q(\tau_r, r, z,)$ and $\phi_t(r, z)$.

The cadmium ratio measurements of most interest, however, are those for U^{238} and U^{235}. These nuclei have many resonances which contribute to the epicadmium activation, and equation (2.5-4) is inappropriate for such a case. But, if the effective resonance integral for such a nuclide in a rod can be represented by

$$ERI = \sum_{j=1}^{n} \sigma_j \quad , \tag{2.5-5}$$

where σ_j is the contribution of each resonance to the total ERI, then equation (2.5-3) may be rewritten as

$$R_f^* - 1 = \left[\frac{0.886 + 0.414\left[\frac{p_o q_o^*}{\phi^* \xi_o \Sigma_s^o}\right]}{0.886 + 0.414\left[\frac{p_o q_o}{\phi_t \xi_o \Sigma_s^o}\right]}\right]\left[\frac{\left[\frac{0.5 p_o q_o}{\phi_t \xi_o \Sigma_s^o}\right] + \sum_{j=1}^{n}\left[\frac{p_j q_j \sigma_j}{\phi_t \xi_j \Sigma_s^j \sigma_o}\right]}{\left[\frac{0.5 p_o q_o^*}{\phi^* \xi_o \Sigma_s^o}\right] + \sum_{j=1}^{n}\left[\frac{p_j^* q_j \sigma_j}{\phi^* \xi_j \Sigma_s^j \sigma_o}\right]}\right][R_f - 1] \quad , \tag{2.5-6}$$

where the subscripts o and j denote the energy at which the quantity denoted by the subscript is to be calculated. The epithermal sub-cadmium range is indicated by o, and the energy corresponding to the j^{th} resonance is indicated by j. The quantity σ_o refers to the

2200. m/sec cross section as previously stated. The quantities q, ϕ_t, and R_f are understood to be functions of position in the assembly and the functional dependence is omitted for convenience.

The first fraction on the right side of equation (2. 5-6), enclosed by brackets on the main line, has a value very close to 1. 0, since, in the thermal lattices to which age-diffusion theory may best be applied, the values of the ratio $p_o q/\phi \xi \Sigma_s$ are in the range 0. 05 to 0. 1. Thus, even a 10 per cent difference between the exponential and critical values of this ratio will change the value of the first fraction in equation (2. 5-6) by 0. 4 per cent, or less, from its asymptotic value of 1. 0. This fraction will be set equal to 1. 0 to simplify the equation.

The experimental quantity most often cited is ρ_{28}, the ratio of the epicadmium to the subcadmium absorption of U^{238} in the rods. Equation (2. 5-6) may be rewritten to give

$$\rho_{28}^{*} = \left[\frac{\left[\frac{p_o q_o^{*}}{\phi^{*} \xi_o \Sigma_s^o} \right] \left[\frac{0.5 \sigma_o}{ERI} \right] + \sum_{j=1}^{n} \left[\frac{p_j q_j^{*} f_j}{\phi^{*} \xi_j \Sigma_s^j} \right]}{\left[\frac{p_o q_o}{\phi_t \xi_o \Sigma_s^o} \right] \left[\frac{0.5 \sigma_o}{ERI} \right] + \sum_{j=1}^{n} \left[\frac{p_j q_j f_j}{\phi_t \xi_j \Sigma_s^j} \right]} \right] [\rho_{28}] \quad , \qquad (2.5\text{-}7)$$

where f_j is the fractional contribution of the j^{th} resonance to the ERI, and where the values of q and ϕ are calculated at the position of the ρ_{28} measurement in the exponential assembly. Equation (2. 5-7) is the relationship desired for correcting exponentially measured values of ρ_{28}. It can be used for any nuclide with more than one resonance, and was used for correction of the ρ_{28} values measured in the Small Exponential Assembly.

An experimental test of this equation can be made by noting that the correction depends upon the experimental position of the test foils, especially in the z direction. Measurements made at different positions should be identical after correction, however, for any particular array. For this reason, two measurements,

each at a different position, were made in all but one of the lattices tested.

It should be emphasized that in a large exponential assembly there will exist an asymptotic region in which a cadmium ratio measurement will have no inherent difference from one made in a critical assembly. If the slowing down density is actually proportional to the thermal flux, which will occur in a large exponential assembly over a region sufficiently distant from the source and the boundaries, then the relationship for the critical assembly applies, and

$$\frac{p_o q(\tau)}{\Sigma_a \phi} = k_\infty \left[\exp(-B_m^2 \tau) \right] , \qquad (2.5\text{-}8)$$

where B_m^2 is the material buckling. Equation (2.5-1) depends only on the assumption that the slowing down density is actually proportional to the thermal flux and not upon the dimensions of the system.

When the critical assembly value of ρ_{28} has been obtained, it can be used for calculation of the resonance escape probability in the infinite assembly using the procedure of Kouts (24).

2.6 CORRECTION OF U^{238}/U^{235} FISSION RATIOS TO INFINITE ASSEMBLY VALUES

The ratio δ_{28} is defined as the number of U^{238} fissions to the number of U^{235} fissions in the rod. It is measured by exposing depleted and natural uranium foils in a split rod in the lattice. The fission product activity of the depleted foil is caused by fast neutron fission of U^{238}. The fission product activity of the natural foil is caused almost entirely by thermal fission of the U^{235} foil atoms.

If a single rod were placed in the moderator, the resulting U^{238} fission product activity of the depleted foil would be caused by fast neutrons arising from thermal fissions in that rod. The resulting value of δ_{28} is referred to as the "single rod" value. It depends primarily on the diameter of the rod. If, however, the

test rod is part of a lattice of rods, fast neutrons arising from thermal fissions in other rods may reach the test rod and cause additional U^{238} fissions in the depleted foil. This effect is known as the "interaction effect" and may amount to several times the single rod fast effect at close lattice spacings. The interaction effect depends mainly on the spacing between the rods in terms of the mean free path for the fast neutrons. The fast neutrons causing the interaction effect may arise at some distance from the test rod, since a fission energy neutron is only removed from the fast fission energy range by an inelastic collision with a fuel atom or by a collision with a moderator atom.

The fission energy neutrons which cause fast fission in U^{238} will be born in the rods of the lattice with a birth rate density proportional to the thermal flux. In an infinite assembly the thermal flux would be the same at identical cell points across the assembly. If the thermal flux in the actual assembly varied in the vicinity of the test rod in a linear fashion, the resulting fission activation of a foil still would be the same as if the measurement were made in a flat flux. For, the sum of fast neutrons born at equal distances from the foil in a linear flux would be identical to the sum of fast neutrons born at the same distance in a flat flux. In an exponential or critical assembly, however, the flux distribution is usually not flat or linear, and a correction must be applied to the measured data to obtain the value for an infinite lattice.

The variation caused in the value of δ_{28} for a single thin rod by the thermal flux shape in an exponential assembly is quite small. It may be safely neglected on geometric considerations alone, because the fast neutrons reaching the foil must originate in the same rod at points very close to the foil and, over this small region, the variation of the thermal flux is nearly linear. A numerical example is given in Appendix B. The neutrons causing the interaction effect come from other rods, and their birth rate density is appreciably different from a linear function over distances

at which they can still contribute to the interaction effect.

In the lattices considered here, the rods were relatively thin, being only 0.250 inches in diameter. They were spaced in three hexagonal arrays of 0.880, 1.128, and 1.340 inches, center to center, respectively. In these cases it is a reasonable approximation to consider the neighboring rods to be line sources of fast neutrons.

Consider a measurement made at position $(0, z_f)$ in an exponential array; the coordinate system is that of Figure 2-1. The fast flux, ϕ_f, arriving at this point from a neighboring rod a distance r_k away is proportional to the thermal flux along the neighboring rod:

$$\phi_f(0, z_f) \propto \int_0^H K_p(\rho)\, \phi_t(r_k, z)\, dz \quad , \tag{2.6-1}$$

where the point kernel for single collisions is

$$K_p(\rho) = \frac{\exp\left(-\Sigma_s^f \rho\right)}{4\pi\rho^2} \quad , \tag{2.6-2}$$

and

$$\rho = \left[[z-z_f]^2 + r_k^2\right]^{1/2} \quad . \tag{2.6-3}$$

The macroscopic scattering cross section along the flight path of the fast neutron is represented by Σ_s^f. These equations would also apply to a bare critical reference assembly or to an infinite assembly, the only difference being in the limits of integration and in the expression for the thermal flux. The appropriate thermal flux expressions for the exponential case could be taken from sections 2.2 or 2.3 but that would lead to undue mathematical labor in the integrations. Good approximations to the thermal flux, for these purposes at least, are given in Table 2-1. In this table, γ is the inverse of the thermal neutron relaxation length in the exponential assembly, and is either measured or estimated from the relationship

Table 2-1

Thermal Flux Shape Approximations

Type of Assembly	$\phi_t(r, z)$	Foil Position in Assembly	Integration Limits
Exponential	$J_o\left(\frac{2.405r}{R}\right) \exp(-\gamma[z-z_f])$	$(0, z_f)$	$\int_0^H dz$
Bare Critical	$J_o\left(\frac{2.405r}{R^*}\right) \sin\left(\frac{\pi z}{H^*}\right)$	$(0, H^*/2)$	$\int_0^{H^*} dz$
Infinite	1	(0, 0)	$2\int_0^\infty dz$

$$\gamma^2 = [2.405/R]^2 - B_m^2 \quad , \qquad (2.6\text{-}4)$$

where B_m^2 is the material buckling of the assembly. The values of R*and H*are appropriate to the reference model of a bare critical assembly, and the thermal flux expressions in Table 2-1 are normalized to the value 1.0 at the experimental position $(0, z_f)$.

Since the experimentally determined value of δ_{28} is proportional to the ratio ϕ_f/ϕ_t and, since equation (2.6-1) is normalized to the same thermal flux at the experimental position through the quantities in Table 2-1, the following expression may be written for the correction to the bare critical case:

$$\delta_{28}^* = \left[\frac{\sum_k [\phi_f^*(0, H^*/2)]_k}{\sum_k [\phi_f(0, z_f)]_k} \right] [\delta_{28}] \quad ; \qquad (2.6\text{-}5)$$

the summation is over the various sources of fast flux. Correction to the bare critical case is a little ambiguous since it depends, in principle, on the reference foil position chosen.

The corresponding relation for correction to the infinite case is

$$\delta_{28}^i = \left[\frac{\sum_k \left[\phi_f^i(0, 0)\right]_k}{\sum_k [\phi_f(0, z_f)]_k} \right] [\delta_{28}] \quad , \qquad (2.6\text{-}6)$$

where the superscript i indicates the theoretical infinite case.

If the single rod value is taken to be identical in both the exponential and infinite assemblies, only the interaction effect need be corrected for the variation in flux shapes. In such a case the value of δ_{28} due to the interaction effect may be substituted in place of δ_{28} in the general correction equation (2.6-6), and the corresponding summations made over only the fast neutrons from neighboring rods. The result of this treatment, obtained by using equation (2.6-1) and the expressions in Table 2-1, is

$$\delta_{28}^{i} - \delta_{28}^{sr} = \left[\frac{2 \sum_{k} \int_{0}^{\infty} K_p\left(\left[z^2 + r_k^2\right]^{1/2}\right) dz}{\sum_{k} \int_{0}^{H} K_p\left(\left[[z-z_f]^2 + r_k^2\right]^{1/2}\right) \exp(-\gamma[z-z_f]) \, J_o\left(\frac{2.405 r_k}{R}\right) dz} \right] \times \left[\delta_{28} - \delta_{28}^{sr}\right] . \quad (2.6\text{-}7)$$

The summations in equation (2.6-7) are over all neighboring rods close enough to be considered as contributors to the fast flux at the foil position. The quantity δ_{28}^{sr} is the single rod value, taken to be identical in the infinite and the exponential lattices.

The integral in the numerator of equation (2.6-7) may be written as

$$\int_{0}^{\infty} \left[\frac{\exp\left(-\Sigma_s^f \left[z^2 + r_k^2\right]^{1/2}\right)}{4\pi\left[z^2 + r_k^2\right]} \right] dz = \frac{1}{4\pi r_k} \int_{0}^{\pi/2} \exp\left(-\Sigma_s^f r_k \sec\phi\right) d\theta$$

$$= \frac{1}{4\pi r_k} \left[F\left(\pi/2, \Sigma_s^f r_k\right)\right] , \quad (2.6\text{-}8)$$

where

$$\sec\theta = \frac{\left[z^2 + r_k^2\right]^{1/2}}{r_k} , \quad (2.6\text{-}9)$$

and $F\left(\pi/2, \Sigma_s^f r_k\right)$ is a tabulated function (31).

The integral in the denominator can be evaluated in two parts, after taking the $J_o(2.405 r_k/R)$ term outside the integral. The procedure is as follows:

$$\int_0^H \left[\frac{\left[\exp\left(-\Sigma_s^f\left[[z-z_f]^2+r_k^2\right]^{1/2}\right)\right]\left[\exp(-\gamma[z-z_f])\right]}{4\pi\left[[z-z_f]^2+r_k^2\right]} \right] dz$$

$$= \frac{1}{4\pi r_k} \int_0^{\theta_1} \exp\left(-\Sigma_s^f r_k \sec\theta\left[1-\gamma\sin\theta/\Sigma_s^f\right]\right) d\theta$$

$$+ \int_0^{\theta_2} \exp\left(-\Sigma_s^f r_k \sec\theta\left[1+\gamma\sin\theta/\Sigma_s^f\right]\right) d\theta$$

$$= \frac{1}{4\pi r_k}\left[F_1\left(\theta_1, \Sigma_s^f r_k, -\gamma/\Sigma_s^f\right) + F_1\left(\theta_2, \Sigma_s^f r_k, +\gamma/\Sigma_s^f\right)\right] , \tag{2.6-10}$$

where

$$\sec\theta = \frac{\left[[z-z_f]^2+r_k\right]^{1/2}}{r_k} , \tag{2.6-11}$$

$$\theta_1 = \arctan\left(z_f/r_k\right) \tag{2.6-12}$$

and

$$\theta_2 = \arctan\left(\frac{H-z_f}{r_k}\right) . \tag{2.6-12}$$

The function F_1 is not listed in standard mathematical tables. A parametric table of the function over a useful range of $\Sigma_s^f r_k$ and γ/Σ_s^f is given in Appendix B; the values were obtained by numerical integration on the IBM 7090 computer at the M. I. T. Computation Center.

Equation (2.6-7), together with the appropriate values for the functions F and F_1, is the desired relation for the correction of exponentially measured values of δ_{28} to the infinite assembly values. This relation was used for correction of the data obtained in the Small Exponential Assembly.

A check of equation (2.6-7) may be made by noting that the

calculated numerator of the right side of the equation should vary in direct proportion to the infinite lattice interaction effect measured in various lattice spacings; the comparison was made for the data given in this report.

2. 7 CORRECTION OF INTRACELL FLUX TRAVERSES TO INFINITE ASSEMBLY VALUES

These measurements are usually made with foils of a 1/v-absorber, with and without cadmium covers, to determine the radial flux dip in the thermal neutron flux in and around a single rod. The data may then be used to calculate the disadvantage factor of the cell. The effect of a small exponential assembly upon these measurements is both spectral and spatial in nature.

If the spectral effects are ignored by assuming a one velocity thermal neutron model, the spatial effect may be adequately corrected by using the theory developed in sections 2. 2 and 2. 3. It is common to assume that the over-all spatial neutron distribution and the localized flux dip near a rod can be separated. This assumption greatly simplifies the analysis and will be used in this report even though it is only an approximation.

The cell flux pattern is commonly shown in terms of the activation of a 1/v detecting foil, with the rod center taken as the center of the coordinate system. The activation is usually normalized to a value of 1. 0 at the rod center. If the radial coordinate in a system centered on a test rod is represented by $\underline{r}$, a normalized flux point for a cell would then be represented by $S(\underline{r})$, where

$$S(\underline{r}) = \frac{\int_0^{v^*} N_n(\underline{r}, v)\, dv}{\int_0^{v^*} N_n(\underline{0}, v)\, dv} . \qquad (2.7\text{-}1)$$

$N_n(\underline{r}, v)$ is the density of neutrons of speed v at radius $\underline{r}$ from the rod center.

If the assumption is made that the over-all spatial distribution and the localized flux dip are separable, then the activation of the foil in an infinite lattice may be found from the equation:

$$S^i(\underline{r}) = \left[\frac{\phi_t(0, z_f)}{\phi_t(r_f, z_f)}\right] [S(\underline{r})] \quad , \qquad (2.7\text{-}2)$$

where the point (r_f, z_f) in the exponential assembly corresponds to the point $(\underline{r})$ in a coordinate system centered on the rod. The total thermal flux, ϕ_t, may be obtained from the equations of sections 2.2 or 2.3. As in the case of the U^{238}/U^{235} fission ratio, there is no particular merit in correcting the values to those which would be measured in a critical assembly. Such measurements, when made in a critical assembly, are invariably corrected to the infinite case before being reported.

If the source distribution of the exponential assembly is a J_o-shaped distribution, the above correction is directly proportional to $1/J_o(2.405r_f/R)$, irrespective of where the measurement is made in the z direction. Even in the case of a plane source, if the measurement is made at some distance from the source, the higher modes will have decayed, and the distribution will be very close to a J_o-shaped distribution in the radial direction. This result can be tested by making a radial flux traverse across the assembly at equivalent cell points. Such a measurement was made in the lattices tested in the Small Exponential Assembly.

The effect of the size of the exponential assembly on the thermal spectrum available at the place of measurement in the assembly can be divided into two parts. One part is the effect of the presence of source neutrons. The other part is the increased possibility of leakage, especially of the higher energy thermal neutrons.

Since the source neutrons are thermal, it is possible that they will, after some collisions, assume the thermal neutron spectrum characteristic of the lattice. Nevertheless, it is desirable to make the measurements at a point where the source neutrons have effectively disappeared and only neutrons born and moderated in the

assembly are available. An estimate of the relative amount of the source neutrons available at the test point can be obtained by calculating the ratio of ϕ_e to ϕ_s from the equations of sections 2. 2 or 2. 3. The theory is then quite useful for finding a region for intracell flux traverses in which there is an adequate flux and a small number of source neutrons.

The effect of leakage on the thermal neutron spectrum is beyond the scope of the theory developed, which used a one velocity thermal neutron model. To estimate this effect, a more sophisticated model must be used. The most useful theory and code for this purpose is the Thermos code developed by Honeck (17) for the IBM 7090 computer. The Thermos code was designed primarily for finding the spectral distribution of thermal neutrons across a cell in an infinite lattice, but it may be used to estimate the effect of leakage. The method is discussed in Appendix C.

2. 8 BUCKLING MEASUREMENTS IN A SMALL EXPONENTIAL ASSEMBLY

One of the most useful measurements made in an exponential assembly is that of the material buckling. This measurement, which requires an accurate determination of the thermal neutron relaxation length along the axis of the assembly, cannot be made in a small assembly because the leakage from the assembly determines the relaxation length almost independently of the material buckling. This property may be seen from the formula for estimating the inverse of the square of the relaxation length along the axis of the assembly:

$$\gamma^2 = \left[\frac{2.405}{R}\right]^2 - B_m^2 \quad . \qquad (2.6\text{-}4)$$

Substitution of the value R=25 cm, as an example of a small assembly, yields the result

$$\gamma^2 = [92.5 \times 10^{-4}] - B_m^2 \qquad (cm^{-2}) \quad .$$

Since a typical value of B_m^2 might be $10. \times 10^{-4}$ cm^{-2}, the inverse

relaxation length, γ, is little affected by changes in the material buckling. Thus, B_m^2 would be difficult to measure accurately, even without the presence of source and end effects.

2.9 PREPARATION OF TABLES FOR THE GENERAL CASE

In the solution of the exponential problem no restriction on the size of the assembly was made aside from the requirement that the assembly be subcritical. It would be expected, however, that the theory would be even more applicable to large exponential assemblies than to small ones. By assuming identical diffusion properties for source and lattice thermal neutrons, the equations developed in sections 2.2 and 2.3 can be simplified somewhat for calculation. This procedure has made possible the preparation of a set of tables for general use.

If the thermal source neutrons have the same average diffusion properties as the thermal lattice neutrons, then

$$\Sigma_a^e = \Sigma_a^s \text{ , and } D_e = D_s \text{ .} \qquad (2.9\text{-}1)$$

The requirement that the extrapolated height of the assembly be equal to the extrapolated diameter,

$$H = 2R \text{ ,} \qquad (2.9\text{-}2)$$

and scaling of the height and radius in terms of the thermal diffusion length, L,

$$\begin{aligned} a &= R/L \text{ ,} \\ 2a &= H/L \text{ ,} \end{aligned} \qquad (2.9\text{-}3)$$

then specifies the size in terms of a dimensionless parameter, a.

For convenience, the roots of the J_o Bessel series will be defined as μ_i, so that

$$J_o(\mu_i) = 0 \text{ ;} \qquad (2.9\text{-}4)$$

the first members of the set of μ_i being

2.4048, 5.5201, 8.6537, $\cdots$.

Then, from equation (2. 2-6), it follows that

$$\psi_i R = \mu_i \quad . \tag{2.9-5}$$

Equation (2. 2-12) now can be written as,

$$\beta_i^2 = \frac{1}{L^2 a^2}\left[a^2 + \mu_i^2\right] \quad ; \tag{2.9-6}$$

furthermore,

$$\beta_i R = \left[a^2 + \mu_i^2\right]^{1/2} \quad , \tag{2.9-7}$$

and

$$\beta_i H = 2\left[a^2 + \mu_i^2\right]^{1/2} \quad . \tag{2.9-8}$$

Equation (2. 2-20) can be written as

$$\frac{\phi_s(r, z)}{F}\left[\frac{D}{L}\right] = \sum_{i=1}^{\infty}\left[\frac{2a}{\mu_i\left[a^2 + \mu_i^2\right]^{1/2}}\right]\left[\frac{J_o\left(\frac{\mu_i r}{R}\right)}{J_1(\mu_i)}\right]\left[\frac{\sinh\left(2\left[a^2+\mu_i^2\right]^{1/2}\left[1-\frac{z}{H}\right]\right)}{\cosh\left(2\left[a^2+\mu_i^2\right]^{1/2}\right)}\right] \quad . \tag{2.9-9}$$

Equation (2. 2-45) can be written as

$$\frac{\phi_e(r, z)}{F}\left[\frac{D}{L}\right] = \sum_{i=1}^{\infty}\sum_{n=1}^{\infty}\left[\frac{4a}{\mu_i\left[a^2+\mu_i^2\right]^{1/2}}\right]\left[\frac{1}{\frac{1}{k_{i,n}} - 1}\right]\left[\frac{n\pi}{n^2\pi^2+4\left[a^2+\mu_i^2\right]}\right]$$

$$\times \frac{\tanh\left(2\left[a^2+\mu_i^2\right]^{1/2}\right)}{J_1(\mu_i)} J_o\left(\frac{\mu_i r}{R}\right) \sin\left(\frac{n\pi z}{H}\right) \quad , \tag{2.9-10}$$

where

$$k_{i,n} = \frac{k_\infty \exp\left(-\frac{\tau_o}{L^2}\left[\frac{\mu_i^2}{a^2} + \frac{n^2\pi^2}{4a^2}\right]\right)}{1 + \frac{\mu_i^2}{a^2} + \frac{n^2\pi^2}{4a^2}} \quad . \tag{2.9-11}$$

Equation (2. 2-47) can be written as

$$\frac{q(\tau, r, z)}{F}\left[\frac{p_o L}{1}\right] = \sum_{i=1}^{\infty}\sum_{n=1}^{\infty}\left[\frac{4a}{\mu_i\left[a^2+\mu_i^2\right]^{1/2}}\right]\left[\frac{k_\infty}{1-k_{i,n}}\right]\left[\frac{n\pi}{n^2\pi^2+4\left[a^2+\mu_i^2\right]}\right]$$

$$\times\left[\frac{\tanh\left(2\left[a^2+\mu_i^2\right]^{1/2}\right)}{J_1(\mu_i)}\right]\left[\exp\left(-\frac{\tau}{L^2}\left[\frac{\mu_i^2}{a^2}+\frac{n^2\pi^2}{4a^2}\right]\right)\right]$$

$$\times J_o\left(\frac{\mu_i r}{R}\right)\sin\left(\frac{n\pi z}{H}\right) \quad . \qquad (2.9\text{-}12)$$

For the case of a J_o-shaped source the corresponding equations can be obtained by taking the first member of the Bessel function series and multiplying by the normalizing factor,

$$\frac{\mu_i}{2}[J_1(\mu_i)] \quad ,$$

in each of the three equations, (2. 9-9), (2. 9-10), and (2. 9-12).

Finally, the equation for the critical case, (2. 5-1), may be rewritten as

$$\frac{q^*(\tau)}{\phi^*}\left[\frac{p_o}{\Sigma_a}\right] = k_\infty\left[\exp\left(-\frac{\tau}{L^2}\left[\frac{\mu_i^2}{a^{*2}}+\frac{\pi^2}{4a^{*2}}\right]\right)\right] \quad , \qquad (2.9\text{-}13)$$

where the parameter a* refers to the critical scaled radius of a reference bare critical reactor of height equal to the diameter.

For any particular exponential assembly characterized by k_∞, τ_o/L^2, and a, the following ratios can be obtained at a given point in the assembly by using equations (2. 9-9), (2. 9-10), (2. 9-11), and (2. 9-12):

$$\phi_e/\phi_s \quad \text{and} \quad \Sigma_a[\phi_e+\phi_s]/p_o q(\tau) \quad ;$$

where ϕ_e/ϕ_s is the ratio of equation (2. 9-10) to equation (2. 9-9), and where the second ratio is given by the sum of equations (2. 9-10) and (2. 9-9) divided by equation (2. 9-12). Furthermore,

since $p_o q^*(\tau)/\Sigma_a \phi^*$ for a bare critical reference assembly can be obtained from equation (2.9-13), the quantity

$$\frac{p_o q(\tau)/\phi_t}{p_o q^*(\tau)/\phi^*}$$

can be calculated at any particular value of the age.

The quantities $[\phi_s/F][D/L]$, $[\phi_e/F][D/L]$, and $[q(\tau)/F][p_o L]$ are shown in Figure 2-2 as functions of position along the central axis of a typical exponential assembly. Figure 2-3 shows the variation of the correction factor

$$\frac{p_o q(\tau)/\phi_t}{p_o q^*(\tau)/\phi^*}$$

with position along the central axis in the same case. The factor is far from 1.0 at the source end, owing primarily to the presence of the thermal source neutrons. As the source neutrons die away in the assembly the correction factor rises until it overshoots 1.0 and then rapidly returns to a value of 1.0. The variation of the quantity

$$\frac{R_f(0,z) - 1}{R_f^* - 1}$$

from equation (2.5-4) should be the exact inverse of that given by this curve. Thus, the theory gives a method of predicting the distance from the source end at which the cadmium ratio becomes constant in the assembly. The region of the assembly over which the cadmium ratio is constant is often referred to as the "asymptotic region". Cadmium ratio traverses are usually used to find this asymptotic region in an exponential assembly. The theory allows prediction of the extent of the region before the assembly is built.

Equations (2.9-9), (2.9-10), (2.9-11), (2.9-12), and (2.9-13) were programmed for machine calculation on an IBM 709 computer and evaluated for a range of values of the parameters, k_∞, τ_o/L^2, and a. The calculations were made in each case for each of twenty equally spaced points along the central axis. Positions along the

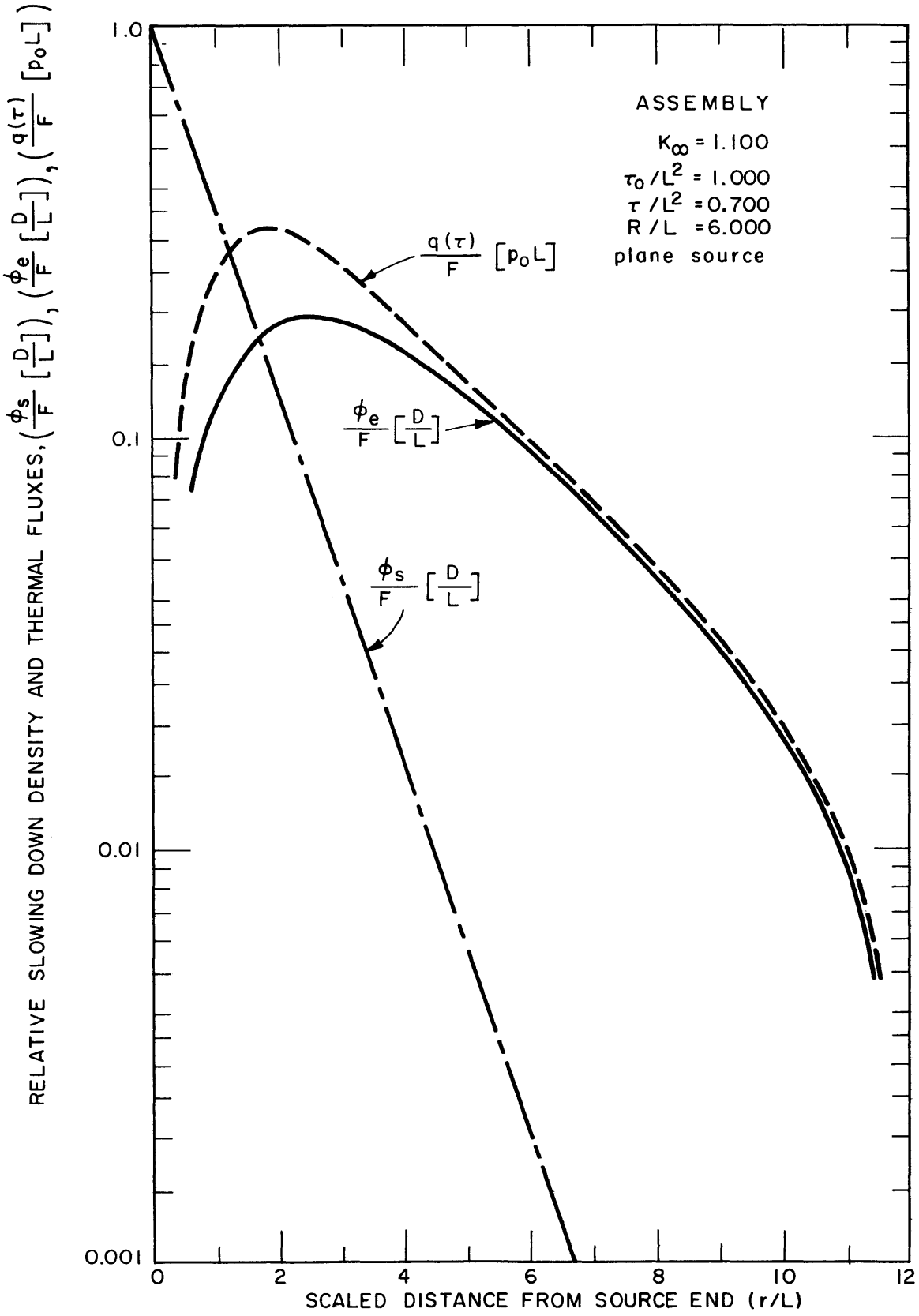

FIG. 2-2 SLOWING DOWN DENSITY AND THERMAL FLUXES IN A TYPICAL EXPONENTIAL ASSEMBLY

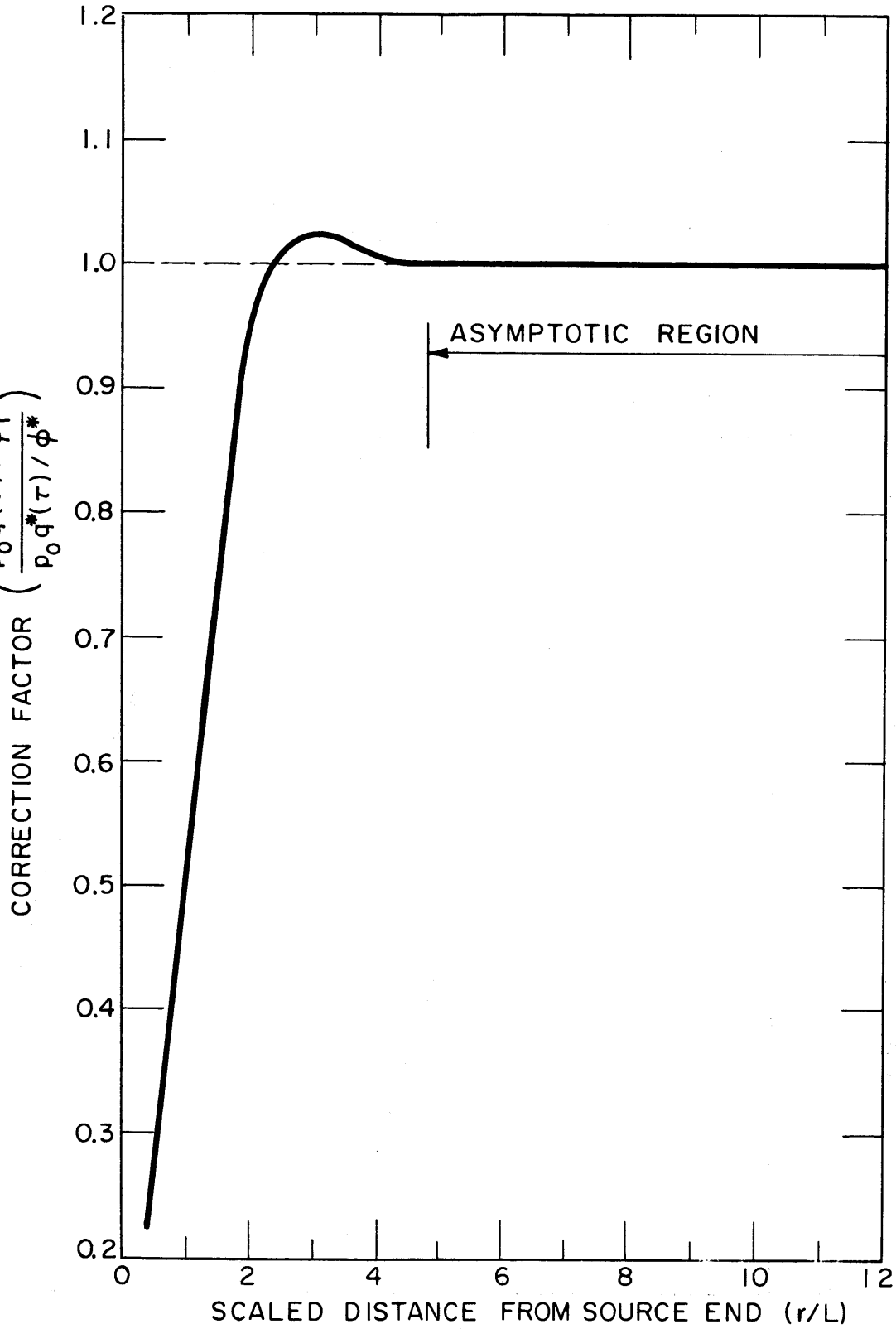

FIG. 2-3 CORRECTION FACTOR IN A TYPICAL EXPONENTIAL ASSEMBLY

central axis are commonly chosen for cell measurements; this choice also shortened the computational time since

$$J_o(\psi_i[0]) = 1.0.$$

The following information was tabulated for each case studied:

a. The distance from the source end, along the central axis, where the asymptotic region begins; the point at which this occurs is called the "asymptotic point".

b. A second point on the central axis, chosen about 30 per cent of the total length farther into the asymptotic region. Parameters are given for this point as well as for the asymptotic point to allow interpolation between the two points.

c. The ratio of the number of lattice born and moderated neutrons to the number of source neutrons at each of the above two points. This ratio is a measure of the quality of the flux spectrum.

d. The value of the quantity, $[\phi_e/F][D/L]$, for each of the above two points. This ratio is a measure of the thermal flux available.

The equations were evaluated over the following ranges of parameters:

a. k_∞ of 1.100, 1.200, 1.300, 1.400.

b. τ_o/L^2 of 0.250, 1.0, 2.0, 3.0.

c. τ of 0.7 τ_o. This value of the age will be in the region of the lowest energy U^{238} resonances.

d. Source distribution, both plane and J_o-shaped.

Four values of R/L were evaluated for each possible combination of k_∞ and τ_o/L^2. These sizes range from just under critical size downward in each case.

The tabulated values of these quantities in Appendix A should be of considerable assistance in the future design of exponential assemblies, as well as in the optimization of present assemblies.

2.10 REMARKS ON THE GENERAL USE OF THE THEORY

The use of age-diffusion theory has some well known deficiencies. The necessity for homogenization of a heterogeneous lattice is the most obvious and it would be expected that, as the fuel becomes thicker and more widely separated, the theory would tend to break down. The lumping of the thermal neutrons into one velocity group is also a serious approximation, especially since the probability of leakage from an assembly depends on the neutron velocity. The use of age theory is probably not acceptable in the case of water moderated lattices, but it should be better in the case of moderators with higher nuclear mass. Finally, the general use of diffusion theory is only an approximation to the actual case of very small assemblies with sharp gradients and close boundaries.

The advantages of using age-diffusion theory are also well known. The chief advantage is the ability to get an exact solution of the equations for the three dimensional case. However, even the exact solution presented in this chapter is relatively complex and requires a computer to evaluate the many cases that might be considered in an experimental program. Another advantage of the simple theory is the relatively small number of variables involved, which makes parametric studies of the general case feasible.

It should be noted, however, that the use of age-diffusion theory for calculating the differences between lattice parameters measured in exponential assemblies and infinite lattice values is much more appropriate than when it is used for calculating the quantities themselves. In every case where the theory was used for corrections in this chapter, as well as in the correction for the U^{238}/U^{235} fission ratio, the assumption was made that

$$\frac{\text{desired measurement}}{\text{exponential measurement}} = \frac{\text{theoretical desired value}}{\text{theoretical exponential value}} ,$$

and the quantities most likely to vary from the exponential to the desired case were selected for theoretical calculation. This approach

is nearly always more accurate than the direct calculation of a quantity. The experimental measurement gives a reference point from which deviations for somewhat changed conditions usually can be calculated accurately using simple theory. This result is based on the fact that deficiencies in the theory will tend to affect the exponential and critical calculations in much the same way, and so tend to cancel out when the ratio is formed.

CHAPTER 3
EXPERIMENTAL PROCEDURES

3.1 THE SMALL EXPONENTIAL ASSEMBLY

The small exponential tank, fabricated at M.I.T. by J. Bratten (3), was modified for these experiments. It is a thin-walled aluminum tank in the form of a right circular cylinder, 21 inches high and 20 inches in diameter, with a removable base plate of 1/2 inch thick aluminum. The tank wall and top are made of 1/16 inch aluminum sheet. The tank is equipped with a wheeled stand, as well as lines and valves to allow filling or draining from a 3/4 inch line. Different lattices can be studied in the facility provided appropriate grid plates are available. Figure 3-1 is a sketch of the assembly.

In an experiment, the assembly is positioned under the thermal neutron beam port in the Medical Therapy Facility of the M.I.T. Reactor. Fast and slow neutron shields are placed around it and the entire assembly, with the shielding, is lifted on the hoist to a position about three feet below the beam port. Figure 3-2 shows the assembly in the experimental position. Owing to its small size and ease of use, a wide variety of experiments can be made at small cost.

The irradiation time for each experiment was two hours when the reactor was at a power of 1.8 megawatts. At this power level there was a reasonably flat flux across the top of the assembly. The flux had a magnitude of about 6×10^8 neutrons/cm^2 sec at the center of the assembly, which slowly fell to about 4×10^8 neutrons/cm^2 sec at the boron carbide shield. The assembly was allowed to sit for about 90 minutes after irradiation in order to reduce the handling exposure. It was then removed, the moderator was drained, and the foils were taken out of the assembly for counting

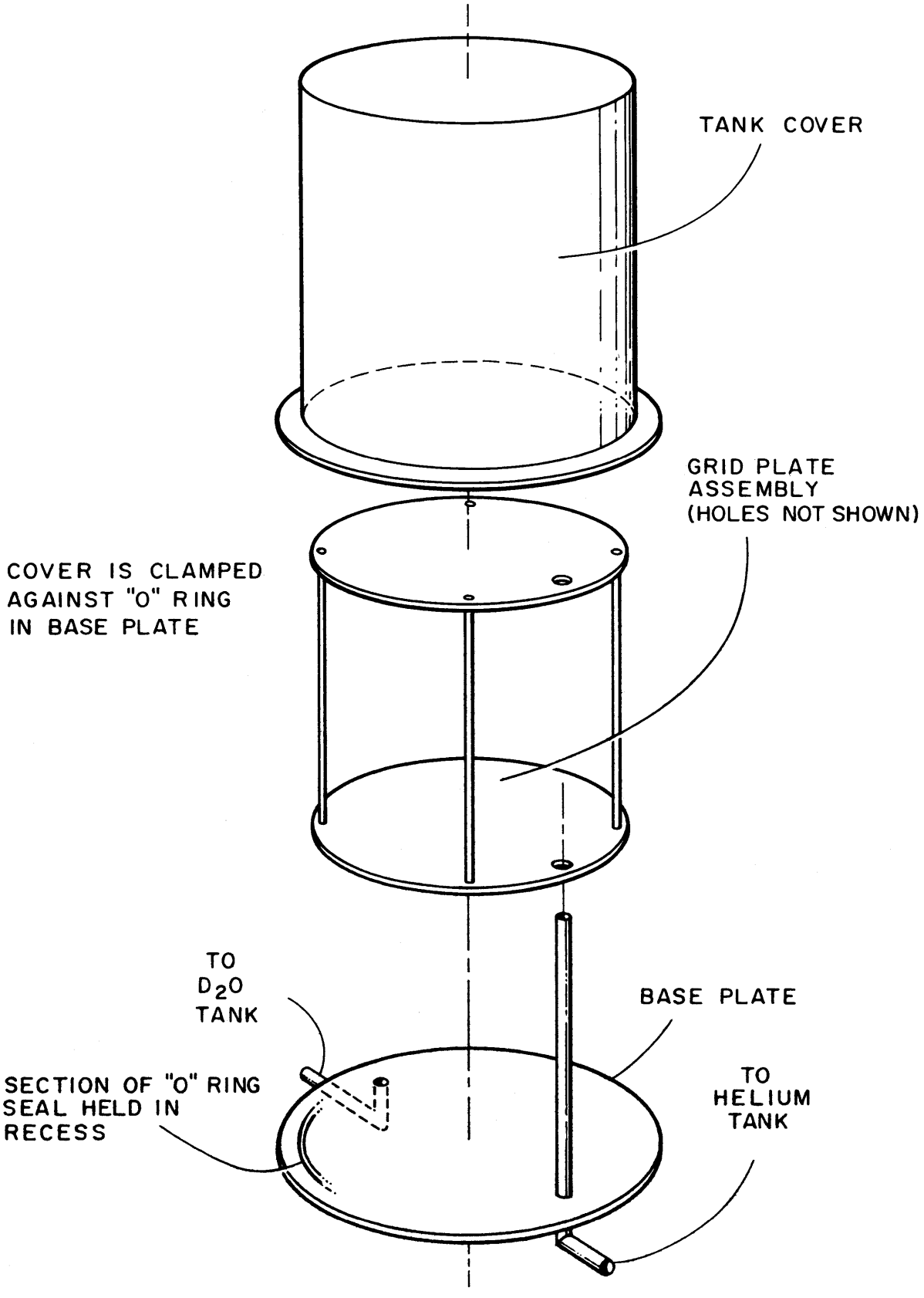

FIG. 3-1 SMALL EXPONENTIAL ASSEMBLY

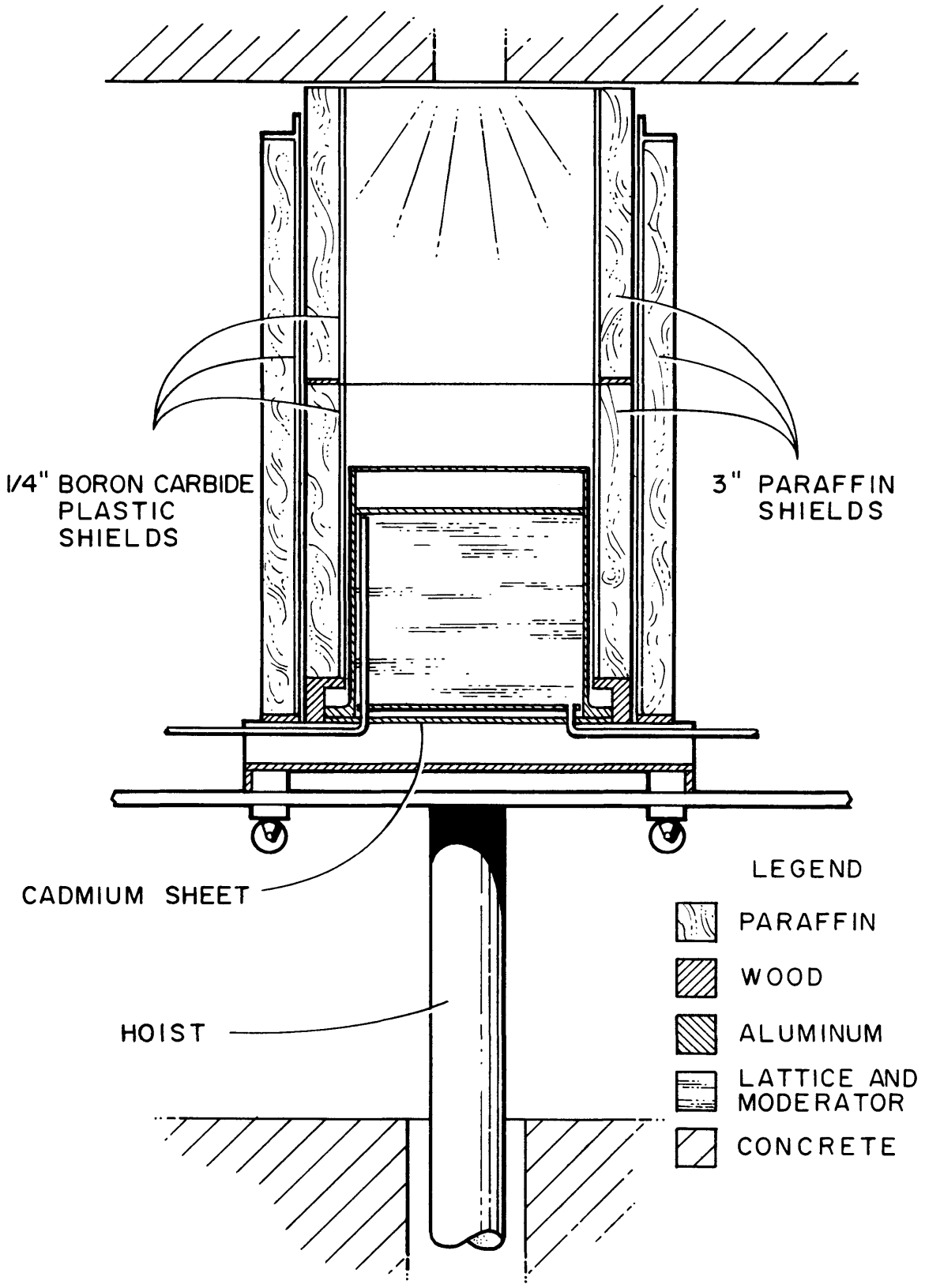

FIG. 3-2 SMALL EXPONENTIAL ASSEMBLY WITH SHIELDING UNDER NEUTRON PORT

3.2 LATTICES TESTED IN THE ASSEMBLY

A set of 290 metallic uranium rods previously used in the "miniature lattice" experiments at the Brookhaven National Laboratory was used for these experiments. The rods had a U^{235} concentration of 1.143 per cent, and were 0.250 inch in diameter. They were enclosed in aluminum tubes of 0.318 inch diameter and 0.028 inch wall thickness. The rods were 16 inches long and were positioned by means of grid plates. The three arrays tested were hexagonal, and had basic center to center rod spacings of 0.880, 1.128, and 1.340 inches, respectively. Since the rods were not long enough to fill the entire tank, an air space of about five inches was present from the top of the rods and the moderator to the source end of the tank. The level of the moderator was maintained by an overflow pipe. Each grid plate assembly had a removable center array to facilitate foil handling.

Three moderator mixtures of water and heavy water were used at each of the above three lattice spacings; they were 99.8, 90.27, and 80.23 mole per cent D_2O in value. The lower values were obtained by using degraded waters from previous fillings of ion exchange columns as well as by mixing D_2O with distilled water. The value of the heavy water content was determined by gravimetric analysis (33). The tank held about 100 liters of moderator when it was filled to the level of the top of the rods.

3.3 MEASUREMENTS MADE IN EACH LATTICE

3.3.1 Axial and Radial Traverses of the Tank

To test the equations derived in sections 2.2 and 2.3, axial and radial traverses were made in each lattice. Gold foils, 0.005 inch thick and 1/8 inch in diameter were used. The axial foils were taped in milled recesses one inch apart on an aluminum stick, 1/16 inch by 1/4 inch thick and 17 inches long. Bare and cadmium covered foils were spaced alternately on the stick; the cadmium covers were 0.020

inch thick. The axial stick was taped along a rod in the second row from the center; thus it was at a distance from the center of 1.7 times the center to center rod spacing.

The radial foils were taped in milled recesses on a similar stick, 20 inches long, but were spaced at distances equal to the center to center rod spacing of each array tested. This insured that the foils were positioned at the same point of each cell in a radial traverse. The radial stick was taped to rods on a main diameter of the assembly and was placed so that each foil was midway between two fuel rods. The foils were alternately bare and cadmium covered as in the axial traverse. Figure 3-3 shows the relative position of the sticks in the removable center array.

The gold foil activities were counted with an automatic Baird Atomic Gas Flow Geiger Counter.

Consideration is given in section 5.1.5 to the possible effect of the foil holder and cadmium covers on the data. Details of the data reduction are given in Appendix D.

3.3.2 U^{238} Cadmium Ratio (R_{28}) Measurement

The average U^{238} cadmium ratio, R_{28}, was measured for 0.250 inch diameter rods, with the equipment and technique set up by A. Weitzberg (38). Two identical foils of uranium depleted to eighteen parts per million U^{235} were irradiated, for each ratio measurement, at equivalent positions in the lattice. The foils were 0.250 inch in diameter and 0.005 inch thick. One foil was placed between two fuel slugs, with thin (0.001 inch thick) aluminum catcher foils on either side to prevent the pickup of fission products from the surrounding uranium. The other foil was placed in a pill box of 0.020 inch thick cadmium, composed of a sleeve 0.375 inch in length imbedded in the aluminum cladding and two 0.250 inch diameter discs which were placed on either side of the depleted foil. Two buttons of enriched uranium 0.094 inch thick were included within the cadmium covers to minimize the streaming of resonance neutrons from the moderator through the cadmium. Figure 3-4 shows the foil assembly in the rod.

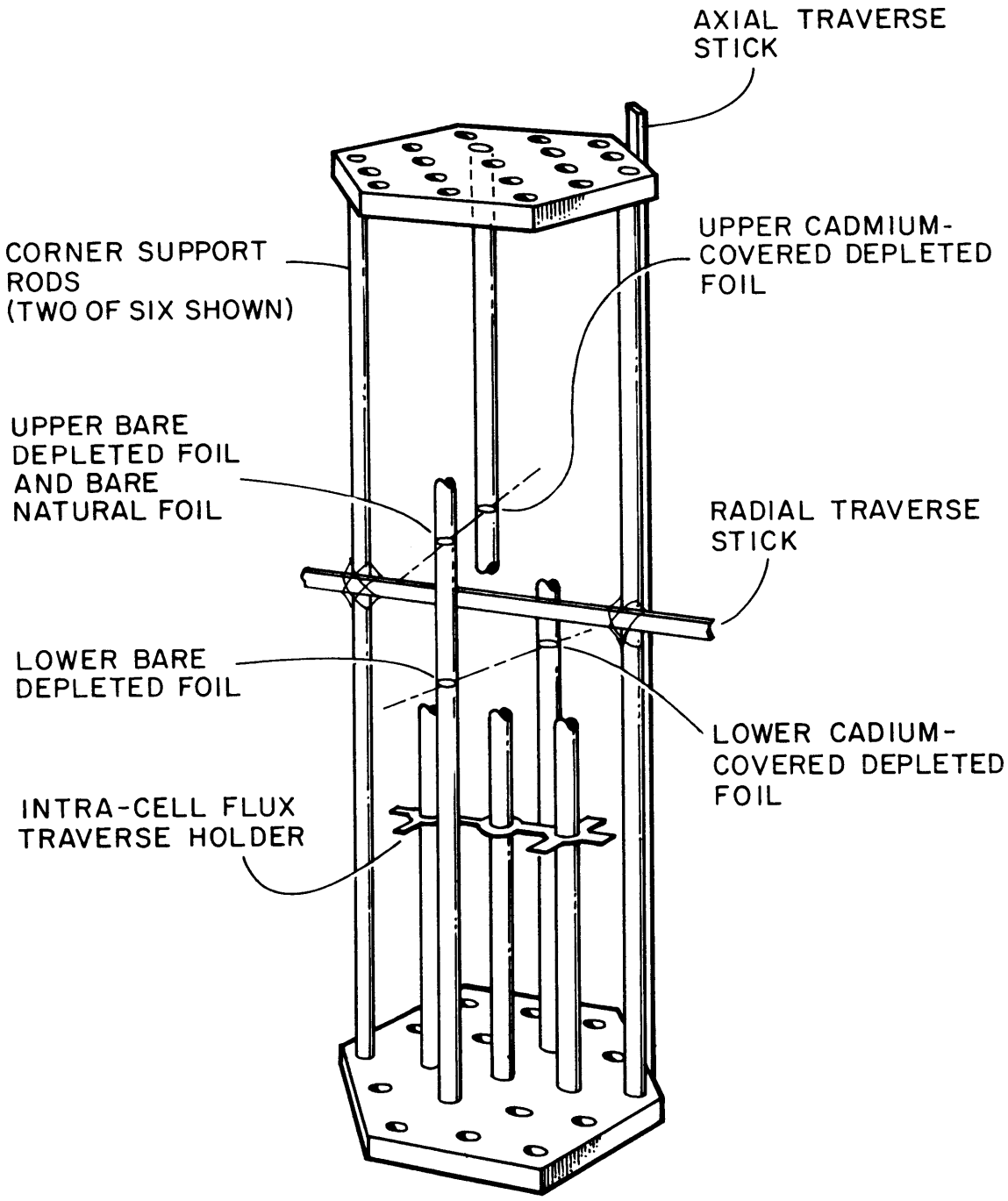

FIG. 3-3 REMOVABLE CENTER ARRAY SHOWING RELATIVE FOIL POSITIONS

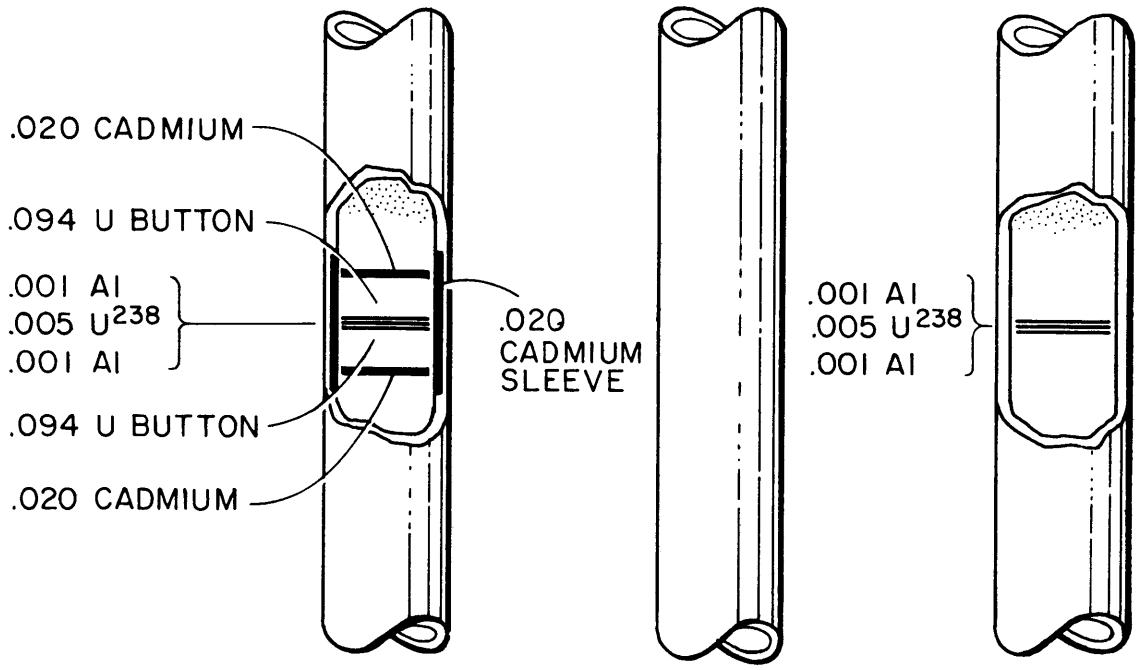

FIG. 3-4 U^{238} CADMIUM RATIO FOIL ARRANGEMENT

Two ratio measurements were made at different heights in all but one of the lattices, in order to test the theory developed in section 2. 5 and to improve the accuracy of the measurements. The relative positions at which these measurements were made, together with the positions for the other measurements, are given with the data. Figure 3-3 shows the relative positions of all the various foils in the removable center array.

A time delay of several hours from the end of the irradiation was observed to allow build-up of Np^{239} from the 23-minute half life decay of U^{239}. Then the foils were counted alternately in a gamma spectrometer system of two identical channels. A block diagram of one channel is shown in Figure 3-6. Details of the system are given by Weitzberg (38). The spectrometers were set to straddle the 103 kev peak of Np^{239} with window widths of 30 kev. The foils were counted several times over a period of two or three days to verify that the observed radiation decayed with the proper half life and to improve the accuracy of the results. Details of the data reduction are given in Appendix D.

3. 3. 3 U^{238}/U^{235} Fission Ratio (δ_{28}) Measurement

The average U^{238}/U^{235} fission ratio, δ_{28}, was measured for 0. 250 inch diameter rods by means of the equipment and technique set up by J. Wolberg (41). A uranium foil depleted to eighteen parts per million of U^{235} and a natural uranium foil were irradiated at the same position in the lattice for each fission ratio measurement. Each foil was 0. 250 inch in diameter and 0. 005 inch thick. The foils were covered with thin aluminum catcher foils and placed back to back between two fuel slugs in a rod. Since the same depleted foil arrangement was used in the measurement of R_{28} and δ_{28}, the same bare depleted foil was used for both measurements; it was only necessary to determine the activity at different times in the two counting systems.

About 90 minutes after the end of the irradiation, the fission product gamma activities of the natural and depleted foils were counted alternately in a gamma ray counter, as shown in Figure 3-7. Details

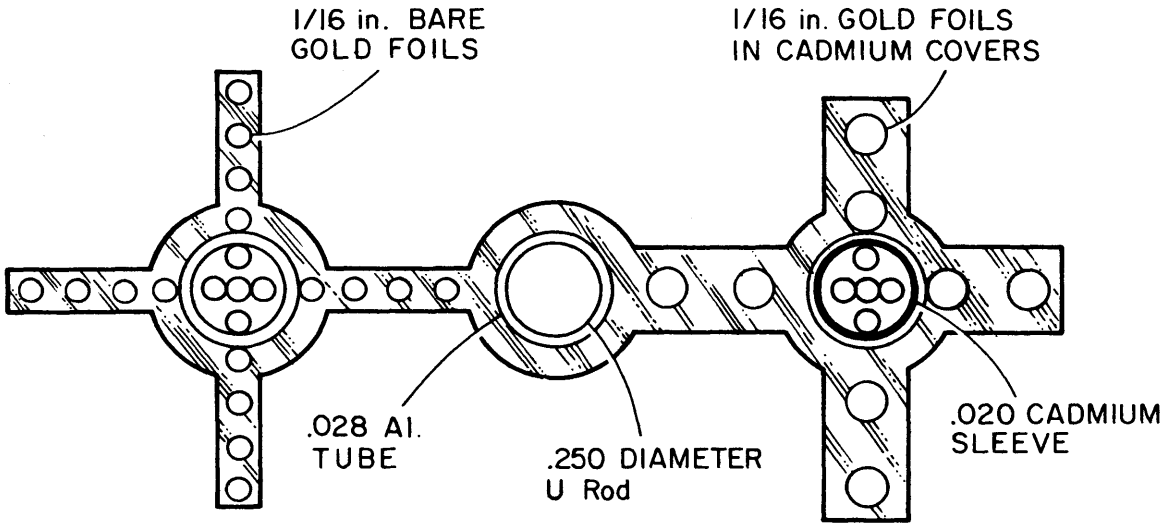

FOIL POSITIONS IN ALUMINUM HOLDER

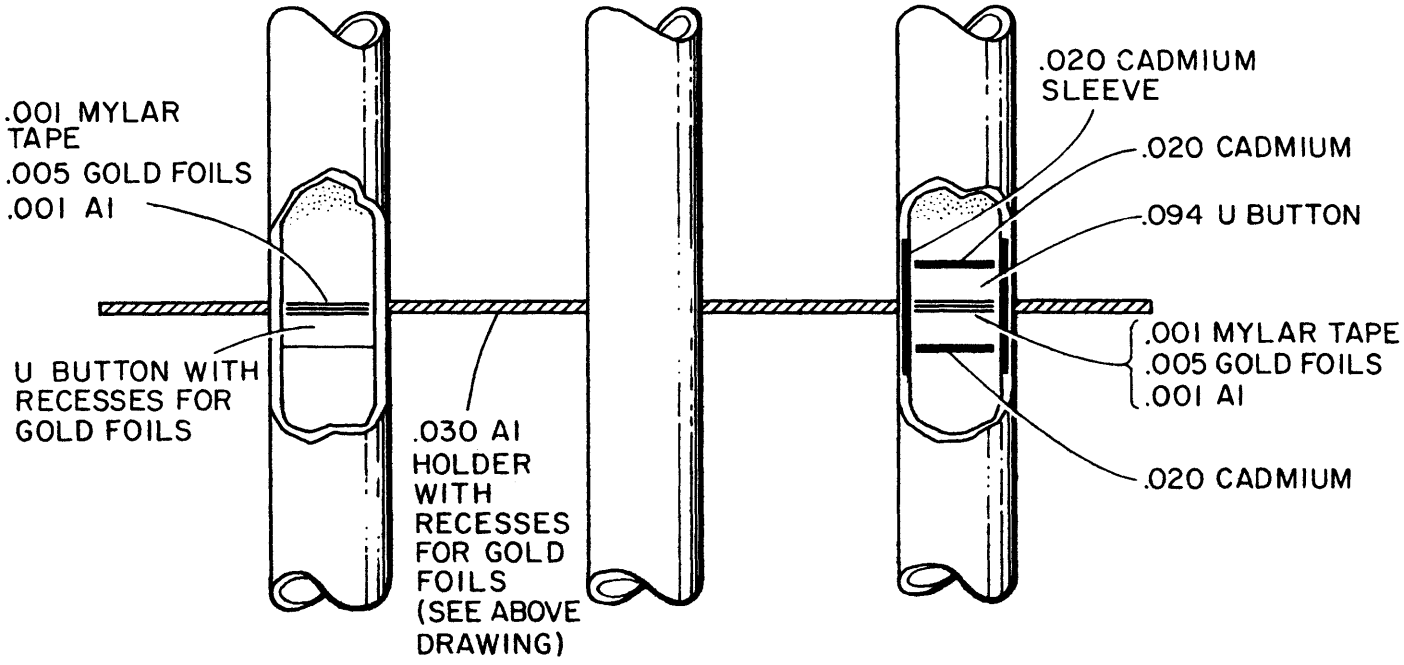

FIG. 3-5 INTRA-CELL FLUX TRAVERSE FOIL ARRANGEMENT

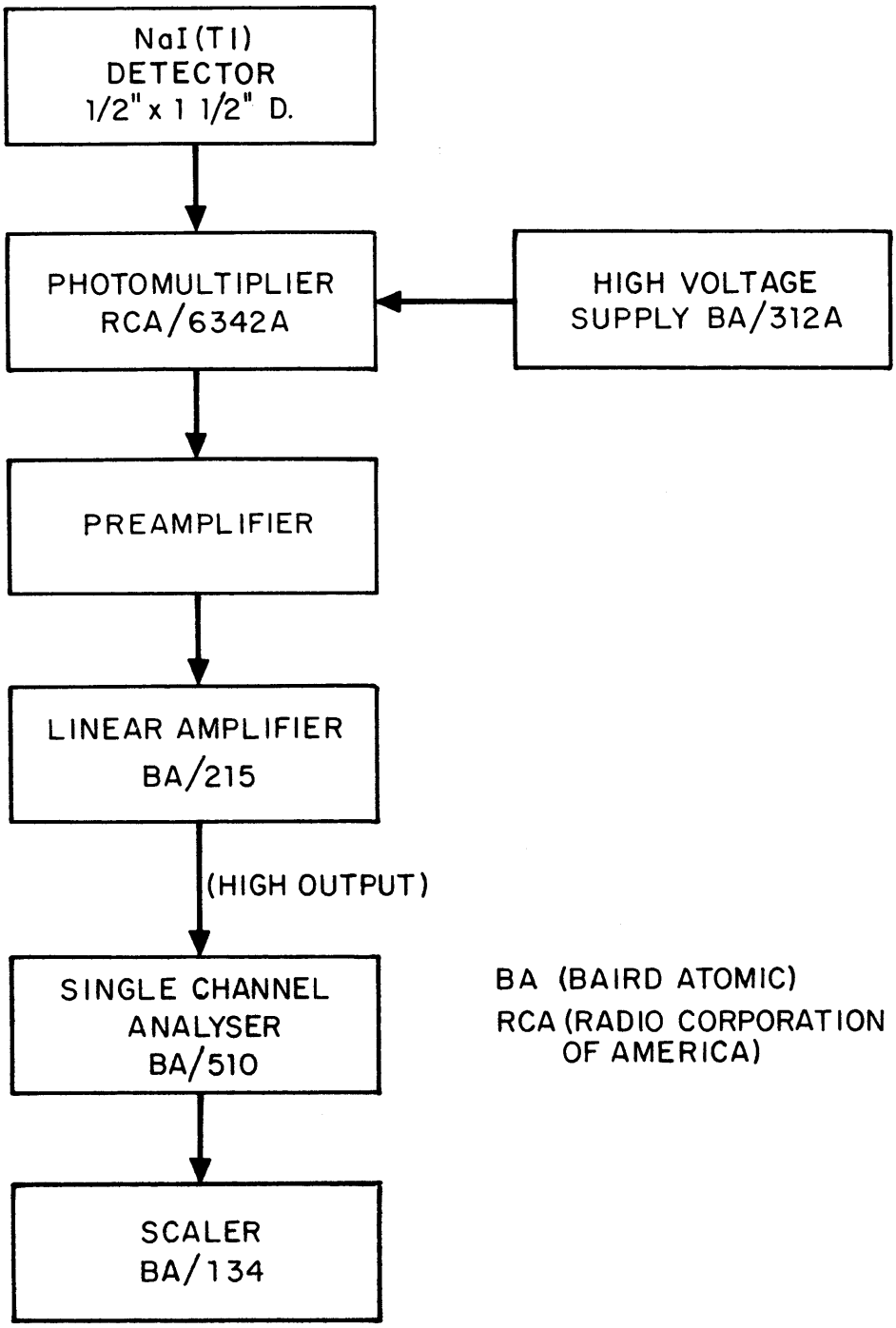

FIG. 3-6 BLOCK DIAGRAM OF U^{238} CADMIUM RATIO COUNTING EQUIPMENT

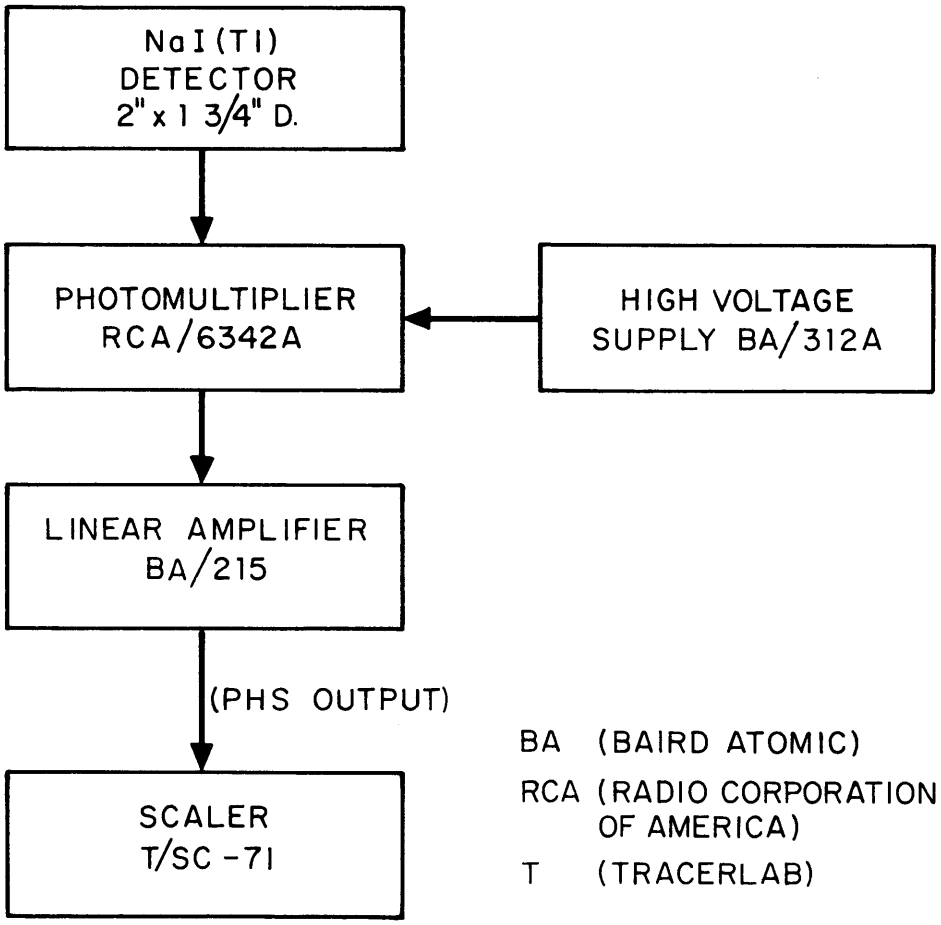

FIG. 3-7 BLOCK DIAGRAM OF U^{238}/U^{235} FISSION RATIO COUNTING EQUIPMENT

of the system are given by Wolberg (41). The bias of the amplifier was set to reject counts below 0.72 Mev. The activity of the two foils was followed for about 1-1/2 hours as it decayed. Details of the data reduction are given in Appendix D.

3.3.4 Intracell Flux Traverse Measurement

Thermal flux traverses were made across a unit cell in each of the lattices moderated with 90 per cent and 80 per cent D_2O. Gold foils, 1/16 inch in diameter and 0.005 inch thick were positioned in milled recesses on an aluminum holder 0.032 inch thick. Similar foils were covered with small cadmium boxes made of 0.020 inch thick cadmium and were positioned on the same holder at equivalent points in another cell of the lattice. The flux at points inside the rod was obtained by placing the gold foils in small recesses machined in a button of the fuel and capped with another button. The epicadmium activity in the rod was measured by using the same kind of button, but surrounded with a cadmium pill box like that used for the U^{238} cadmium ratio measurement. The traverses were made along the two basic directions of the hexagonal cell. Figure 3-5 shows the foil holder and the foil assembly in the rods.

The gamma activity of the gold foils was counted, at convenient times after the irradiation by using a gamma spectrometer system shown in Figure 3-8. The spectrometer was set to straddle the 412 kev γ-ray peak of gold with a 40 kev window. Details of the data reduction are given in Appendix D.

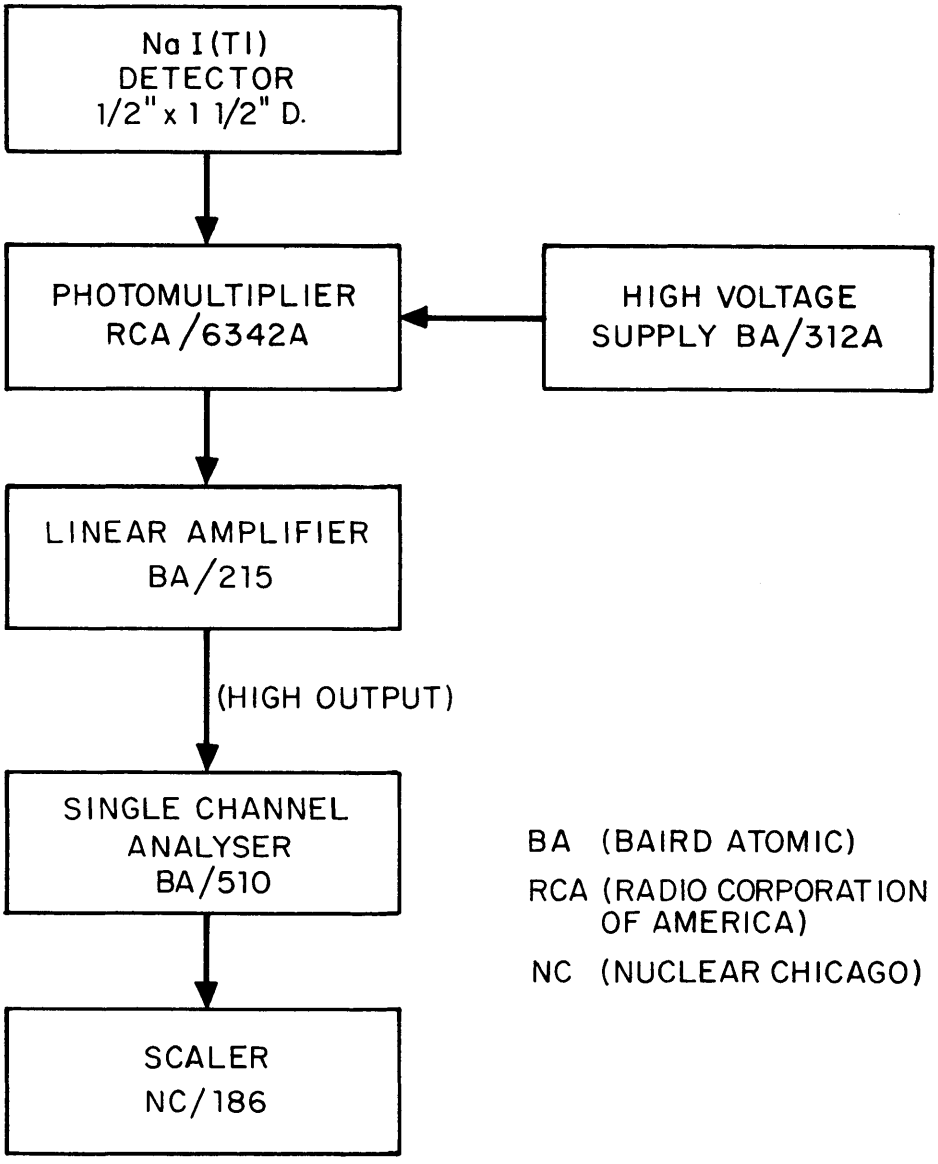

FIG. 3-8 BLOCK DIAGRAM OF INTRA-CELL FLUX TRAVERSE COUNTING EQUIPMENT

CHAPTER 4
RESULTS

4.1 AXIAL AND RADIAL TRAVERSES OF THE ASSEMBLY

To test the theory developed in section 2.2, axial and radial traverses were made in every lattice used. The axial traverses provide the most informative comparison of the theory with the experiment. The nine axial traverses are shown in Figures 4-1 through 4-9. The radial traverses were nearly identical and only one of the traverses is shown (Figure 4-10).

The solid curves on the nine axial traverses were calculated from equations (2.2-20), (2.2-45), and (2.2-47). The upper curve in each case represents the total thermal flux along the central axis corresponding to an incoming source neutron current of one neutron/cm^2 sec. The lower curve in each case represents the slowing down density at the gold resonance along the central axis, corresponding to the same incoming current. A plane source was used for the calculations. For convenience in plotting, each axial traverse was normalized by multiplying by the appropriate value of (D/L). This normalization does not affect the shape or spacing of the curves in any way; it merely makes the value of the total thermal flux equal to 1.0 at the extrapolated boundary of the source end of the lattice. The scale on the right side of each graph pertains to the slowing down density curve and is smaller by a factor of 10 than the scale on the left side which pertains to the total thermal flux. The right scale also has dimensions of cm^{-1} owing to the normalization of the slowing down density to the source current. Thermal input parameters for the calculations were obtained from the Thermos 709 code. All of the input parameters for the calculations are listed in Table 4-1. The use of the Thermos code itself, and the input data

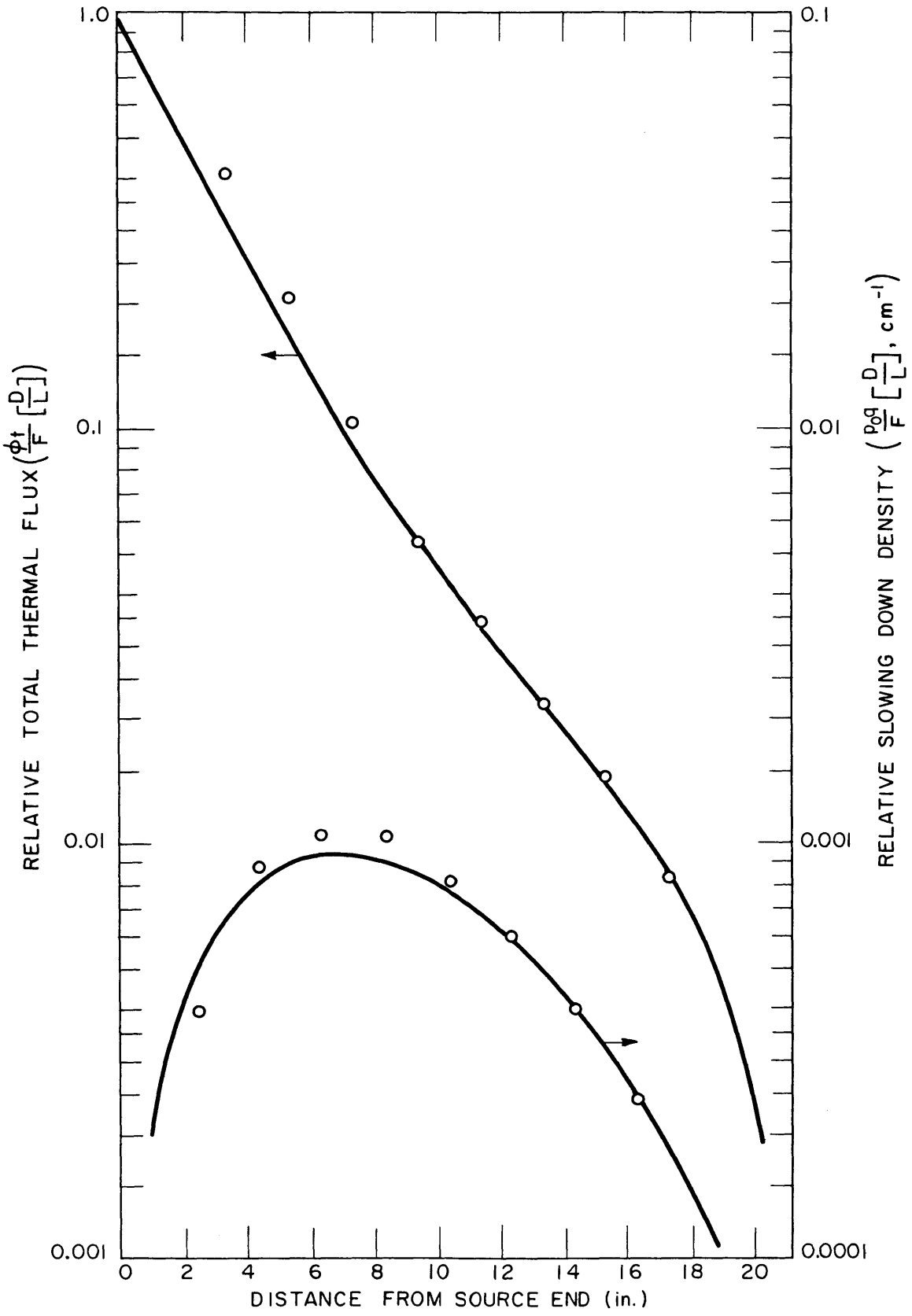

FIG. 4-1 AXIAL FLUX TRAVERSE (99.8% D_2O, 0.880 in. SPACING)

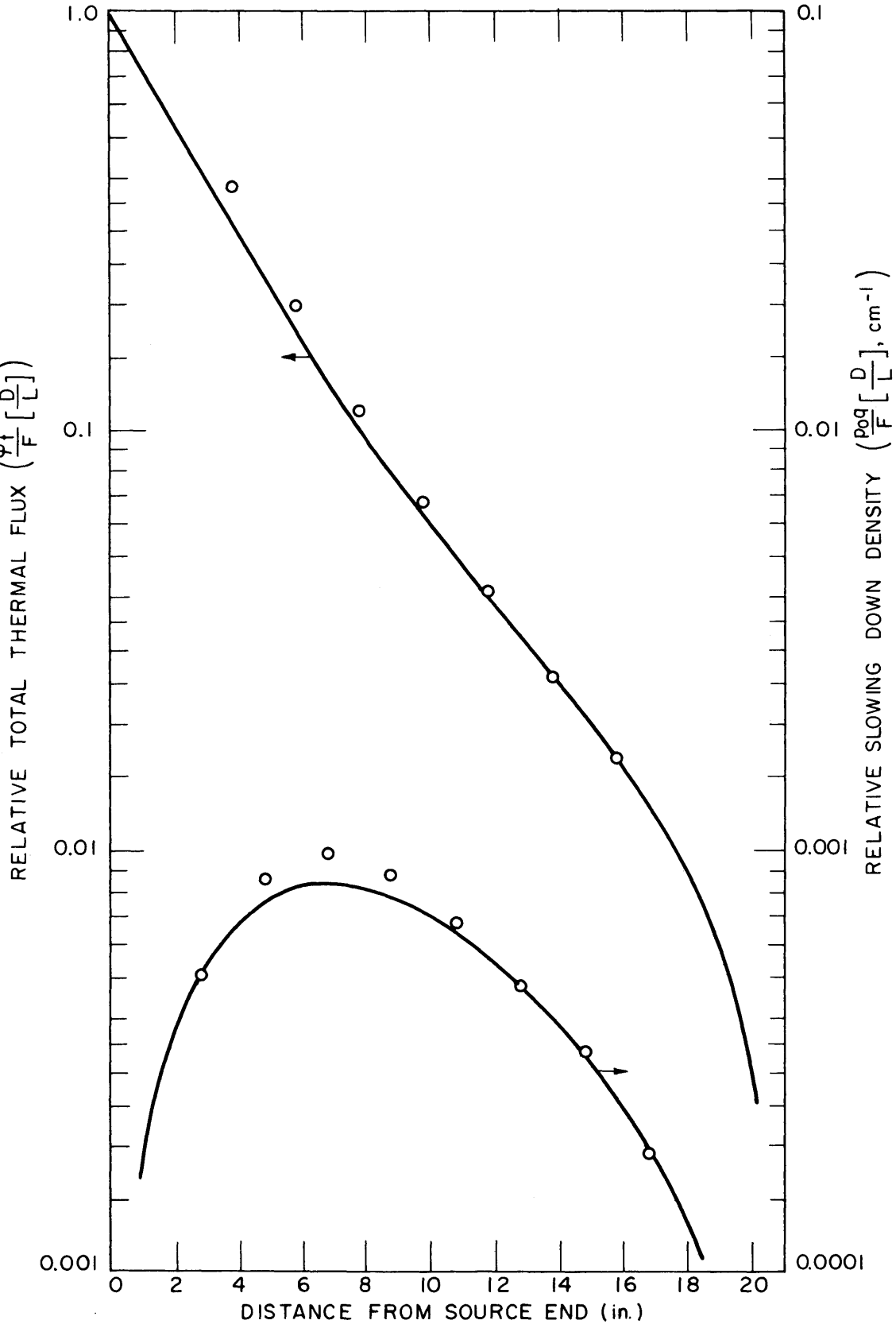

FIG. 4-2 AXIAL FLUX TRAVERSE (99.8% D_2O, 1.128 in. SPACING)

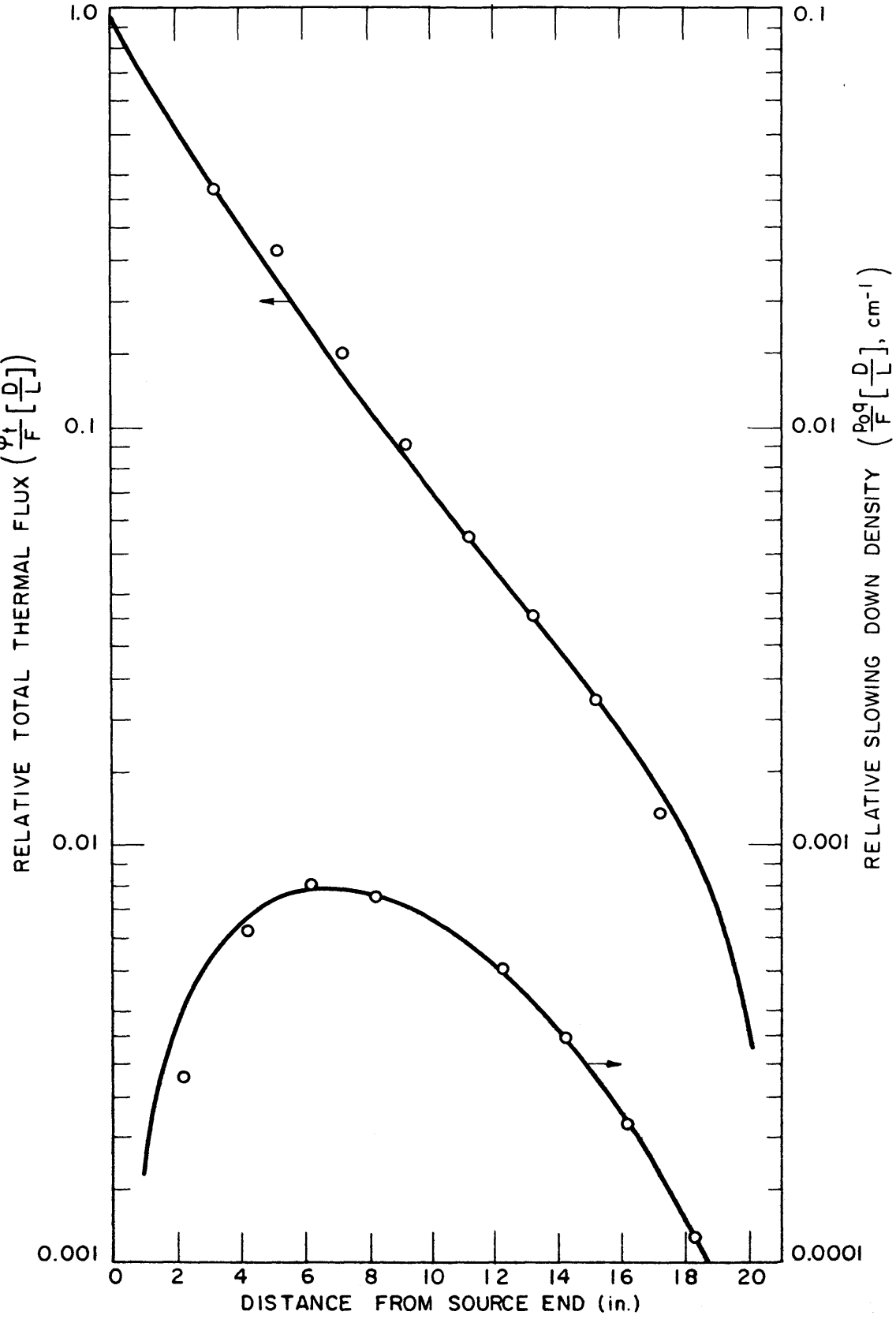

FIG. 4-3 AXIAL FLUX TRAVERSE (99.8% D_2O, 1.340 in. SPACING)

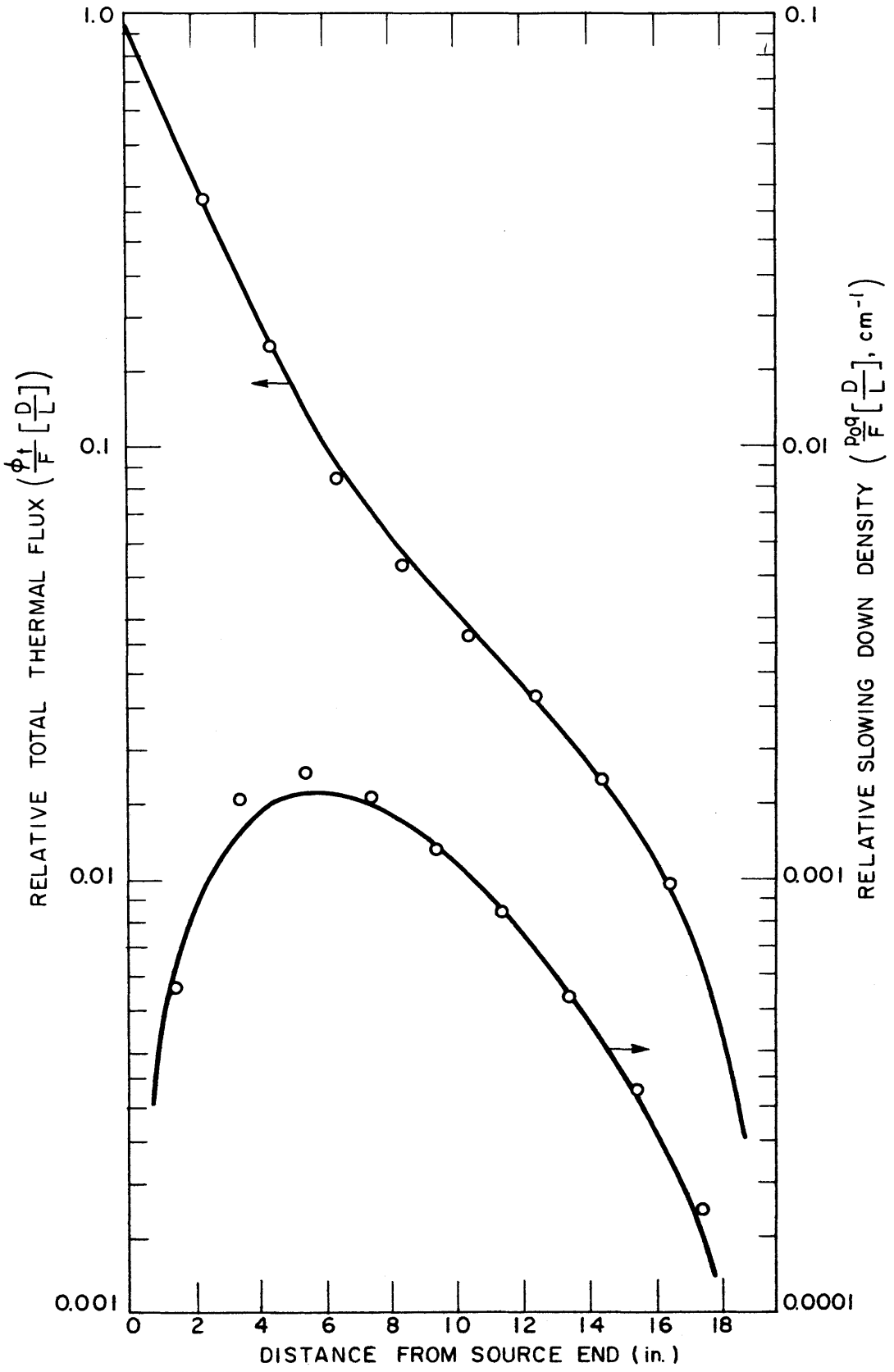

FIG. 4-4 AXIAL FLUX TRAVERSE (90.3% D_2O, 0.880 in. SPACING)

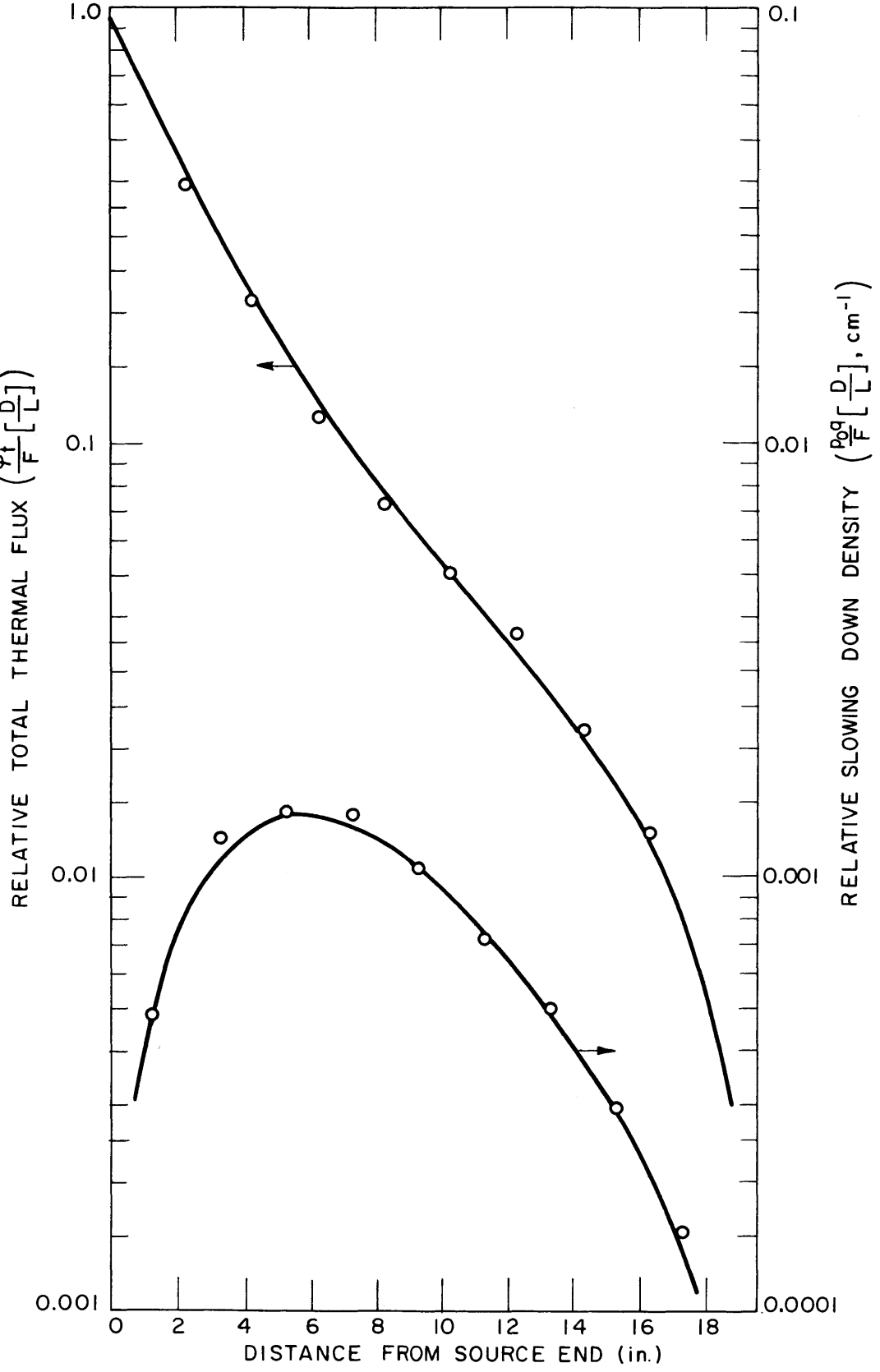

FIG. 4-5 AXIAL FLUX TRAVERSE (90.3% D_2O, 1.128 in. SPACING)

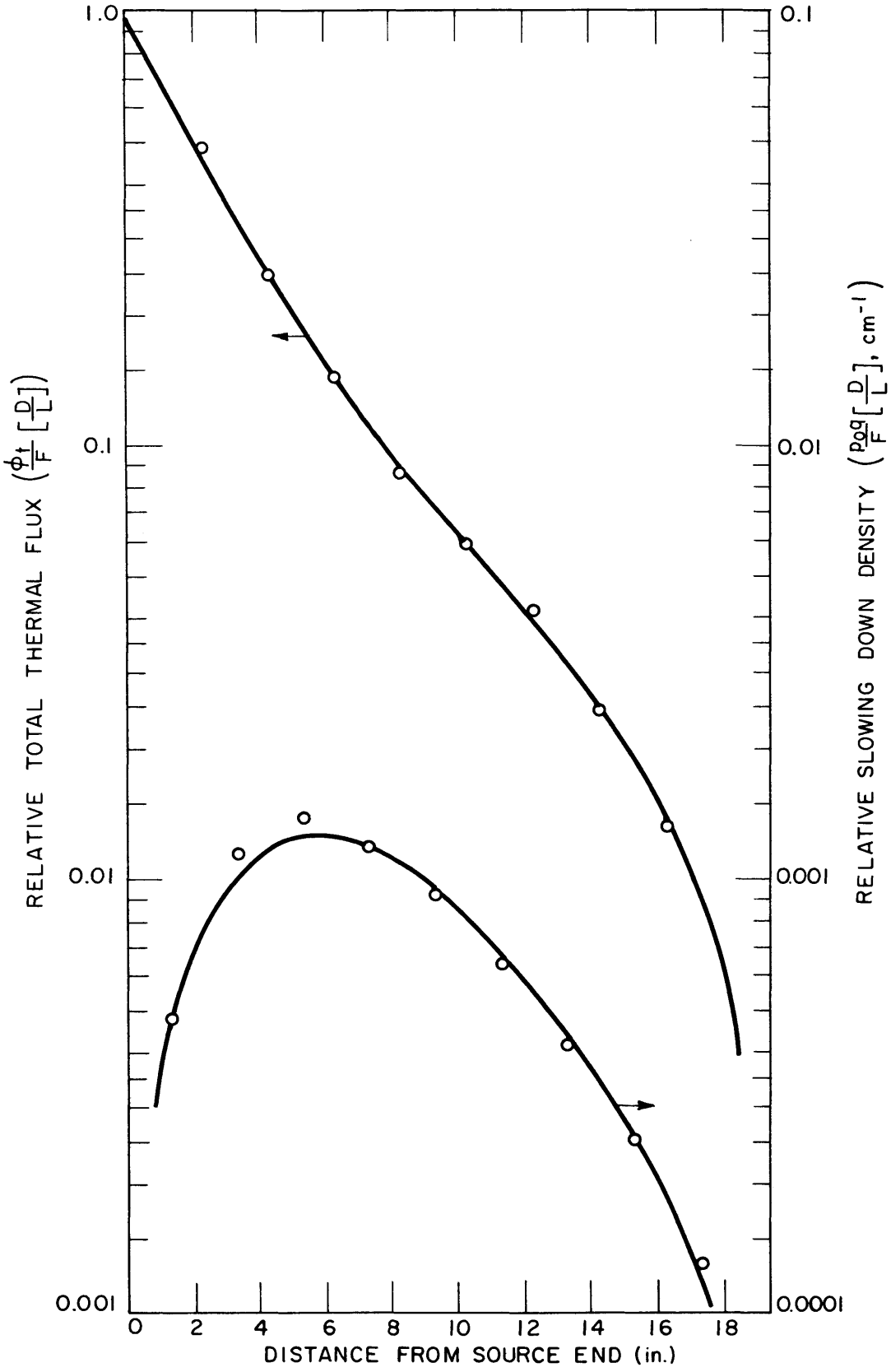

FIG. 4-6 AXIAL FLUX TRAVERSE (90.3% D_2O, 1.340 in. SPACING)

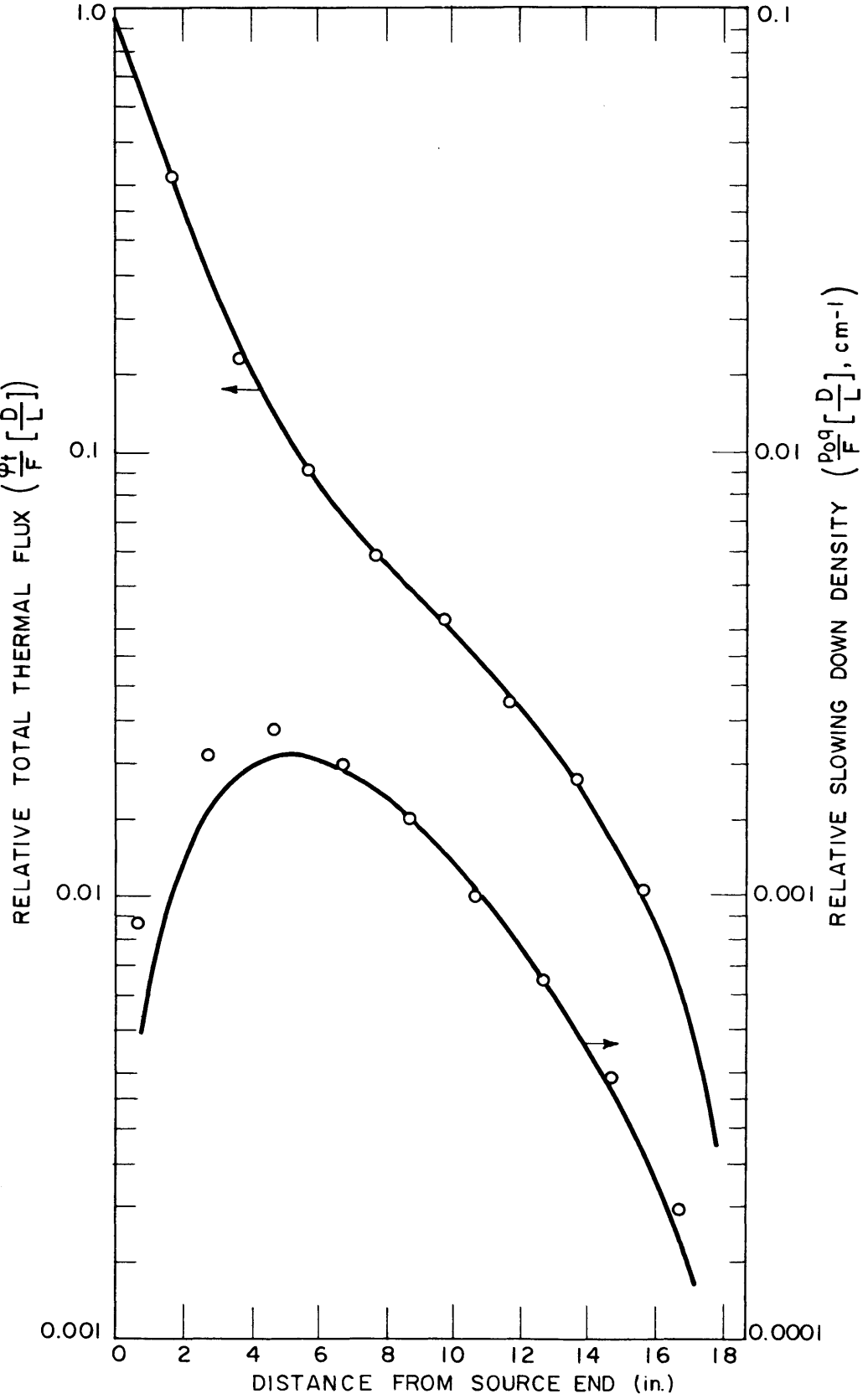

FIG. 4-7 AXIAL FLUX TRAVERSE (80.2% D_2O, 0.880 in. SPACING)

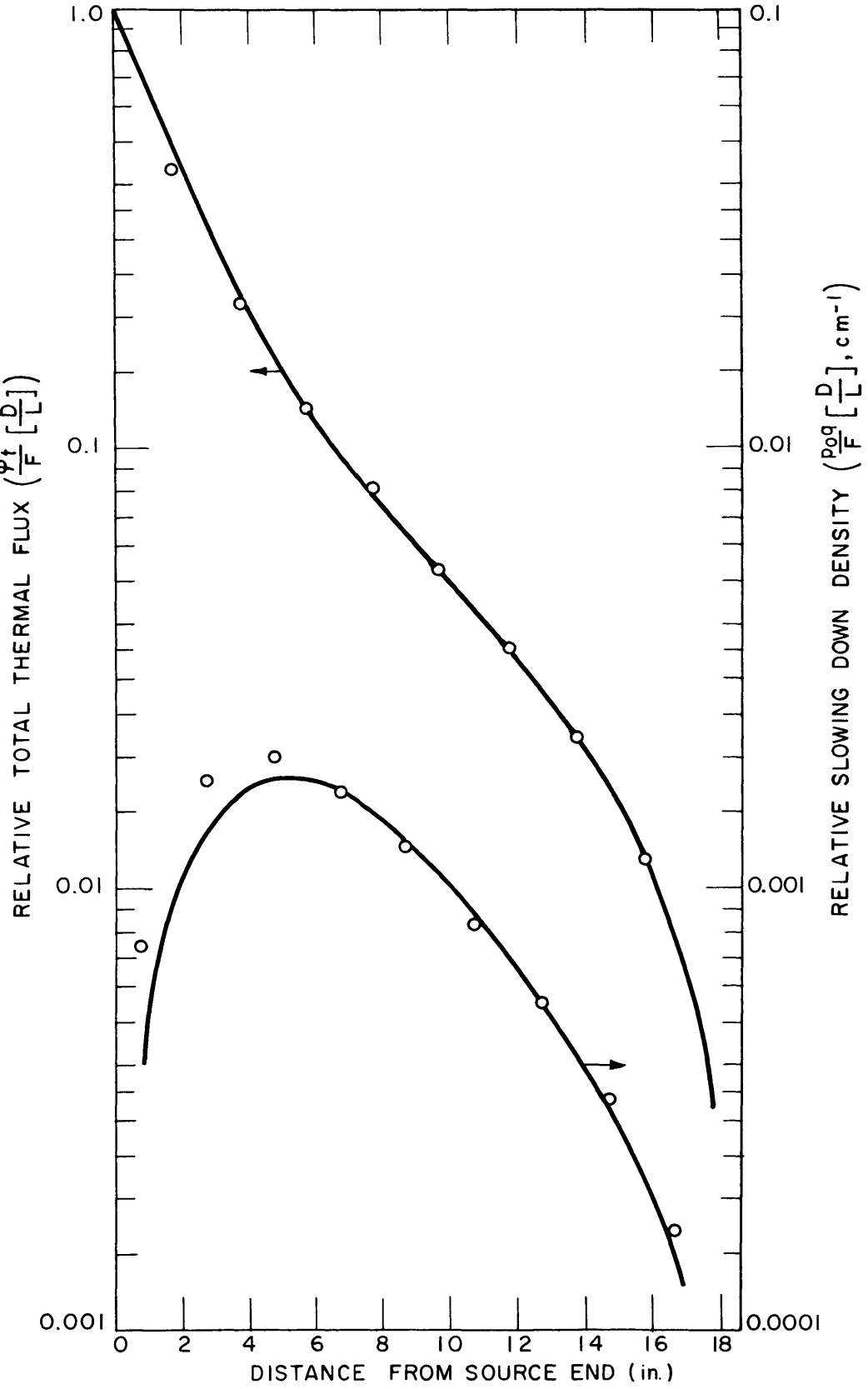

FIG. 4-8 AXIAL FLUX TRAVERSE (80.2% D_2O, 1.128 in. SPACING)

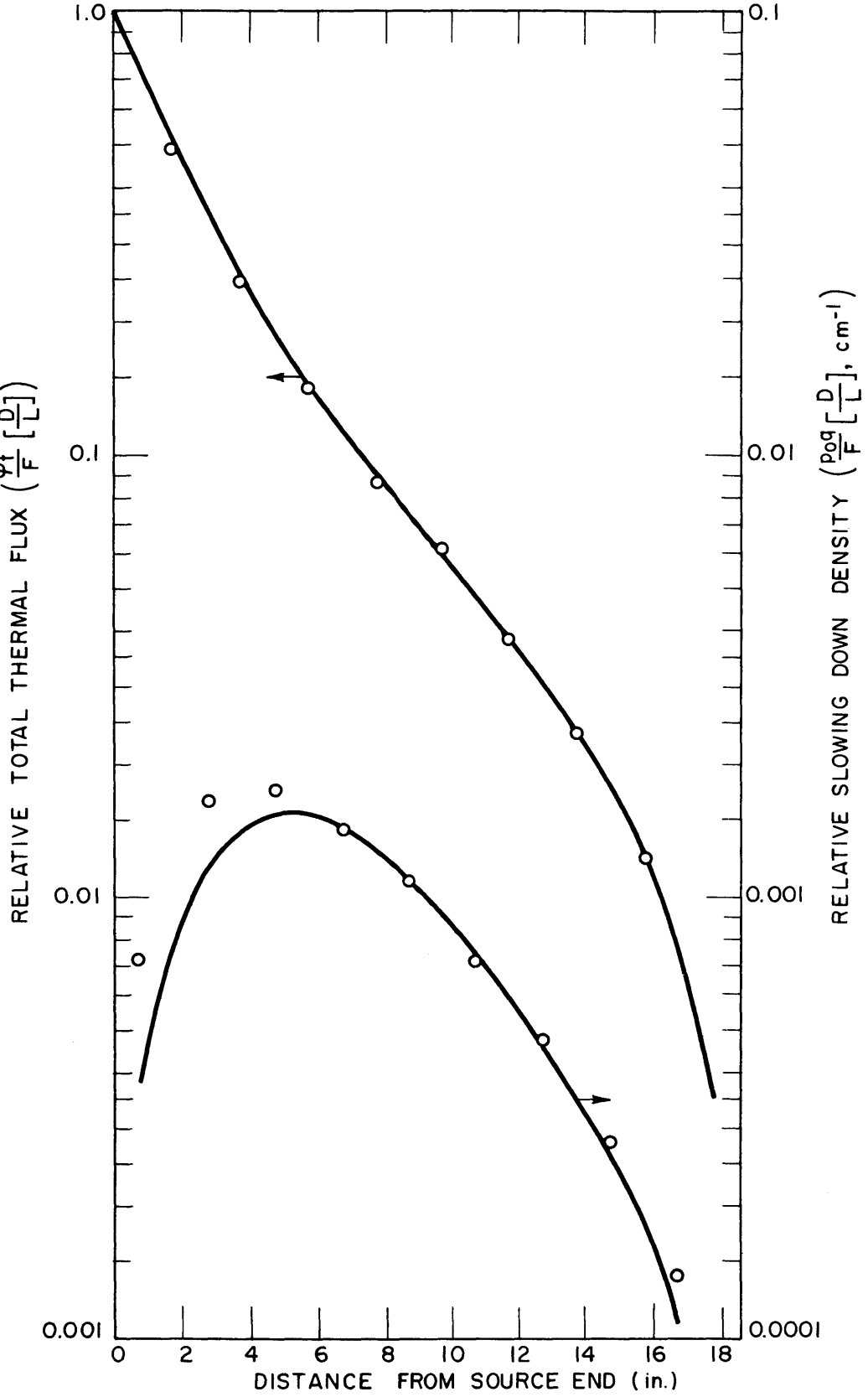

FIG. 4-9 AXIAL FLUX TRAVERSE (80.2% D_2O, 1.340 in. SPACING)

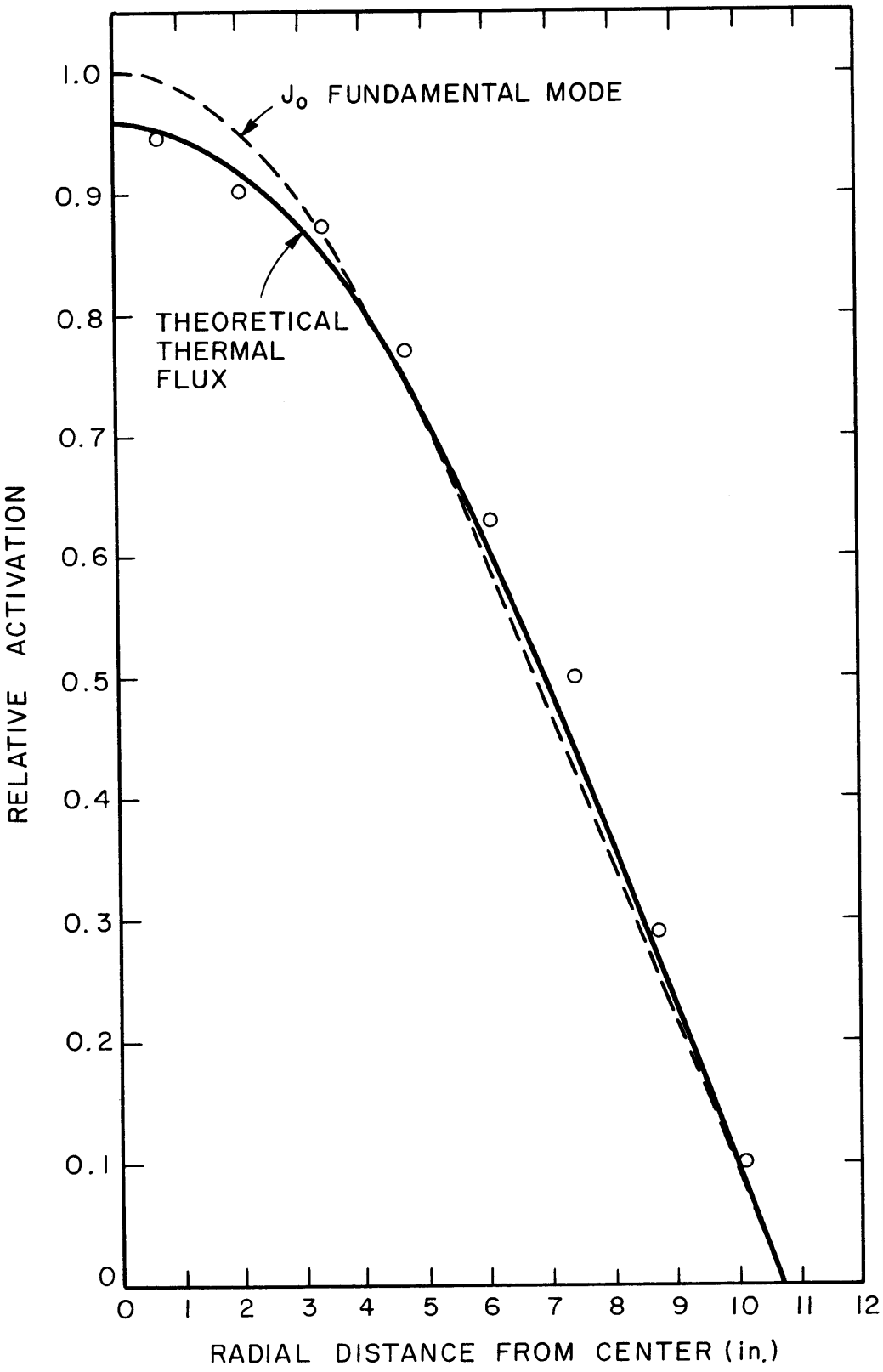

FIG. 4-10 RADIAL FLUX TRAVERSE
(80.2% D_2O, 1.340 in. SPACING)

Table 4-1

Input Parameters for the Exponential Code

D_2O Conc.	Rod Spacing	Volume Mod. / Volume Fuel	Extrap. Radius (cm)	Extrap. Height (cm)	Age to Thermal (cm^2)	Age to 4.9 ev (cm^2)
99.8%	0.880	12.0	29.2	53.7	151.	117.
99.8%	1.128	20.8	29.1	53.5	143.	110.6
99.8%	1.340	30.0	29.1	53.4	139.	107.7
90.3%	0.880	12.0	28.2	49.0	100.8	80.4
90.3%	1.128	20.8	28.1	48.6	95.2	75.9
90.3%	1.340	30.0	28.1	48.4	92.7	73.9
80.2%	0.880	12.0	27.6	45.4	75.7	61.7
80.2%	1.128	20.8	27.6	45.2	71.5	58.3
80.2%	1.340	30.0	27.5	45.2	69.6	56.8

Input parameters dependent upon or inferred from Thermos calculations

D_2O Conc.	Rod Spacing	k_∞	$\overline{D}$ (cm)	$\overline{\Sigma}_a$ (cm^{-1})	L^2 (cm^2)
99.8%	0.880	1.121	1.093	0.01815	60.2
99.8%	1.128	1.177	1.078	0.01255	85.9
99.8%	1.340	1.281	1.070	0.00953	112.2
90.3%	0.880	1.145	0.765	0.02251	34.0
90.3%	1.128	1.160	0.743	0.01550	47.9
90.3%	1.340	1.182	0.731	0.01196	61.1
80.2%	0.880	1.147	0.571	0.02556	22.3
80.2%	1.128	1.121	0.552	0.01779	31.0
80.2%	1.340	1.079	0.542	0.01395	38.9

used to obtain the parameters, are explained in Appendix C.

To obtain satisfactory quantitative agreement between the theoretical and the experimental traverses, it was necessary to use as parameters the extrapolation distance, d_a, at the axial boundary and the value of ERI/σ_o of the gold foils. The values used, as well as the calculated values of $\xi\Sigma_s$ and $\bar{\Sigma}_a$, are listed in Table 4-2, and the results are discussed in section 5. 1.

The radial thermal neutron density distribution shown in Figure 4-10 is for the 80. 2% D_2O-1. 340 inch lattice. The theoretical curve was calculated by using equations (2. 2-20) and (2. 2-45). The scale is normalized to a value of 1. 0 at the central axis for the fundamental J_o mode.

The experimental points shown on Figures 4-1 through 4-10 were obtained from the activation of gold foils as explained in section 3. 3. 1. The routine data reduction was made by using equations (2. 4-10) and (2. 4-11).

4. 2 U^{238} CADMIUM RATIO MEASUREMENTS

The average U^{238} cadmium ratio of the rods was measured in each of the nine lattices. The calculation of the correction factors for ρ_{28} was made using equation (2. 5-7) and values of $p_o q/\phi_t \bar{\Sigma}_a$ computed by the exponential code. The experimental results, the calculated correction factors, and the resulting critical assembly values of ρ_{28} found are given in Table 4-3. A graph and discussion of the results are given in section 5. 2.

4. 3 U^{238}/U^{235} FISSION RATIO MEASUREMENTS

The average U^{238}/U^{235} fission ratio in the rods was measured for each of the nine lattices. The calculation of the corrections to obtain the infinite lattice values was made by using equation (2. 6-7). The experimental results, the calculated infinite lattice correction factors, and the resulting infinite lattice values are given in Table 4-4. A graph and a discussion of the results are given in section 5. 3.

Table 4-2

Data Used in Comparing Experimental to Theoretical Flux Traverses

D_2O Conc.	Rod Spacing	d_a (cm)	$\bar{\lambda}_t$ (cm)	$d_a/\bar{\lambda}_t$	ERI/σ_o ±3%	$\xi\Sigma_s$ (cm^{-1})	$\bar{\Sigma}_a$ (cm^{-1})
99.8%	0.880	6.55	3.28	2.0	6.07	0.1617	0.01815
99.8%	1.128	6.45	3.23	2.0	5.82	0.1703	0.01255
99.8%	1.340	6.4	3.21	2.0	5.10	0.1741	0.00953
90.3%	0.880	4.2	2.30	1.8	5.00	0.260	0.02251
90.3%	1.128	4.0	2.23	1.8	4.89	0.274	0.01550
90.3%	1.340	3.9	2.19	1.8	4.60	0.280	0.01196
80.2%	0.880	2.4	1.71	1.4	4.86	0.364	0.02556
80.2%	1.128	2.3	1.66	1.4	4.71	0.384	0.01779
80.2%	1.340	2.3	1.63	1.4	4.22	0.392	0.01395

Table 4-3

Measurements of the Ratio of Epicadmium to Subcadmium Capture in U^{238} (ρ_{28})

D_2O Conc.	Rod Spacing	Distance from End (in.)	ϕ_e/ϕ_s	ρ_{28} Measured	Corr. Factor	ρ_{28} Critical	ρ_{28} Best Value
99.8%	0.880	5.73	0.42	1.36 ±.03	1.178	1.60 ±.03	1.58 ±.03
99.8%	0.880	9.68	1.50	1.90 ±.10	0.817	1.55 ±.08	
99.8%	1.128	11.28	1.49	1.45 ±.04	0.860	1.25 ±.03	1.25 ±.03
99.8%	1.340	5.64	0.29	0.598±.010	1.341	0.802±.013	0.796±.012
99.8%	1.340	11.31	1.19	0.883±.023	0.895	0.790±.021	
90.3%	0.880	5.71	1.04	1.242±.012	0.971	1.206±.012	1.219±.013
90.3%	0.880	7.66	2.37	1.462±.026	0.843	1.233±.022	
90.3%	1.128	5.61	0.73	0.647±.007	1.082	0.700±.007	0.708±.008
90.3%	1.128	9.58	2.80	0.809±.012	0.885	0.716±.011	
90.3%	1.340	5.67	0.60	0.506±.011	1.132	0.573±.012	0.582±.011
90.3%	1.340	9.61	2.05	0.653±.020	0.907	0.592±.019	
80.2%	0.880	5.72	1.88	0.960±.009	0.919	0.882±.008	0.941±.006
80.2%	0.880	9.68	12.1	1.030±.006	0.914	0.941±.006	
80.2%	1.128	5.61	1.23	0.588±.012	0.995	0.585±.012	0.633±.005
80.2%	1.128	9.57	5.73	0.688±.005	0.920	0.633±.005	
80.2%	1.340	5.70	0.95	0.397±.001	1.042	0.414±.001	0.414±.002
80.2%	1.340	9.60	3.88	0.446±.003	0.925	0.413±.003	

Table 4-4

Measurements of the U^{238}/U^{235} Fission Ratio (δ_{28})

D_2O Conc.	Rod Spacing	δ_{28} Measured	Interaction Effect (Exponential)	Interaction Corr. Factor ± 2%	Interaction Effect (Infinite)	δ_{28} (Infinite)
99.8%	0.880	0.0424 ± .0013	0.0298	0.895	0.0266	0.0392 ± .0013
90.3%	0.880	0.0414 ± .0012	0.0288	0.972	0.0280	0.0406 ± .0012
80.2%	0.880	0.0386 ± .0012	0.0260	0.972	0.0253	0.0379 ± .0012
99.8%	1.128	0.0303 ± .0030	0.0177	0.943	0.0167	0.0293 ± .0030
90.3%	1.128	0.0267 ± .0008	0.0141	0.970	0.0137	0.0263 ± .0008
80.2%	1.128	0.0266 ± .0008	0.0140	0.970	0.0136	0.0262 ± .0008
99.8%	1.340	0.0225 ± .0007	0.0099	0.930	0.0092	0.0218 ± .0007
90.3%	1.340	0.0219 ± .0007	0.0093	0.930	0.0087	0.0213 ± .0007
80.2%	1.340	0.0230 ± .0007	0.0104	0.930	0.0097	0.0223 ± .0007
Single rod (41)						0.0126 ± .0003

Average of the three measurements at each spacing

Spacing (in.)	δ_{28} (Infinite)
0.880	0.0392 ± .0008
1.128	0.0263 ± .0006
1.340	0.0218 ± .0003

4.4 INTRACELL FLUX TRAVERSES

Thermal and epithermal gold flux traverses were made across a unit cell in six of the nine lattices. The results are shown compared with the Thermos theoretical flux traverse curves in Figures 4-11 through 4-16. The square points represent a traverse from the center to a point of the hexagonal cell, and the circular points represent a traverse from the center along a line normal to a flat of the cell. The activations are normalized to a value of 1.0 at the cell center.

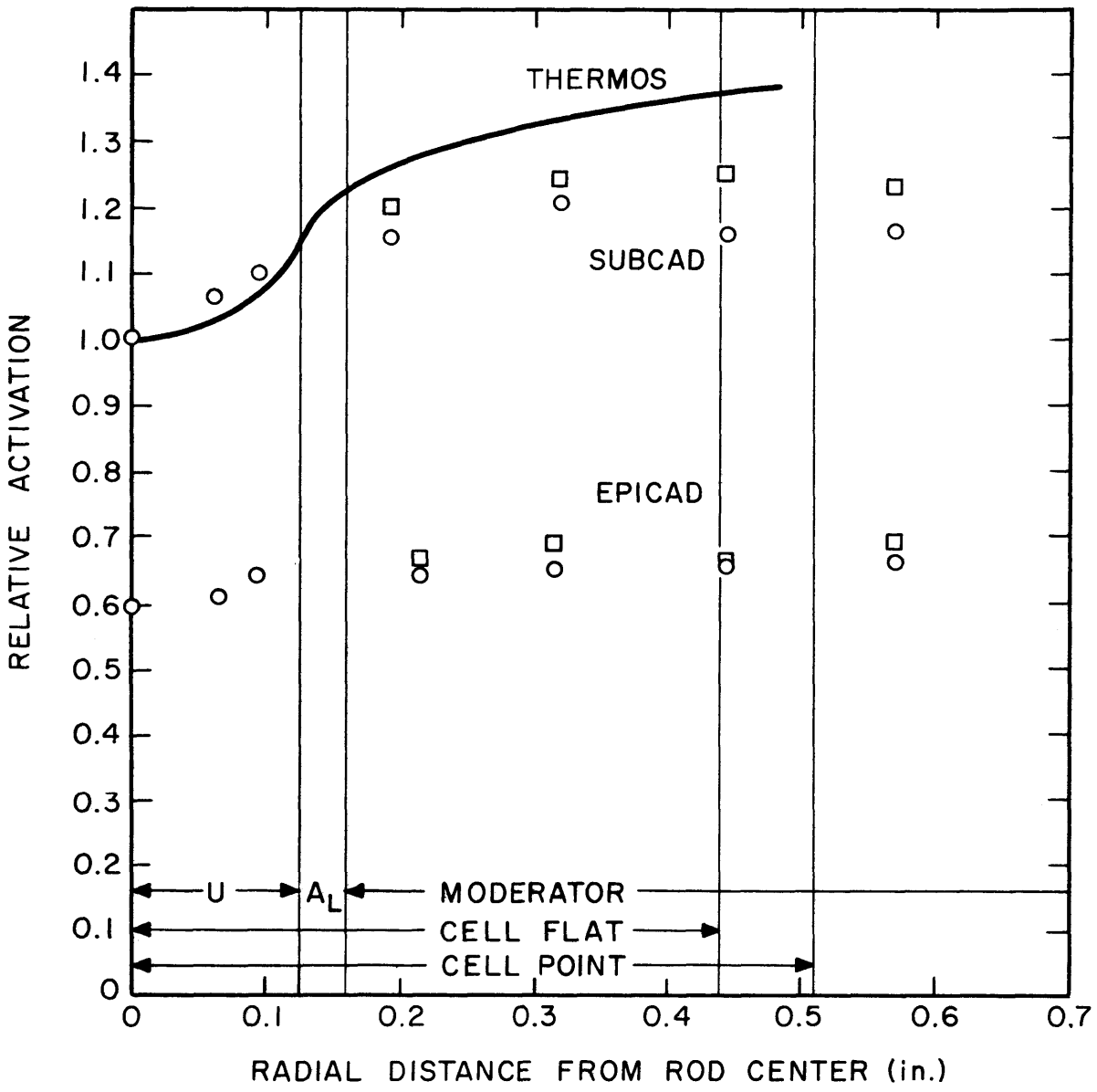

FIG. 4-11 INTRA-CELL GOLD FLUX TRAVERSE
(90.3% D_2O, 0.880 in. SPACING)

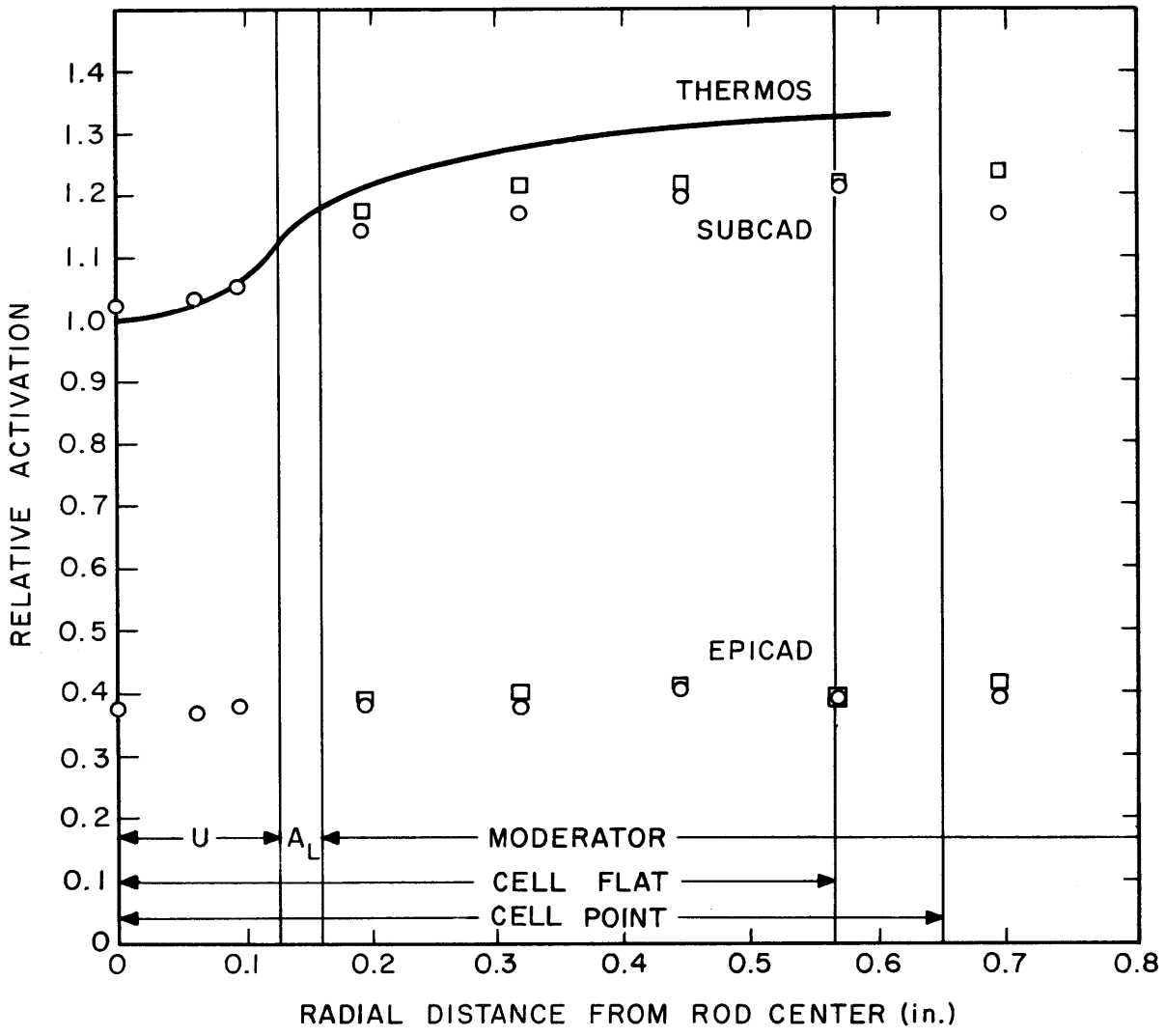

FIG. 4-12 INTRA-CELL GOLD FLUX TRAVERSE
(90.3% D_2O, 1.128 in. SPACING)

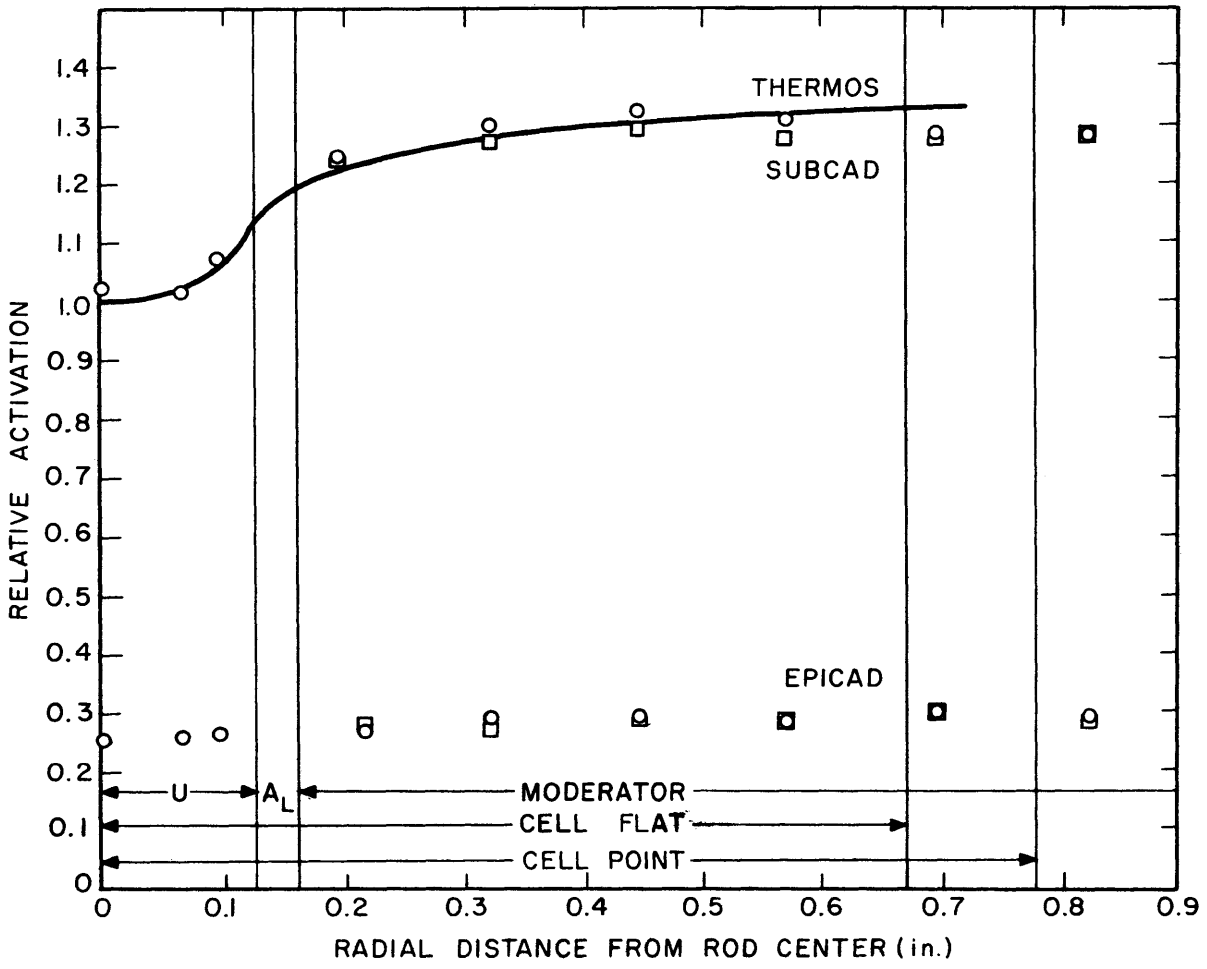

FIG. 4-13 INTRA-CELL GOLD FLUX TRAVERSE (90.3% D_2O, 1.340 in. SPACING)

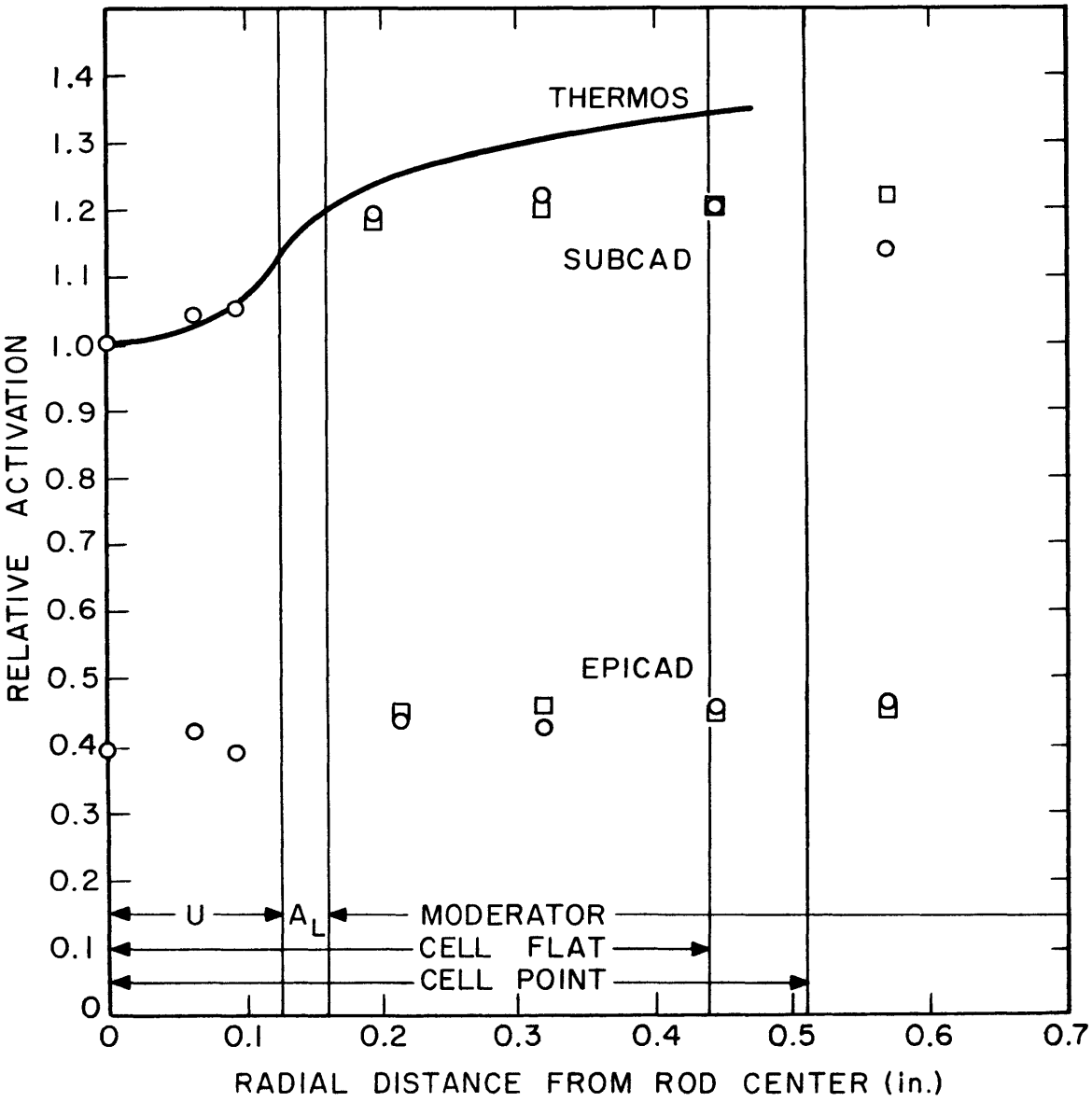

FIG. 4-14 INTRA-CELL GOLD FLUX TRAVERSE
(80.2% D_2O, 0.880 in. SPACING)

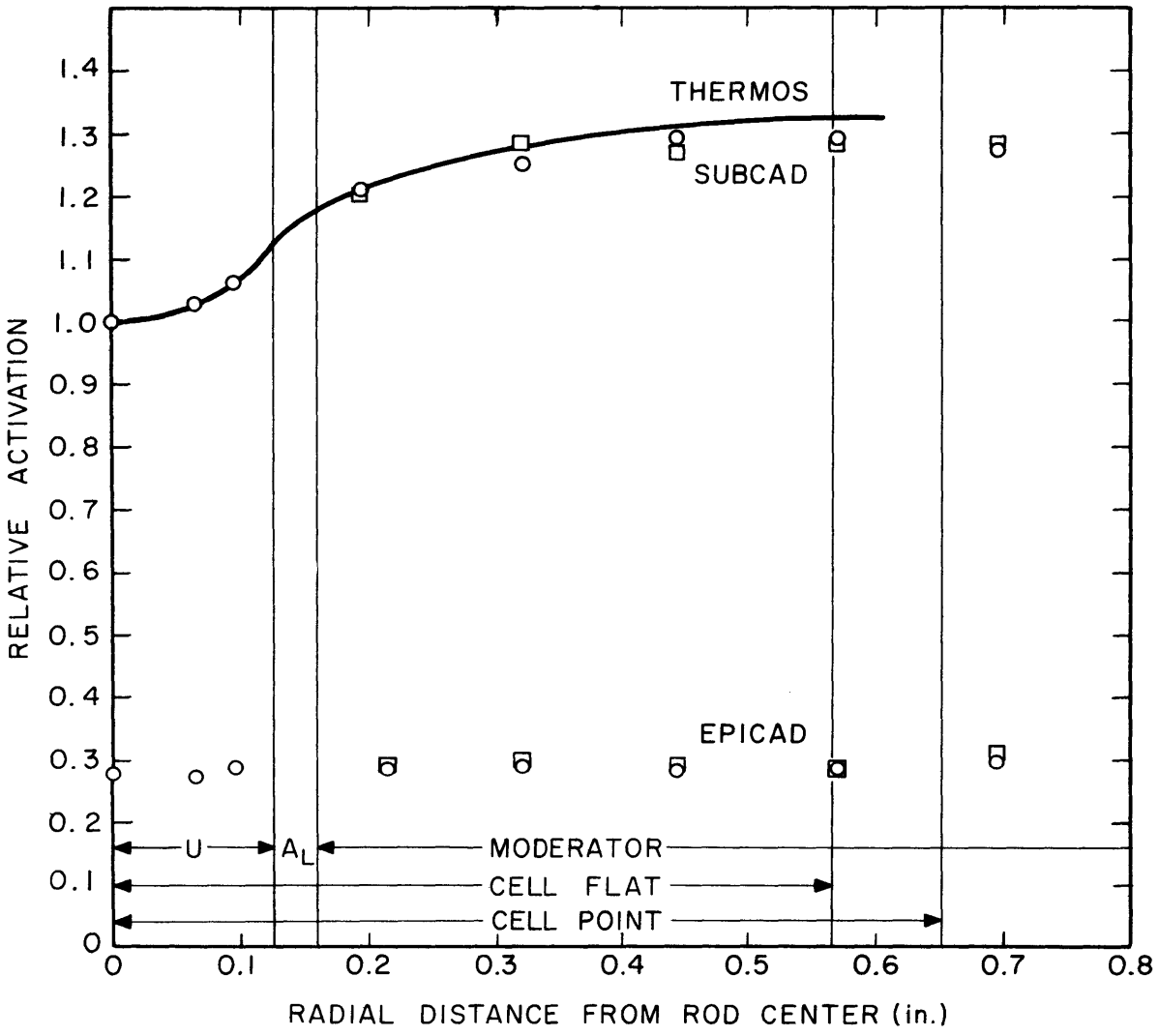

FIG. 4-15 INTRA-CELL GOLD FLUX TRAVERSE
(80.2% D_2O, 1.128 in. SPACING)

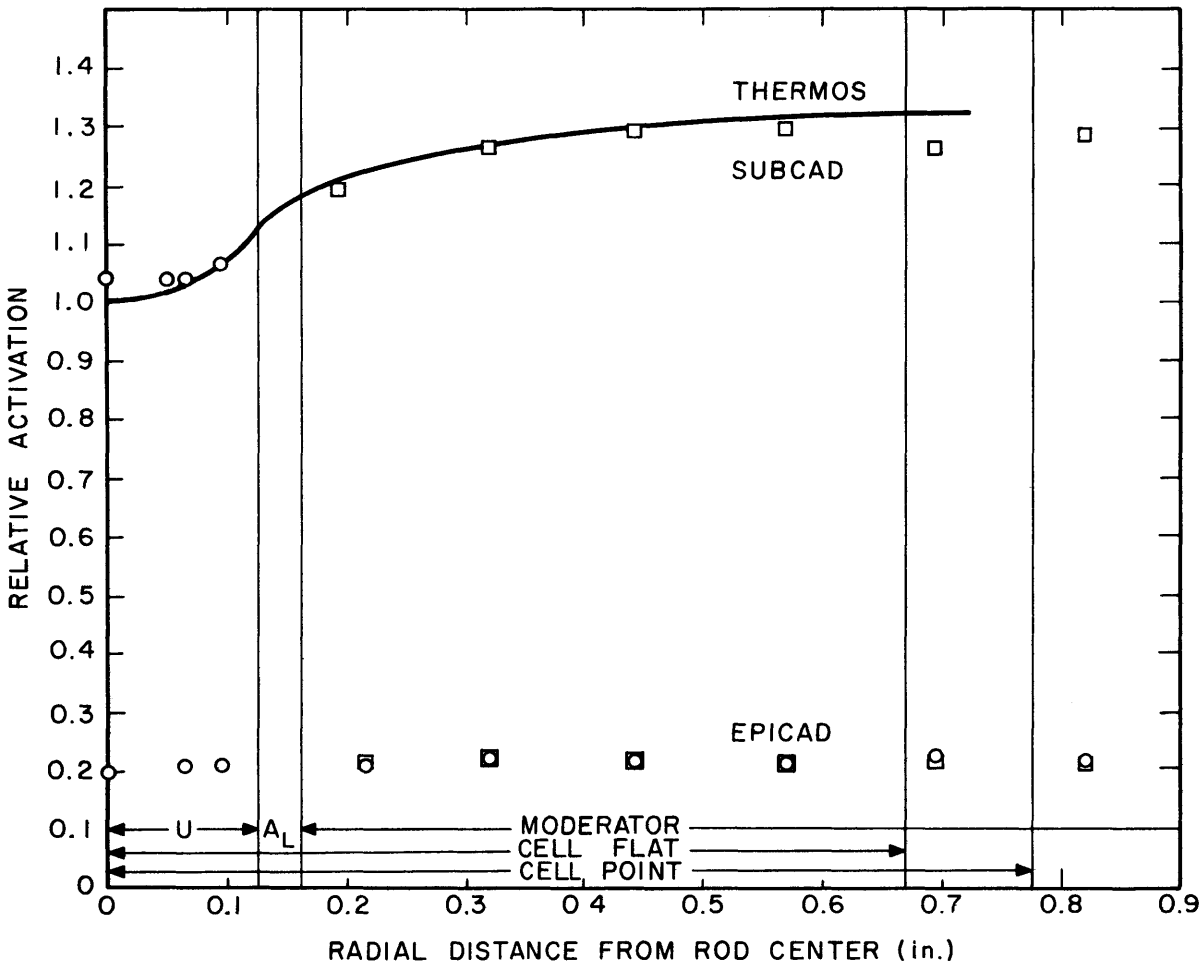

FIG. 4-16 INTRA-CELL GOLD FLUX TRAVERSE (80.2 % D O, 1.340 in. SPACING)

CHAPTER 5
DISCUSSION OF RESULTS

5.1 AXIAL AND RADIAL TRAVERSES OF THE ASSEMBLY

5.1.1 Theoretical Problems Introduced by the Size of a Small Assembly

The flux shapes in a small assembly are determined primarily by the leakage of the neutrons in both the thermal energy region and in the slowing down region. In a large assembly the multiplication also has an important influence on the flux shapes. Thus, the size of a small assembly must be carefully considered in a theoretical treatment.

It can be seen from section 2.9 that the size of an assembly may be completely specified by using the ratios, R/L, H/L, and τ_o/L^2. The first two ratios are simply the extrapolated dimensions in terms of the thermal diffusion length. The third ratio is a measure of the leakage during slowing down compared with the thermal leakage.

The extrapolated dimensions are found by adding an extrapolation distance to the physical dimensions of the assembly. This is a useful and justifiable mathematical device which allows the use of simpler mathematical treatments in describing neutron behaviour in a lattice. In a large assembly, defined as one which has a radius equal to perhaps four or more diffusion lengths, the use of an extrapolated boundary has been shown to give good results in many different investigations. In small assemblies, such as those considered in this report (where the radius was as small as 2.75 thermal diffusion lengths), the choice of an extrapolated boundary may reflect the following problems:

a. It is not entirely correct to use the same extrapolated boundary at the source end for the thermal flux due to the source and for the lattice born and moderated thermal flux. In principle, no extrapolation distance should be taken at this end for the source flux. Nevertheless, the same boundary was used for both the source flux and the lattice born thermal flux in the theoretical treatment in order to obtain a Fourier sine transform of the source flux which could be introduced into the lattice born thermal neutron flux equation.

b. The source flux for these experiments was a non-isotropic beam rather than an isotropic flux as was assumed in the theoretical treatment. This non-isotropy would persist for several mean free paths into the assembly, and the flux shape might reflect its presence.

c. The extrapolation distance may be different for slowing down neutrons and thermal neutrons. This problem is a common one in most treatments of the flux shape inside an assembly. In the theoretical treatment these extrapolated boundaries were taken to be the same in order to use the same Fourier transforms in the different equations.

d. The assembly was not surrounded by a vacuum as was assumed, but by shields consisting of alternate layers of paraffin and boron carbide plastic. These shields may return some of the neutrons and thus increase the apparent extrapolation distance.

e. The thermal diffusion length may be different for the energy spectrum of the source neutrons from that of the lattice born thermal neutron spectrum. Thus, the apparent size of the assembly may vary, depending upon the ratio of the source neutrons to the lattice born neutrons.

All of the above considerations are important since the small size of the assembly makes every part of the lattice relatively close to a boundary.

5. 1. 2 Theoretical Traverse Curves

The theoretical axial traverse curves, Figures 4-1 through 4-9, have several interesting features common to all of the nine lattices. The first feature is the point of inflection found on all the subcadmium semi-log plots. This inflection point is characteristic of a small exponential assembly and it occurs at the place where the lattice born thermal flux begins to predominate. The initial part of the thermal curve, near the source end, is a straight exponential decay of the thermal source neutrons in the assembly. The point of inflection is reached when the lattice born and moderated thermal neutrons become a significant fraction of the total thermal flux. As the number of the lattice born thermal neutrons becomes larger than the remaining source neutrons, the slope of the thermal curve changes to become characteristic of the inverse relaxation length of the multiplying assembly. The sharp downturn of the thermal curve at the end far from the source is a consequence of the requirement that the thermal flux extrapolate to zero at that boundary.

The second interesting feature of the theoretical curves is the change in the shape of the curves of the slowing down density as the H_2O content of the moderator is increased. One effect of the H_2O addition is to increase the non-escape probability of both the slowing down and the thermal fluxes. Thus, the lattice becomes "larger" in terms of the non-escape probabilities as H_2O is added, and the curves of the slowing down density reflect this change. They change from a rounded form in the "smallest" assemblies which, in terms of the non-escape probabilities are the 99. 8 per cent D_2O cases, to a more peaked form. Far from the source, the slowing down density curve tends to become parallel to the thermal flux curve. If the physical size of the assemblies had been increased

also, thus further increasing the non-escape probabilities, the slowing down density curves would have eventually assumed a shape parallel to the thermal flux over most of the assembly. These parallel curves are characteristic of large exponential assemblies in which the thermal flux is proportional to the slowing down density. In the 99.8 per cent D_2O lattices this proportionality is not approached, but in the 80.2 per cent D_2O cases, the two curves are nearly proportional over approximately half of the assembly.

5.1.3 The Use of the Extrapolated Distance and the Value of ERI/σ_o in Comparison of the Theory with Experiment

The extrapolated distance and the value of ERI/σ_o are used as parameters in the comparison of theoretical with experimental values for the slowing down density at the gold resonance and the thermal flux. The effect of using these quantities will be illustrated.

The extrapolation distance affects the position of the theoretical curves as well as the size of the assembly. If the extrapolation distance is increased at the source end, the theoretical curves are shifted toward the source end by approximately the same amount as the increase in the extrapolation distance. The effect of increasing the extrapolation distance in a small assembly is illustrated in Figures 5-1 and 5-2. In Figure 5-1, the theoretical flux shapes were calculated by using the conventional extrapolation distance of $0.71\lambda_t$ on all boundaries. In Figure 5-2, the theoretical flux shapes were calculated by using an extrapolation distance of $2.0\lambda_t$ at each end and $1.0\lambda_t$ at the radial boundary. Otherwise, all the input parameters in each calculation were identical. It can be seen that the shapes of the curves are little affected by the increase in the extrapolation distance. The primary effect is to move both of the curves to the left; this shift is caused by the movement of the source end to the left when the extrapolation distance is increased.

The value of the quantity ERI/σ_o for the foils used in the traverse affects the experimental values of the slowing down density. This is illustrated by Figures 5-2 and 4-3. The calculations leading

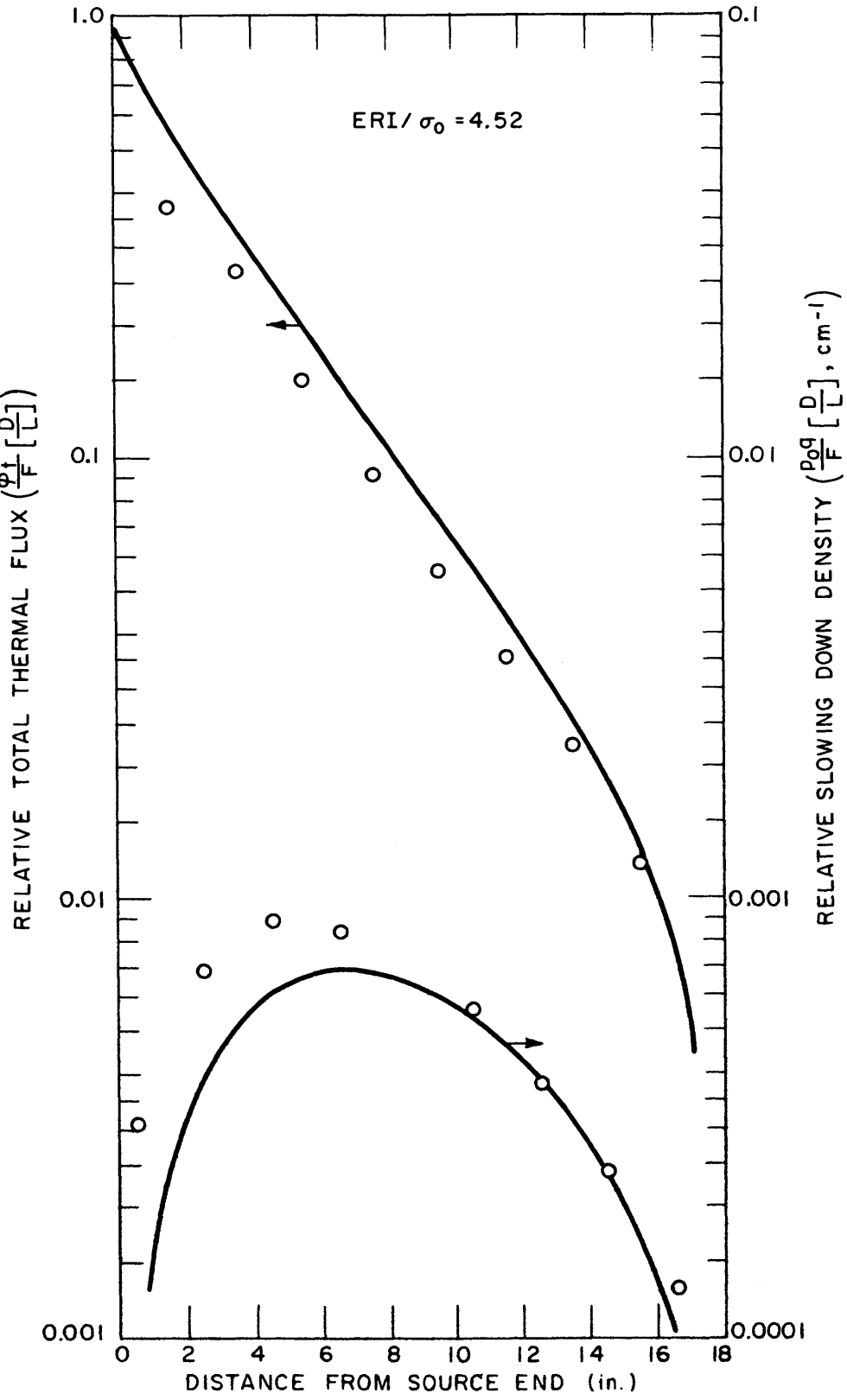

FIG. 5-1 COMPARISION OF AXIAL FLUX TRAVERSE WITH THEORY. EXTRAPOLATION DISTANCE = 0.71 λ_t (99.8 % D_2O, 1.340 in. SPACING)

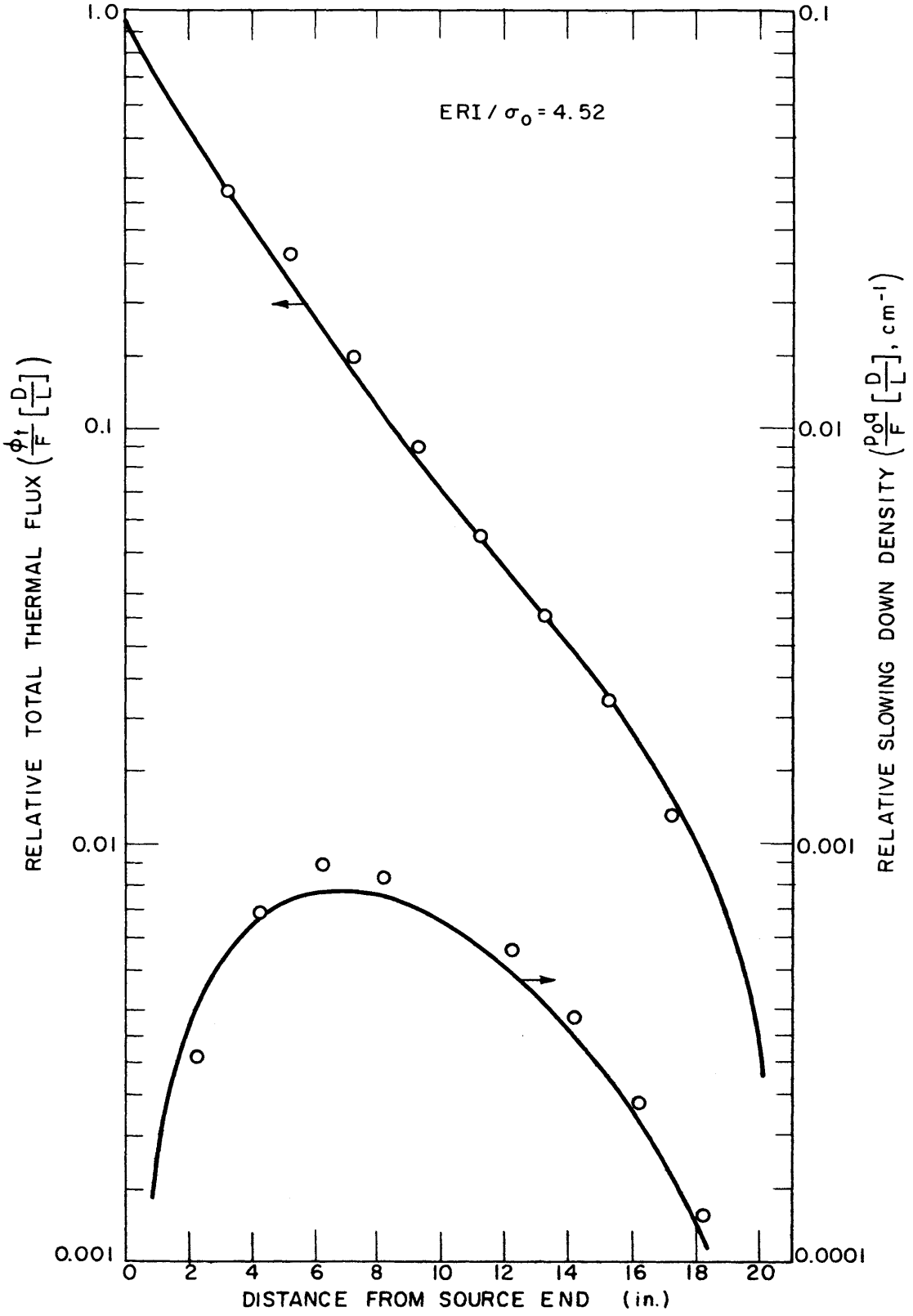

FIG. 5-2 COMPARISION OF AXIAL FLUX TRAVERSE WITH THEORY. EXTRAPOLATION DISTANCE = 2.0 λ_t (99.8% D_2O, 1.340 in. SPACING)

to these two graphs are identical aside from the value used for ERI/σ_o; in Figure 5-2, the value of ERI/σ_o is taken to be 4.52, and in Figure 4-3 it is taken to be 5.10. It can be seen from the two graphs that the effect of the value of ERI/σ_o is to move the entire set of experimental points for the slowing down density downward as the value of ERI/σ_o is increased.

The significance of the values of the extrapolation distance and ERI/σ_o will be considered in following parts of this section.

5.1.4 Detailed Comparison of the Experiments with the Theory

In general, the agreement of the experimental points with the theoretical curves is good throughout the nine graphs, Figures 4-1 through 4-9. The correspondence is better than might be expected in view of the approximations involved in the application of age-diffusion theory to such small assemblies. The experimental points, however, show the actual flux shapes to have real deviations from the theoretical curves. For purposes of clarity the actual flux points were not connected by lines to show the experimental flux shapes; however, the experimental errors were small and a smooth curve can easily be drawn through these points.

In the three graphs representing the 99.8 per cent D_2O lattices, there is a systematic deviation of the thermal flux points near the source end from the theoretical thermal neutron curve. In all of the nine graphs there is a systematic deviation of the measured slowing down density points near the source end from the theoretical slowing down density curves. In both cases, the measured points tend to fall above the theoretical curve. The values of the extrapolation distance, the deviations of the thermal and slowing down density curves, and the values of the ERI/σ_o used for the gold foils will each be considered in detail.

5. 1. 4. 1 The Extrapolation Distance

The most striking point in the comparison of these curves with the experimental values is the use of an extrapolation distance larger than $0.71\lambda_t$. The values for the extrapolation distance used in the nine graphs are given in Table 4-2. The values were chosen, as demonstrated in section 5. 1. 3, to bring the theoretical flux shapes into reasonable alignment with the data. The value of the extrapolation distance for a given lattice, shown in Table 4-2, was used on both ends, while an extrapolation distance of $1.0\lambda_t$ was used for the radius when the theoretical curves were calculated.

As mentioned in section 5. 1. 2, the validity of the value of the extrapolated boundary used in a small assembly is subject to discussion. The use of larger extrapolation distances in the smaller assemblies, as shown in Table 4-2, indicates that the conventional boundary conditions begin to break down in small assemblies, and that the theory is near the limit of its validity.

One possible explanation of the need to use the larger extrapolation distance at the source end is the non-isotropy of the source flux. The same extrapolation distance was used on the end far from the source as at the source end and may be justified, in part, for another reason. For structural purposes, there were 1-1/2 inches of aluminum and moderator between the ends of the uranium rods and the absorbing boundary at the end of the assembly far from the source. This material is quite different from a vacuum and tends to increase the extrapolation distance. The curves are sensitive to the choice of this boundary only near the last experimental point, so this effect is important only over a small part of the curve. The radial boundary condition is discussed in the section dealing with the radial traverse curve.

5. 1. 4. 2 Deviation of the Theoretical Thermal Flux Curves

The deviation of the thermal flux curves from the measured points near the source end in the three 99. 8 per cent D_2O cases may be caused by the boundary problem. Another possible cause,

however, is that the same thermal diffusion length was assumed for both the source and the lattice born neutrons in the theoretical calculations. This assumption simplified the theory for machine calculation, as can be seen in section 2.9, but it may have been unjustified for the cases in which the assembly was quite small, in terms of diffusion lengths. In these cases, the source neutrons constituted a significant part of the total thermal flux everywhere in the lattice. The effect of this assumption would be less noticeable in the lattices containing H_2O and would help explain why the fit of the thermal data with theory becomes very good in these "larger" lattices.

5.1.4.3 Deviation of the Theoretical Slowing Down Density Curves

The first experimental point on the slowing down density curves, aside from Figure 4-2, must be regarded to have less significance than the other points; it represents a measurement made 1/4 inch closer to the source than the physical end of the assembly. Regardless of this first point, there is a sharper peak near the source end in the measured values of the slowing down density at the gold resonance than in the theoretical curves. This effect may be due to the value of the age used in the calculations. The theoretical curve in this region is very sensitive to the value chosen for the age to the gold resonance energy. To illustrate this, a sample case was computed with input parameters close to those for the 90 per cent-1.128 inch lattice. The results are shown in Figure 5-3; while the slowing down density at zero age is not shown, it would be directly proportional to the thermal flux. As the age of the neutron increases, the slowing down density drops rapidly in value near the source end, owing to escape of the slowing down neutrons, but it remains relatively constant further inside the assembly. It follows from this property, illustrated by Figure 5-3, that all the theoretical slowing down density curves of Figures 4-1 through 4-9 could have been fitted more closely to the experimental values if values of the age to the gold resonance from 10 per cent to 20 per cent smaller had been used for the theoretical calculation.

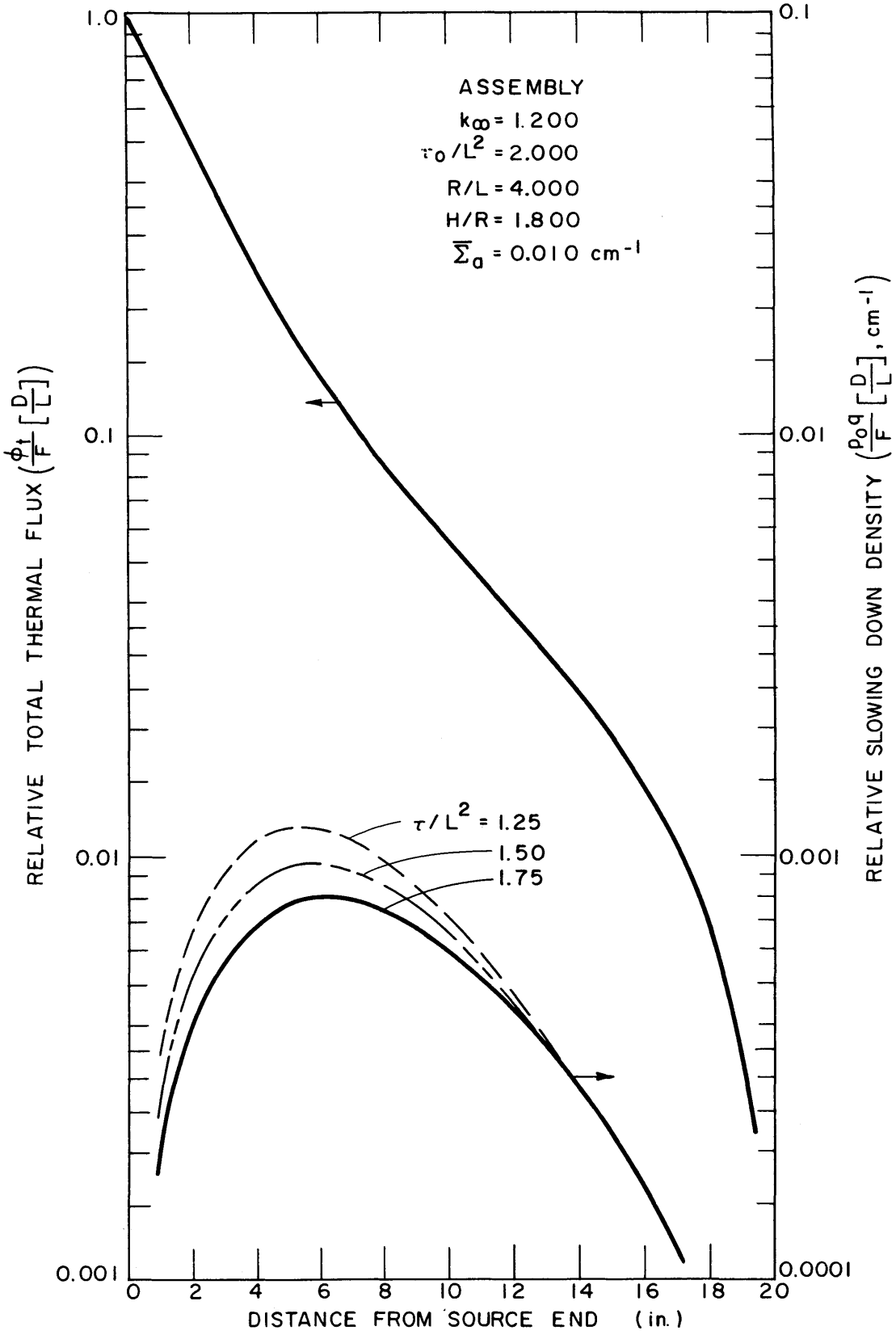

FIG. 5-3 TYPICAL THERMAL FLUX AND SLOWING DOWN DENSITIES AT THREE PARTIAL AGE VALUES

This was not attempted because the present agreement is fairly good and it has the virtue of a consistent theoretical treatment of the Fermi age.

Experimental values of the age of fission neutrons to the indium resonance in H_2O/D_2O mixtures have been obtained by Wade (36). They are plotted in Figure 5-4. The age from the indium resonance at 1.46 ev to thermal energies was obtained by using a formula derived for a mixture of two species:

$$\frac{1}{\tau_{mix}} = \frac{n_1^2}{\tau_1} + \frac{n_2^2}{\tau_2} + \frac{n_1 n_2}{\tau_2}\left[\frac{D_2}{D_1}\right] + \frac{n_1 n_2}{\tau_1}\left[\frac{D_1}{D_2}\right] \qquad (5.1\text{-}1)$$

where n_i = the mole fraction of species i. This equation can be obtained from the age equation with the assumption that the values of the transport and scattering cross sections and the value of ξ are constant for each of the two species. Since the age from the indium resonance to thermal energies is only a fraction of the total age, the use of this equation should not introduce any significant errors. Table 5-1 shows the data used in equation (5.1-1) and the total ages from fission to thermal energies obtained by using the values from equation (5.1-1) and Figure 5-4.

The total ages were then corrected for the presence of uranium and aluminum in the cell by using the approximation of Driggers and St. John (6):

$$\tau_{cell} = \tau_{mod}[1 + 2V_a + V_u] \ , \qquad (5.1\text{-}2)$$

where V_a = the volume fraction of the aluminum and

V_u = the volume fraction of the uranium.

This approximation is obtained by assuming that the aluminum does not moderate the neutrons significantly, and that the inelastic scattering of uranium is about one half as effective as the elastic scattering of the moderator. The results are listed in Table 4-1.

In order to obtain values of the age to intermediate energy levels, including the gold resonance, the following formula was used:

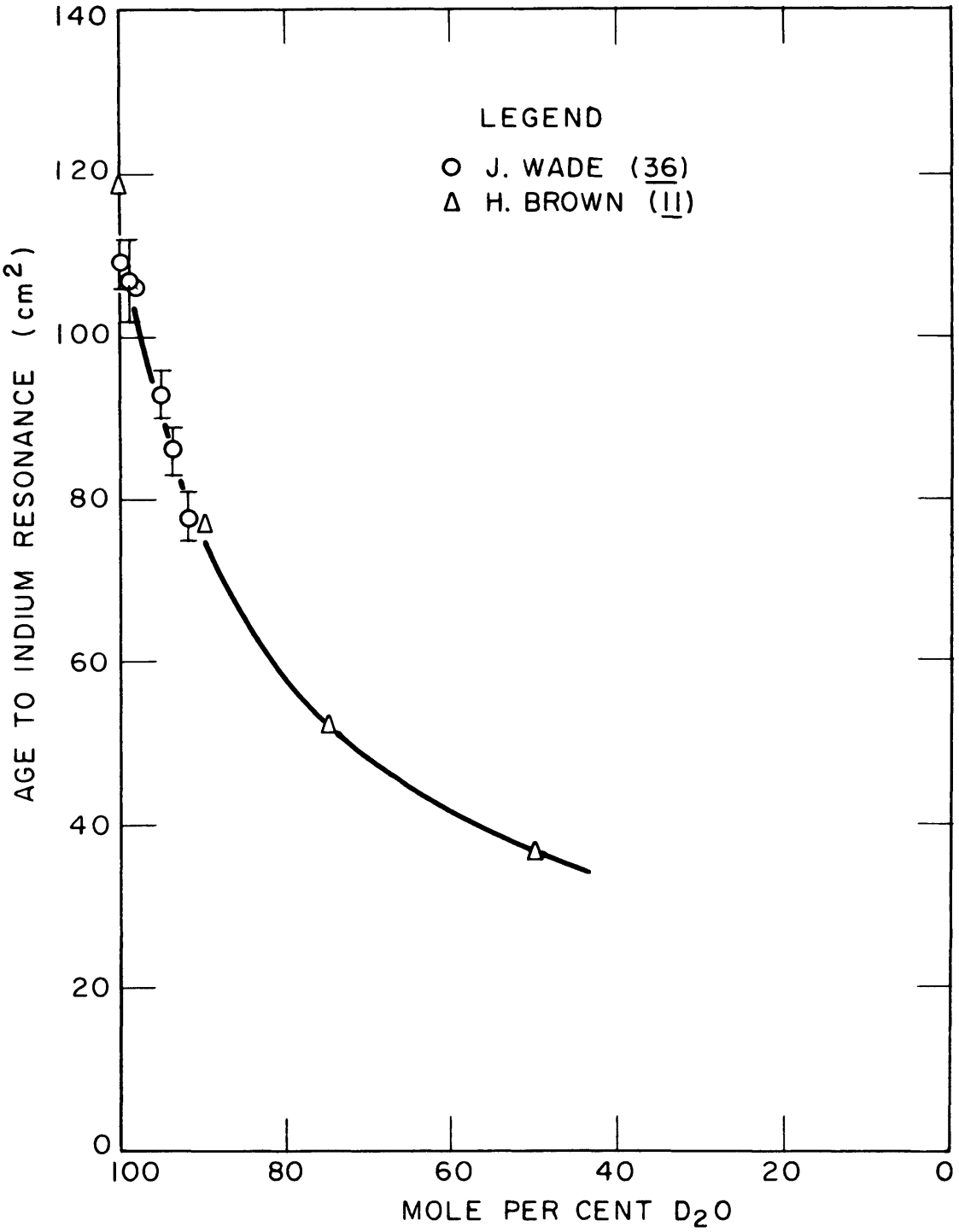

FIG. 5-4 AGE TO INDIUM RESONANCE IN MIXTURES OF D_2O AND H_2O

Table 5-1

Data for the Calculation of the Age to Thermal Energies in Mixtures of H_2O and D_2O

Age from indium resonance to thermal energies (29).

100% D_2O	20. cm^2
100% H_2O	1. cm^2

Thermal transport mean free path (29).

100% D_2O	2.65 cm
100% H_2O	0.48 cm

Age from indium resonance to thermal energy using equation (5.1-1), and the above data.

99.8% D_2O	20. cm^2
90.3% D_2O	11.1 cm^2
80.2% D_2O	7.0 cm^2

Age from fission energy to indium resonance from Figure 5-4.

99.8% D_2O	110. cm^2
90.3% D_2O	75.5 cm^2
80.2% D_2O	58.0 cm^2

Total age from fission to thermal energies.

99.8% D_2O	130. cm^2
90.3% D_2O	86.6 cm^2
80.2% D_2O	65.0 cm^2

$$\tau_r = \tau_{in}\left[\frac{\ln\left[\frac{2\times10^6}{E_{res}}\right]}{\ln\left[\frac{2\times10^6}{1.46}\right]}\right], \qquad (5.1\text{-}3)$$

where τ_{in} = cell age to the indium resonance. This formula assumes an average fission neutron energy of 2 Mev, and a constant value of $D/\xi\Sigma_s$ down to the indium resonance energy. The latter assumption is the more serious one. Unfortunately, there are no experimental data for the age to resonances other than indium in mixtures of H_2O and D_2O, but the reasonably good agreement between the experimental results and the theoretical slowing down curves seems to indicate that no serious errors are introduced by the use of equation (5.1-3).

To obtain correction factors for the U^{238} cadmium ratios, values of the age to each of the main uranium resonances must be calculated. Thus, for the sake of consistency, throughout this report equation (5.1-3) was used to calculate the partial ages in each lattice to the gold and uranium resonance energies. Probably the most serious deficiency in the input data for the theoretical calculations is the lack of experimental values to use for ages to resonances other than indium. The effect of this age approximation on the correction factor for ρ_{28} is considered in section 5.2, and the possibility of improving the treatment by using machine calculations is discussed in section 6.

5.1.4.4 The Effective Resonance Integral Used for Gold

The values of the quantity ERI/σ_o shown in Table 4-2 were chosen to give a good fit of the data to the theory. The effect of changing this value, as shown in section 5.1.3, is simply to move the measured slowing down density curve up or down without changing its shape. The calculated quantity $[p_o q/F][L/1]$ must be multiplied by $\bar{\Sigma}_a$ while the epicadmium activations must be multiplied by $\xi\Sigma_s/[[ERI/\sigma_o] + 0.5]$ in order to yield the plotted values

of $[p_o q/F][D/L]$. For this reason, the values of $[ERI/\sigma_o] + 0.5$ are directly proportional to the values chosen for $\xi\Sigma_s$ and inversely proportional to the values chosen for $\bar{\Sigma}_a$. The values of $\bar{\Sigma}_a$ are from the Thermos code, and the values of $\xi\Sigma_s$ at the gold resonance of 4.9 ev were calculated from the data shown in Table 5-2.

According to the theory of section 2.4, the value of the quantity ERI/σ_o should be constant for any particular size of foil, thickness of cadmium cover, and type of counting system. However, some variation in the apparent value of the ratio, depending upon the lattice parameters of the assembly in which the foils are activated, is often noted. A separate direct measurement of the value of ERI/σ_o for 0.005 inch thick gold foils with 0.020 inch thick cadmium covers was made by P. Brown (5) at the M.I.T. Lattice Facility. This measurement was made in an assembly of natural uranium rods one inch in diameter, triangularly spaced at 4.5 inches in 99.8 per cent D_2O. A foil wheel, suspended in the middle of a lattice from which the three middle rods had been removed, was used. The foil size, cadmium covers, and counting system were identical with those used in the experiments discussed in this report. The value of ERI/σ_o was calculated from Brown's measured values for the cadmium ratios of an infinitely dilute foil and a 0.005 inch thick gold foil by using the formula

$$\frac{R_o - 1}{R_f - 1} = \frac{[ERI/\sigma_o + 0.5]_{.005}}{[ERI/\sigma_o + 0.5]_{dil}} \quad . \tag{5.1-4}$$

He found the cadmium ratio of the infinitely dilute gold foil (R_o) to be 2.78 ± 1 per cent and the cadmium ratio of an 0.005 inch thick gold foil to be 6.67 ± 1 per cent. A value of 15.2 was used for the ratio ERI/σ_o of the infinitely dilute foil. The value of ERI/σ_o found from the above equation and data is 4.42 for a 0.005 inch thick gold foil. This value lies among those presented in Table 4-2.

Considering the possible error in the calculated quantities which affect the values found for ERI/σ_o, the values appear reasonable.

Table 5-2

Data for the Calculation of $\xi\Sigma_s$

Moderator atom	Hydrogen	Deuterium	Oxygen
ξ	1.0	0.725	0.12
Scattering cross section at 4.9 ev (barns)	20.0(18)	3.44(8)	3.8(18)
Atomic concentration in 99.8% D_2O (barn cm)$^{-1}$	1.33×10^{-4}	6.65×10^{-2}	3.33×10^{-2}
Atomic concentration in 90.3% D_2O (barn cm)$^{-1}$	0.649×10^{-2}	6.02×10^{-2}	3.33×10^{-2}
Atomic concentration in 80.2% D_2O (barn cm)$^{-1}$	1.33×10^{-2}	5.33×10^{-2}	3.33×10^{-2}

The uranium and aluminum were assumed to have no moderating effect at 4.9 ev. Consequently, the values of $\xi\Sigma_s$ found for the moderators were multiplied by the volume fraction of the moderator in the cell.

Rod spacing (in.)	Volume fraction of moderator
0.880	0.880
1.128	0.929
1.340	0.951

5. 1. 5 Possible Effects of the Foil Holders and Cadmium Covers

The aluminum foil holders could produce at least two possible effects on the axial traverses. The first one is that the 0. 030 inch thick aluminum stick might act as a pipe, transmitting source neutrons along its length. Such transmission, however, would be blocked at the first foil which was covered with cadmium and located 1/4 inch closer to the source than the physical end of the assembly.

The second possibility is that the stick might depress or enhance the slowing down and thermal fluxes along its entire length because the scattering cross section of aluminum is different from that of the moderator. Since the foil activation measurements are relative to each other, this effect would cancel out in the data reduction.

The cadmium covers on alternate foils might have the effect of depressing the ratio of subcadmium to epicadmium neutrons at the bare foils between them on the stick. Such a depression would affect the value found for the ratio ERI/σ_o, which would be proportionately higher. Direct measurements by P. Brown (5) of this effect, based on the use of identical foils and covers, show that it is less than 1 per cent for a one-inch spacing of the bare and cadmium covers; an error well within the limits assigned to the values of ERI/σ_o in Table 4-2. Thus, the influence of the aluminum foil holder and cadmium covers upon these measured traverses appears to be negligible.

5. 1. 6 Effect of Calculations Along the Central Axis

One small source of error in the theoretical curves is the radial position of the calculated axial flux curve. In order to save computer time, the axial traverses were computed along the central axis. This procedure avoids the evaluation of the Bessel functions, since all the arguments of the Bessel functions at this point are zero, and the functions all have the value of 1. 0. The experimental traverses were actually made at a distance from the central axis of

1. 7 times the basic center to center rod spacing. The foil stick was taped to a rod in the second hexagonal ring from the center to avoid influencing other measurements inside the first ring of rods.

The difference between the theoretical case at the center line and the theoretical case at the actual experimental radius was determined for the 80. 2 per cent - 1. 340 inch lattice where the deviation of the two theoretical curves from each other would be greatest. The average difference between the two theoretical total thermal curves was less than 1 per cent and the maximum deviation, at the far end from the source, was less than 3 per cent. Slightly smaller deviations were found between the two slowing down density curves. This error was the only known error greater than 1 per cent which was not corrected for in the theoretical or experimental values given in this report. It was not corrected because its evaluation would have involved a complete calculation of the flux curves off the center axis, and would have involved a large amount of computer time. The error, caused by this procedure, in the calculation of the ρ_{28} correction is much smaller, owing to the tendency of similar errors to cancel out in the ratios used in that calculation. It is considered in section 5. 2.

5. 1. 7 Radial Traverse of the Assembly

Figure 4-10 shows a typical radial traverse of the assembly. It was made at a distance of 7. 62 inches inside the assembly from the actual source end. The rods were spaced at 1. 340 inches in 80. 2 per cent D_2O. At the radial traverse position, the ratio of the lattice born and moderated neutrons to the source neutrons was calculated to be 2. 0. The solid line on the graph represents the theoretical total thermal flux and it shows the presence of harmonics when it is compared with the fundamental J_o-curve (dotted line). The experimental flux points agree more closely with the theoretical curve than with the fundamental J_o-distribution.

An extrapolated boundary of 10. 75 inches was used for the theoretical calculation. This value, which is the sum of the physical

radius of 10.2 inches and one transport mean free path, leads to a theoretical curve in good agreement with the experiment. The choice of the extrapolation distance would not affect the J_o-curve near r = 0. This extrapolation distance, which is slightly larger than the conventional value of $0.71\lambda_t$, probably results from reflection of some of the neutrons by the boron carbide shield around the assembly.

5.2 U^{238} CADMIUM RATIO

5.2.1 Choice of Best Experimental Value

The values of ρ_{28} listed in Table 4-3 shown close agreement, after correction to the critical assembly value, in six of the eight lattices in which two measurements were made. In the two lattices in which the corrected measurements disagree beyond the experimental error, the measurement taken for the best value was the one farther from the source. This choice was made because the correction factor closer to the source end is more sensitive both to boundary assumptions and the values chosen for the partial ages. The simple equation (5.1-3) was used to estimate the ages to the various uranium resonances. The effect of an error in the partial age calculations on the correction factor for ρ_{28} is discussed in section 5.2.2.

5.2.2 Effect of Approximations on the Correction Factor

Equation (2.5-7) was used to evaluate the correction factors; the variable in the equation which had to be calculated, and which depends on the value of the age, was the ratio $p_j q_j/\phi$. A graph of this ratio for various ages is shown in Figure 5-5 for the same case as shown in Figure 5-3. The values of the ratios, for different ages, do not differ greatly from each other over the last third of the assembly; hence, a measurement made in that region should be relatively insensitive to the values used for the age. The measurement made farther from the source in each case was in that region; thus the correction factor for the measurement should not be affected seriously by the age approximation used. For this reason, the

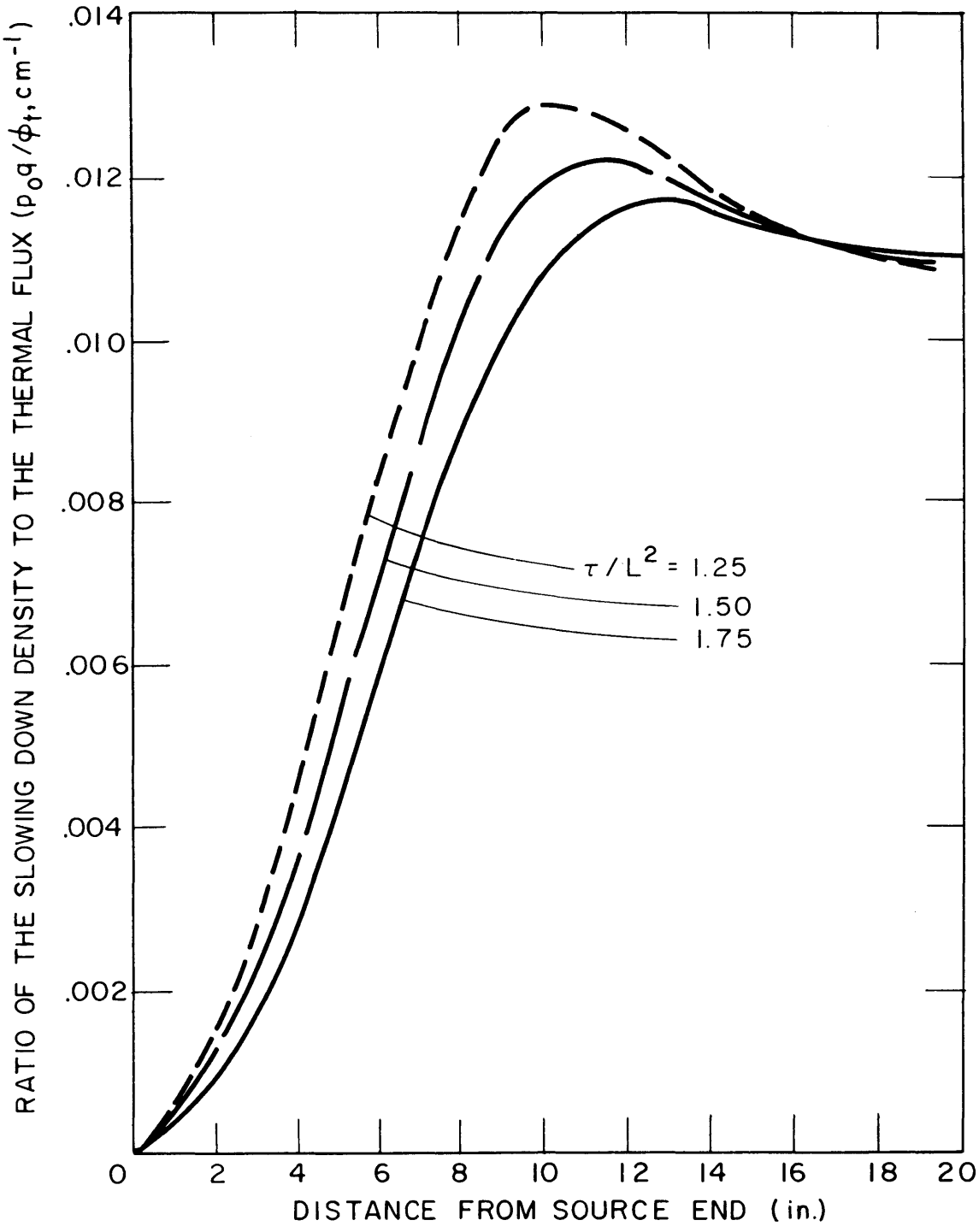

FIG. 5-5 TYPICAL RATIOS OF THE SLOWING DOWN DENSITY TO THE THERMAL FLUX AT THREE PARTIAL AGE VALUES

measurement made farther from the source is preferred over the measurement closer to the source when the two disagree. The disagreement between the two measurements in the 80 per cent - 1.128 inch, and the 80 per cent - 0.880 inch lattices may be caused by the effect of the age approximation on the correction factor; the effect may be relatively large on the measurement closer to the source.

The values of the quantity f_j also had to be known for the calculation. These could be obtained from the infinite dilution resonance integral for uranium, if necessary, but it would be more appropriate to use values for the size of rod actually used in the experiment. Values of the effective resonance integral for a 0.250 inch uranium rod were made available by D. Wehmeyer (37) from machine calculations performed at the Babcock and Wilcox Company. The formula of Hellstrand (13), with corrections taking into account the lattice shielding factor of Bell (2), was used for these calculations. The results are given in Table 5-3 as well as values for the infinite dilution resonance integrals.

For the purposes of the correction factor calculations, the numerous U^{238} resonances above 66.3 ev were lumped into one value assumed to be at 200 ev. The calculations are insensitive to the energy chosen for these lumped resonances. Since the exponential code calculates the quantity $p_o q/\phi_t \bar{\Sigma}_a$, where p_o is the total resonance escape probability, the values obtained from the machine calculations must be multiplied by the factor p_j/p_o, where p_j is the resonance escape probability to the j^{th} energy. These partial resonance escape probabilities were estimated from the formula (10),

$$p_j(E) = \exp\left(\frac{-N_u V_u \phi_u [\,ERI(E)\,]}{\xi \Sigma_s V_m \phi_m}\right), \qquad (5.2\text{-}1)$$

in which the values of the ERI for a 0.250 inch rod shown in Table 5-3 were used. Because of the tendency of similar deviations in the critical and exponential calculations to cancel each other, as mentioned in section 2-10, the approximations used for the values of f_j and p_o have little effect on the correction factors. This was shown

Table 5-3

Resonance Integrals for U^{238}

Resonance Energy (ev)	ERI (32) for Infinite Dilution (barns)	Fraction of Total. f_j	ERI (37) for 0.250 in. diam. rod (barns)	Fraction of Total. f_j
(all above 66.3)	19.5	0.074	7.915	0.3674
66.3	11.6	0.044	0.614	0.0285
36.9	42.3	0.160	1.722	0.0799
21.0	60.8	0.230	2.740	0.1272
6.7	130.2	0.492	8.551	0.3970
Total	264.4	1.000	21.542	1.0000

by recalculating the correction factors for the two measurements made in the 80 per cent - 1.340 inch lattice, with different approximations for the values of p_j and f_j. In the first recalculation, the partial resonance escape probabilities were all taken to be 1.0, and the rod values of f_j from Table 5-3 were used. In the second recalculation, the dilute resonance integral values of f_j from Table 5-3 were used and the partial resonance escape probabilities were again taken as 1.0. The results are shown in Table 5-4. The changes in the correction factors are small, despite the large changes in the values of p_j and f_j.

Since theoretical values were calculated along the central axis, while the measurements were made in the next adjoining rod, a systematic error exists in the theoretical values of $p_o q/\phi_t \bar{\Sigma}_a$. The amount of this error was calculated in the case of the 80.2 per cent - 1.340 inch lattice in which the error would be the largest. The error in the values of $p_o q/\phi_t \bar{\Sigma}_a$ was less than 0.2 per cent at the experimental positions and is, therefore, negligible.

In using the exponential code to compute the values of $p_o q/\phi_t \bar{\Sigma}_a$, a value of k_∞ must be supplied as an input datum. The value of p_o for the calculation of k_∞ thus must be estimated in advance in order to find the correction factor for ρ_{28}. Hence, the critical assembly

Table 5-4

Variation in the Calculated Correction Factor for ρ_{28} Depending on the Values Used for the Fractional Resonance Integral and the Partial Resonance Escape Probability (80. 2% - 1. 340 inch Lattice)

Distance of measurement from source end (in.).	5. 70	9. 60
Correction factor using f_j for 0. 250 inch diam. rods and partial resonance escape probabilities.	1. 042	0. 925
Correction factor using f_j for 0. 250 inch diam. rods and ignoring partial resonance escape probabilities.	1. 048	0. 925
Correction factor using f_j for infinite dilution and ignoring partial resonance escape probabilities.	1. 081	0. 925

value of ρ_{28}, and the experimental value of p_o derived from it, depend on the estimated value of p_o. If the experimental value differs from the previously estimated value, the calculation must be repeated using the new value of p_o. The iteration converges very rapidly on a consistent value of p_o since the function ρ_{28} varies more rapidly than the value of p_o calculated from it. This iteration procedure was used for each of the nine lattice calculations reported here. Table 5-5 shows the progress of the iteration for the 99. 8 per cent - 12. 0 inch lattice.

5. 2. 3 Consideration of Experimental Values

A graph of the values of ρ_{28} is shown in Figure 5-6. It would be expected that the change in the values from 0. 2 per cent H_2O to 10 per cent H_2O would be about the same as the change from 10 per cent H_2O to 20 per cent H_2O for any particular lattice spacing. The expectation is borne out by the results except for the discrepancy in

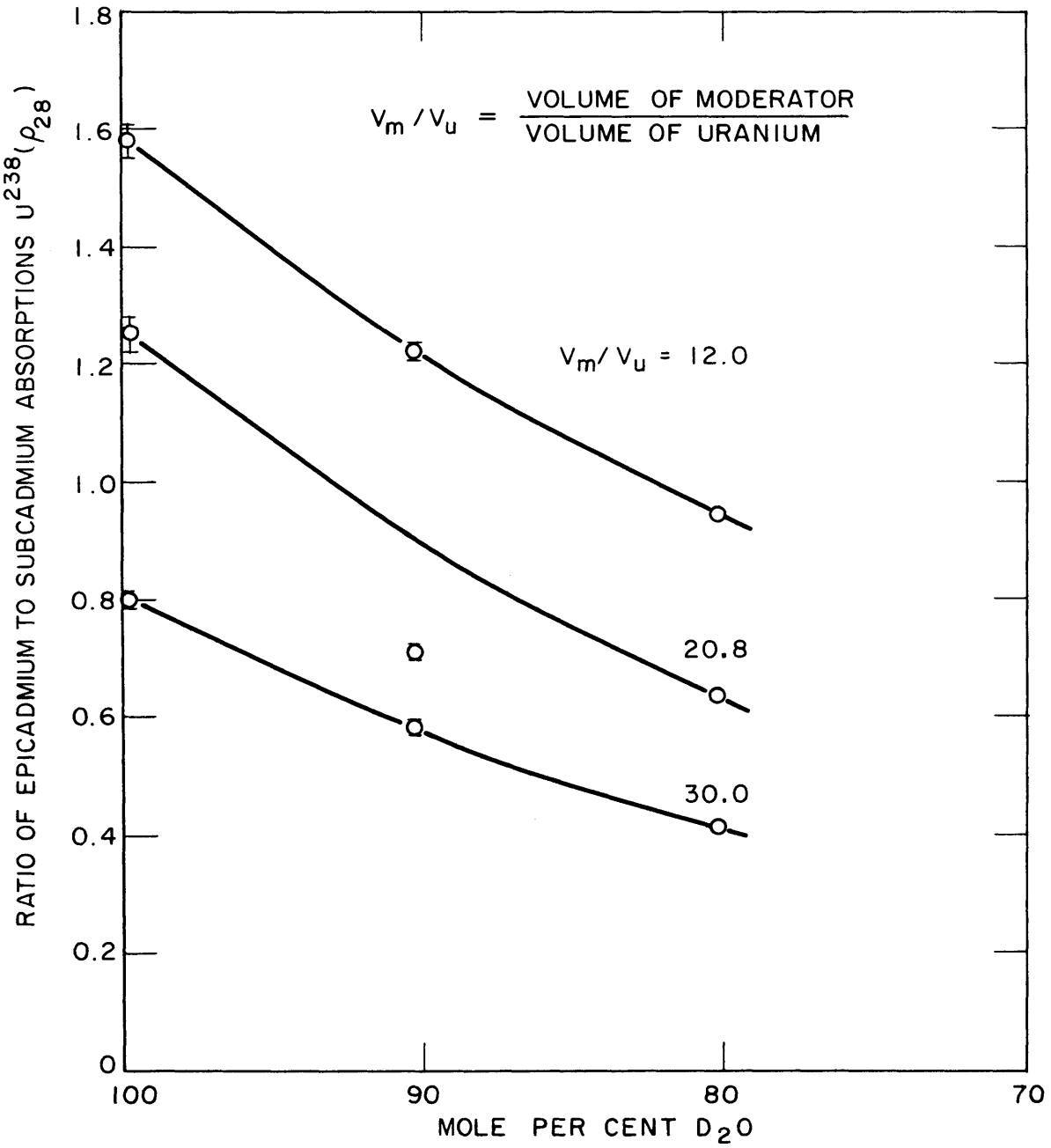

FIG. 5-6 CORRECTED EXPERIMENTAL VALUES OF ρ_{28}

Table 5-5

Progress of the Iteration
to Find the Correction Factor for ρ_{28}

(99. 8% - 0. 880 inch Lattice)

Calculation	First	Second
k_∞/p_o	1. 531	1. 531
Estimated p_o	0. 682	0. 732
k_∞ used	1. 044	1. 121
Correction factor calculated at 5. 73 inches from source end.	1. 200	1. 178
Correction factor calculated at 9. 68 inches from source end.	0. 817	0. 817
Average value of ρ_{28} found.	1. 59	1. 58
Value of p_o calculated from (5. 2-2).	0. 732	0. 735

the 90 per cent - 1. 128 inch lattice. These measurements of ρ_{28} are considered to be consistent and in good agreement, with the exception of that one point. Unfortunately, that particular measurement could not be repeated because the water with 90 per cent D_2O content had been degraded to 80 per cent; the cost of degrading more 99. 8 per cent D_2O to make 100 more liters of 90 per cent D_2O was considered prohibitive. The experimental records show, however, that the result is anomalous. Two measurements were made in the 90 per cent - 1. 128 inch lattice; both of them were low and they were consistent with each other. Each of the two measurements was counted twice on different days, and the activity of the foils agreed with the expected Np^{239} decay activity to 2 per cent. The two measured cadmium ratios on each foil agreed with each other to 0. 4 per cent in one pair and to 1. 2 per cent in the second pair.

The experimental measurement may be erroneous, but all of the following variables were eliminated as sources of error through routine procedures carried out for each experiment or by analysis:

a. Weight difference in the foils. (Corrected.)

b. Previous activation of the foils. (Investigated by counting the background of each foil before irradiation.)

c. Omission of the cadmium covers. (This would have raised the value of ρ_{28}; not lowered it.)

d. Calibration of the counting equipment. (Calibrated several hours before counting. The equipment is very stable over a period of several days.)

e. Counting wrong gamma activity. (Since the calibration was made with an irradiated U^{238} foil, and the appropriate half-life was also obtained, this possibility is unlikely.)

f. Mix-up in lattices or heavy water. (The measurements of δ_{28}, made at the same time, were precisely on the final value.)

g. Wrong correction factor. (This could not account for a 23 per cent discrepancy.)

The measurements appear to be consistently lower than those which would be expected. For this reason, two values have been carried throughout the rest of this analysis; an estimated value of 0.9, and a measured value of 0.707.

5.2.4 Calculation of the Resonance Escape Probability

The calculation of the resonance escape probability from the measured values of ρ_{28} depends upon the formula used (38). Two formulas are used here. The simpler form is

$$p_o = \frac{1}{1 + Gf\rho_{28}} \qquad (5.2\text{-}1)$$

where G is the ratio of thermal neutron absorptions in U^{238} to

thermal neutron absorptions in the fuel, and where f is the thermal utilization. The second form, given by Kouts and Sher (24), is more complicated; it is consistent with the values of f from Thermos and with the values calculated for ϵ from equation (5.3-1). It is,

$$p_o = \frac{1 + \left[[\epsilon - 1]\, a_{28} / \epsilon [\nu_{28} - 1 - a_{28}]\, \ell_1 \right]}{1 + \left[fG\ell_2 \ell_3 \rho_{28} [1 - \delta/\rho_{28}] / [1 + \delta] \right]} \quad . \qquad (5.2\text{-}2)$$

where ℓ_1, ℓ_2, and ℓ_3 are non-escape probabilities in the fast, resonance, and thermal regions, respectively. The quantity δ is defined in section 5.4.4.

Table 5-6 shows the input data for both formulas and the resulting values of the resonance escape probability. Thermal parameters were calculated by using the Thermos code. The values of δ used in the calculation are from the intracell flux traverse measurements and are discussed in section 5.4.4.

Equation (5.2-2) takes into account leakage from the assembly in which the measurement is made. The equation is for measurements made in a critical assembly or in the asymptotic region of an exponential assembly. In application it is quite different from equation (2.5-7), which is to correct measurements made in a non-asymptotic part of the assembly to critical assembly values. In principle, the bucklings and, from them, the non-escape probabilities could be calculated from the data available and used in equation (5.2-2). The equation then would have to be iterated with the new values of p and the consequent change in the bucklings and the non-escape probabilities. It would be desirable in such a case to have experimental measurements of the buckling to use, since the estimated non-escape probabilities still would have some error in them. Because experimental values of the buckling were not available, the non-escape probabilities were simply set equal to 1.0 for the calculations shown in Table 5-6.

Table 5-6

Parameters for Calculation of the Resonance Escape Probability

D_2O Conc.	Rod Spacing	fG (U^{238} abs.) (Thermos)	ρ_{28} (Measured)	ϵ (Measured)	δ (Measured) ± 2%
99.8%	0.880	.2614	1.58 ±.03	1.026±.001	0.0725
99.8%	1.128	.2586	1.25 ±.03	1.018±.001	0.0515
99.8%	1.340	.2569	0.796±.012	1.015±.001	0.0396
90.3%	0.880	.2439	1.219±.013	1.026±.001	0.0625
90.3%	1.128	.2324	0.900 (est.)	1.018±.001	0.0406
90.3%	1.128	.2324	0.708±.008	1.018±.001	0.0406
90.3%	1.340	.2220	0.582±.011	1.015±.001	0.0300
80.2%	0.880	.2291	0.941±.006	1.026±.001	0.0452
80.2%	1.128	.2105	0.633±.005	1.018±.001	0.0330
80.2%	1.340	.1941	0.414±.002	1.015±.001	0.0263

$$\alpha_{28} = 0.107$$
$$\nu_{28} = 2.76 \pm 0.09$$
$$\nu_{25} = 2.43 \pm 0.03$$

Results of Resonance Escape Probability Calculations

D_2O Conc.	Rod Spacing	p_o - Eq. (5.2-1)	p_o - Eq. (5.2-2)
99.8%	0.880	0.707±.004	0.735±.004
99.8%	1.128	0.755±.005	0.774±.005
99.8%	1.340	0.830±.002	0.845±.002
90.3%	0.880	0.771±.002	0.794±.002
90.3%	1.128	0.828 (est.)	0.840 (est.)
90.3%	1.128	0.859±.002	0.872±.002
90.3%	1.340	0.887±.002	0.895±.002
80.2%	0.880	0.824±.002	0.839±.002
80.2%	1.128	0.882±.002	0.893±.002
80.2%	1.340	0.925±.002	0.932±.002

5.3 U^{238}/U^{235} FISSION RATIOS

5.3.1 Calculation of the Fast Fission Factor

The values listed for δ_{28} in Table 4-4 show reasonably close agreement for each lattice spacing regardless of the H_2O content of the moderator. This result can be attributed to the fact that the scattering cross section for neutrons in the fast fission range is nearly the same for both deuterium and hydrogen. Since the experimental values for a given spacing are practically independent of the composition of the moderator, they were averaged to obtain the final result for each spacing. These values were then used to calculate the fast fission factor from the usual relationship.

$$\epsilon = 1 + \frac{\delta_{28}}{\nu_{25}}(\nu_{28}-1-\alpha_{28}) \qquad (5.3\text{-}1)$$

in which the following values were used:

$\nu_{25} = 2.43 \pm 0.03$

$\nu_{28} = 2.76 \pm 0.09$ (25)

$\alpha_{28} = 0.107$ (24) .

The results are given in Table 5-7.

Table 5-7

Fast Fission Factor (ϵ) in 0.250 Inch Diameter Rods

Rod spacing (in.)	Average δ_{28}	Fast fission factor (ϵ)
0.880	0.0392 ± .0008	1.026 ± .001
1.128	0.0263 ± .0006	1.018 ± .001
1.340	0.0218 ± .0003	1.015 ± .001

5. 3. 2 Consideration of the Correction Factor for the Interaction Effect

The value of the correction factor for the interaction effect is less than 1. 0 in all cases. Equation (2. 6-10) shows that it depends upon the parameters chosen for Σ_s^f, the scattering cross section of the moderator for fast neutrons, and γ, the inverse axial relaxation length. In these small assemblies, the value of γ changes over the length of the assembly because the relaxation length shifts from one characteristic of the source neutrons being absorbed to one characteristic of the multiplying medium. This change in the value of γ introduces the error shown in Table 4-4 in the values of the correction factor for the interaction effect. The correction factor estimated by using equation (2. 6-7) took into account both the exponential shape of the thermal flux in the axial direction and the J_o-shape in the radial direction. Allowance was made also for the fact that the measurements were not made upon the central axis but in the next adjoining rod. Rods were considered to contribute to the interaction effect and were counted in the summation indicated in equation (2. 6-7) until the contribution of an individual rod was less than 0. 2 per cent of the total interaction effect. The summation included 90 rods in the case of the closest spacing.

The most interesting fact about the correction to the infinite case for the interaction effect is that the part of the correction due to the axial exponential flux distribution is always less than 1. 0, while the part due to the radial flux distribution is always greater than 1. 0. As can be shown from equation (2. 6-7), the correction factor is the product of the two parts; thus the deviation of the two distributions from a flat flux tend to cancel each other in their influence on the interaction effect. Correction for the J_o-shape alone might be less accurate than making no correction at all if the measurement were made in an exponential assembly. In a large assembly, the correction for either effect is quite small. In the small exponential assembly, the exponential effect tends to dominate.

5. 3. 3 Test of Theory

A test of the theory used in the correction of the interaction effect was mentioned in section 2. 6. It is made by finding the ratio, for each lattice spacing, of the numerator of equation (2. 6-7) to the corrected experimental value of the interaction effect. The results of this comparison are shown in Table 5-8. The agreement is very good, almost within the limits of the experimental error, and it indicates that values of δ_{28} for other spacings of these lattices could be calculated safely with the use of this equation. In similar lattices, the value of δ_{28} could be estimated with one measurement of the interaction effect at a particular spacing and a measurement of the single rod value of δ_{28}.

Table 5-8

Comparison of the Numerator of Equation (2. 6-7) to Interaction Effect Found for Infinite Lattices

Rod Spacing (in.)	Numerator of Eq. (2. 6-7)	Interaction Effect for Infinite Case	Ratio
0. 880	1. 190	0. 0266 ± . 0008	44. 8 ± 1. 4
1. 128	0. 666	0. 0137 ± . 0006	48. 6 ± 2. 3
1. 340	0. 441	0. 0092 ± . 0004	48. 0 ± 2. 1

5. 3. 4 Comparison with Other Measurements

Figure 5-7 shows the final values of δ_{28} compared with those obtained at much closer lattice spacings in H_2O at the Brookhaven National Laboratory (23). The two curves show fair agreement, although they do not look as if they would join in a smooth curve. The discrepancy may be due to a small difference in the interaction effect between lattices moderated by H_2O and lattices moderated by a mixture consisting mostly of D_2O. A very small difference between

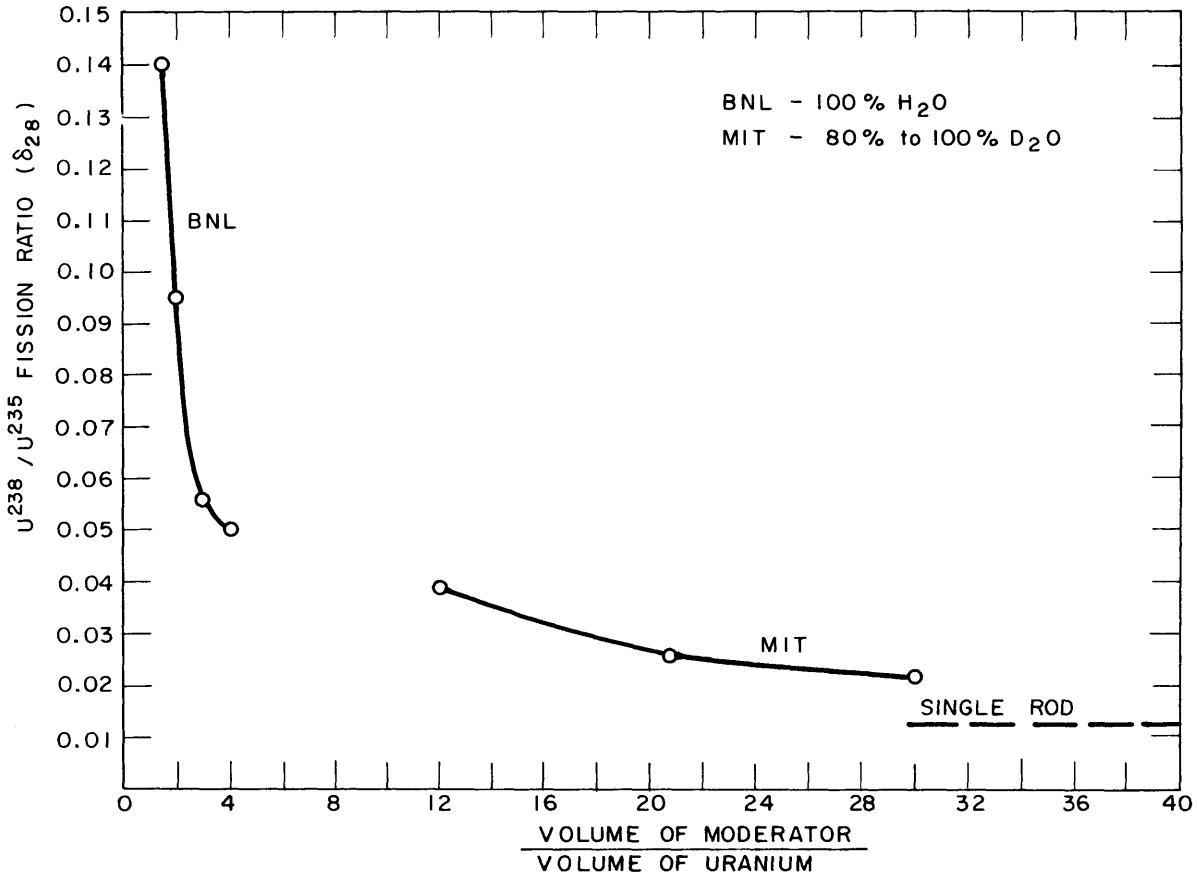

FIG. 5-7 EXPERIMENTAL VALUES OF δ_{28} IN ¼ in. DIAMETER URANIUM RODS

effects in the two moderators probably would be smaller than the experimental error of the measurements made here which covered the range only from 80. 2 per cent D_2O to 99. 8 per cent D_2O.

5. 4 INTRACELL FLUX TRAVERSE MEASUREMENTS

5. 4. 1 Effect of Leakage on the Measurements

It is possible to consider, in an approximate way, the effect of leakage from the assembly on the theoretical intracell flux traverses by introducing the leakage term DB^2 into the cell calculations as an additional energy dependent absorption term. The method is discussed in Appendix C. The theoretical effect upon a relative measurement of neutron density made with a 1/v absorber such as gold is quite small. In all nine of the cases computed, the difference was never more than 0. 3 per cent in the theoretical traverses. For this reason, the intracell flux traverses are plotted against the infinite assembly values. A cadmium cut-off energy of 0. 415 ev was used for the theoretical calculations.

5. 4. 2 Consideration of the Data

A hexagonal cell has two basic lengths; one from the center to a point of the hexagon, and the other normal to one of the sides and passing through the center. Flux traverses were made along both lengths. The traverse to the cell corner is represented by a square point on the graphs and the traverse to the cell side is represented by a circular point. The results for the 90. 3 per cent D_2O and 80. 2 per cent D_2O cases are shown in Figures 4-10 through 4-16. In Figure 4-16, the traverse to the cell side was rejected because of scatter. Similar measurements were made in the 99. 8 per cent D_2O case; beta counts were made on these traverses on an automatic gas flow Geiger counter, but they were too inaccurate to be meaningful. The cause of the inaccuracies probably was the varying surface area of the very small foils used in the experiment. The same type of foils counted on the gamma counter system of Figure 3-8 yielded much

better results, and this system was used for the cases shown in Figures 4-11 through 4-16.

Equation (2. 7-2) was used for correction of the traverses to the infinite assembly. The harmonic content of the radial Bessel function expansion at the axial position of these measurements was less than 1. 0 per cent of the fundamental J_o mode. For this reason, a radial J_o function was assumed to represent the flux distribution in equation (2. 7-2).

Of the six traverses shown in Figures 4-11 through 4-16, the agreement with the Thermos calculations is good only in the lattices with the widest spacing (1. 340 inches). In the tighter lattices, there is a clear discrepancy between the theoretical and the measured neutron densities.

5. 4. 3 Possible Causes of the Disagreement Between the Thermos Calculated Flux Traverses and the Experiments

The explanation of the discrepancy between theory and experiment is not yet known, but some possible causes are listed:

a. In the theoretical calculation, the properties of the mixed moderator were handled by treating the moderator as a collection of three atomic gases, hydrogen, deuterium, and oxygen, with atomic densities equal to their actual values in the mixture. The scattering properties were handled by using a Brown and St. John free gas kernel (4) for the deuterium and oxygen, and a Nelkin kernel (26) for the bound hydrogen. This treatment is based on consideration of the properties of a molecule of D_2O and H_2O. In the mixture, however, the hydrogen probably is bound primarily in the form of HDO molecules and the effect that this might have on the scattering kernels is unknown.

b. In these experiments, the foils were held in a thin aluminum holder, 0. 030 inches by 1/8 inch thick. This was found to have less than 1 per cent effect upon measurements

made in D_2O in an experiment performed by P. Brown (5). However, at the Brookhaven National Laboratory (23), it was found that even a small amount of aluminum can cause a discrepancy in measurements made in H_2O. In the mixtures used here, the aluminum holder should not have been the cause of the discrepancy since the lowest moderator D_2O content was 80 per cent.

c. The possibility of fission product contamination of the foils in the rod giving an artificially high value of their activation was eliminated by using a 0.001 inch shield of aluminum or Mylar tape between them and the adjoining pieces of uranium.

d. If the cadmium covers were transmitting thermal neutrons, the effect on the results would have been in the opposite direction to that which was found.

e. The effect of cylindricalization of the hexagonal cell in the theoretical calculation is also a possible cause of the discrepancy between the theoretical and the experimental cases. This effect, if it is a serious one, would become more pronounced at the smaller spacings, but, it does not seem reasonable to ascribe the discrepancy to this factor alone.

f. The last possibility is that the neutron flux distribution in the small assembly may not be representative of that in the critical assembly and, at the smallest spacings, the experimental flux plots are the least representative. The lattices with the smallest spacings have the highest absorption in the cell and, consequently, the highest neutron temperatures. The presence of source neutrons may then lead to a spectral distribution in the cell markedly different from that in a critical assembly, and, hence, to a measurement which is not comparable with predictions based on Thermos. The calculated ratio of lattice born neutrons to source neutrons for each intracell traverse is listed in Table 5-9. This ratio is the highest in the cases of the greatest discrepancy, which

seems to be at variance with the possibility just outlined.

Since the experimental intracell traverses in a small assembly may be open to question, Thermos calculated values of the thermal utilization were used for the calculations of section 5. 5 below. The difference between the experimental and theoretical values of f are small since most of the neutron absorptions are in the fuel. If the experimental values of the flux traverse had been used, the values of f (and k_∞) would be about 1. 2 per cent higher in the 80. 2 per cent - 0. 0880 inch lattice.

5. 4. 4 Calculation of δ

One measurement of interest is the cadmium ratio of an infinitely dilute gold foil in the rod. From these data the value of a parameter, δ, can be obtained, where δ is defined by the statement (24): "δ/ρ_{28} is the fraction of epicadmium capture that is 1/v capture". It enters into the expression (5. 2-2) which was used for p_o in order to avoid counting epicadmium 1/v absorption in U^{238} in the resonance escape probability. The value of δ can be obtained from the cadmium ratio (R_o) of an infinitely dilute gold foil by using the relationship (24)

$$\delta = 0.0327[R_o-1]^{-1} \quad . \qquad (5.4\text{-}1)$$

The values of δ found for each lattice are listed in Table 5-9. These values were obtained by first finding the cadmium ratio in the rod from the gold flux traverses. The experimental points obtained in the rods were volume-weighted to obtain the cadmium ratio. The activities measured by gamma-ray counting were converted to equivalent cadmium ratios measured by beta-ray counting by use of the following relationship for 0. 005 inch gold foils;

$$[R_f-1]_\beta = 0.764[R_f-1]_\gamma \quad , \qquad (5.4\text{-}2)$$

which was determined by counting identical foils in both the gamma-ray counter and the beta-ray counter. The cadmium ratios were

Table 5-9

Experimental Values of δ from Gold Cadmium Ratios

D_2O Conc.	Rod Spacing	Distance from End (in.)	ϕ_e/ϕ_s	R_f^* (beta)	δ ± 2%
99.8%	0.880	11.37	2.4	2.08	0.0725
99.8%	1.128	9.57	1.0	2.58	0.0515
99.8%	1.340	9.65	0.84	3.31	0.0396
90.3%	0.880	11.39	8.7	2.49	0.0625
90.3%	1.128	11.28	4.4	3.35	0.0406
90.3%	1.340	11.31	3.1	4.35	0.0300
80.2%	0.880	11.38	23.0	3.12	0.0452
80.2%	1.128	11.29	10.4	3.98	0.0330
80.2%	1.340	11.32	6.3	5.13	0.0263

corrected to the critical assembly values using equation (2.5-4). The cadmium ratio of an infinitely thin foil was then found by using the relationship (5.1-4) together with the value of ERI/σ_o listed in Table 4-2, and by using a value of ERI/σ_o equal to 15.2 for the infinitely thin foil. Figure 5-8 is a graph of the results, which appear to be consistent with each other.

5.5 CALCULATION OF THE INFINITE MULTIPLICATION FACTOR OF THE LATTICES

With the data found in the lattices and the results of machine calculations, it was possible to calculate the infinite multiplication factor of the lattices. The various quantities entering the calculation and the results are summarized in Table 5-10. The errors quoted for the infinite multiplication factor reflect only the experimental errors of the resonance escape probability and the fast fission factor.

It is interesting to observe the effect of the addition of H_2O to the moderator. At the smallest lattice spacing of 0.880 inches, the infinite multiplication factor is increased by the addition of H_2O owing

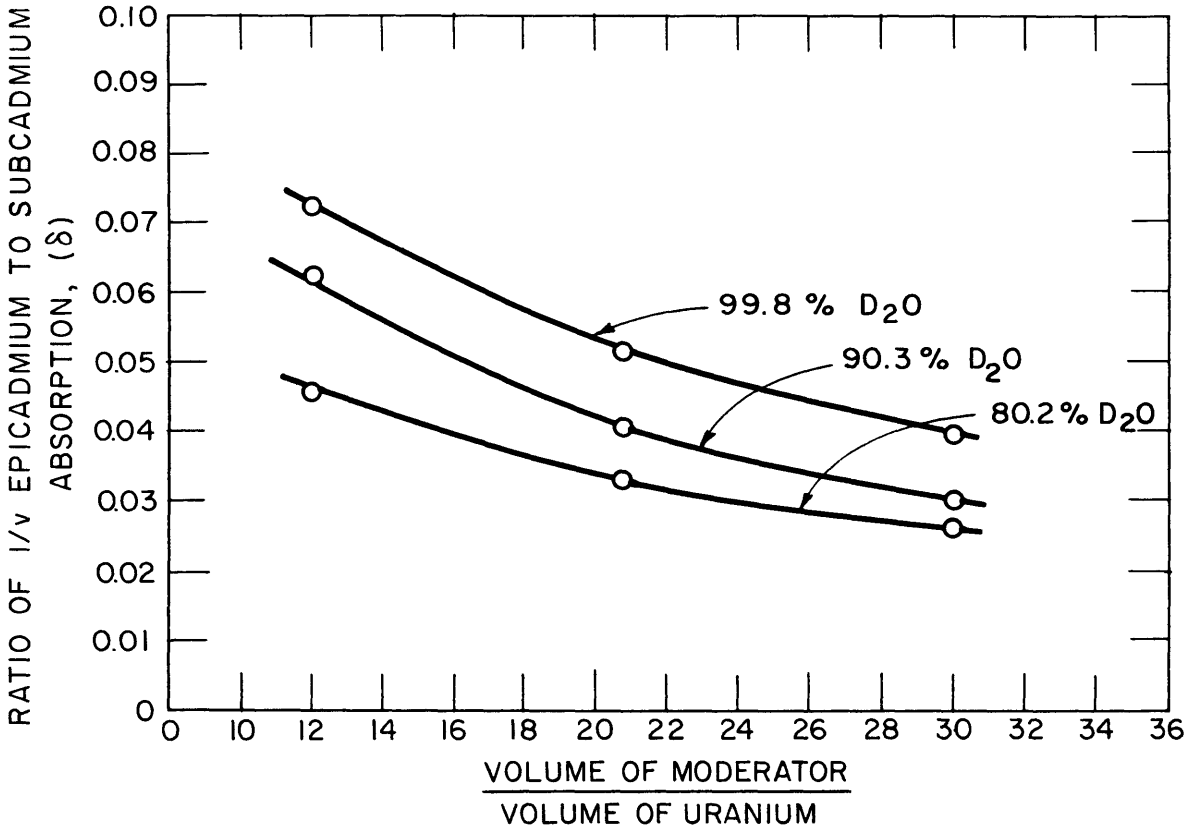

FIG. 5-8 EXPERIMENTAL VALUES OF δ IN 1/4 in. DIAMETER URANIUM RODS

to the increase in the resonance escape probability. At the widest lattice spacing of 1.340 inches, the infinite multiplication factor is decreased by the addition of H_2O owing to the decrease in the thermal utilization. At the intermediate spacing of 1.128 inches, the two effects nearly cancel each other as the H_2O content of the moderator is increased.

Table 5-10

Calculated Infinite Multiplication Factor (k_∞)

D_2O Conc.	Rod Spacing	η (Thermos)	ϵ (Measured) ± .001	p_o (Measured)	f (Thermos)	k_∞
99.8%	0.880	1.529	1.026	.735 ± .004	.976	1.126 ± .006
99.8%	1.128	1.536	1.018	.774 ± .005	.974	1.178 ± .008
99.8%	1.340	1.540	1.015	.845 ± .002	.971	1.282 ± .003
90.3%	0.880	1.537	1.026	.794 ± .002	.919	1.151 ± .003
90.3%	1.128	1.542	1.018	.840 ± .002	.880	1.160 ± .003
90.3%	1.340	1.544	1.015	.895 ± .002	.843	1.182 ± .003
80.2%	0.880	1.540	1.026	.839 ± .002	.866	1.148 ± .003
80.2%	1.128	1.543	1.018	.893 ± .002	.799	1.121 ± .003
80.2%	1.340	1.545	1.015	.932 ± .002	.738	1.079 ± .002

CHAPTER 6
CONCLUSIONS AND RECOMMENDATIONS

6.1 THEORY OF A SMALL ASSEMBLY - CONCLUSIONS

6.1.1 The Size of a Subcritical Assembly

One of the principal purposes of this work was to determine whether a small lattice could be used for cell measurements without loss of validity. The theory that has been developed here shows that the size of an assembly is important only in terms of the scaled dimensions of R/L and H/L, and the ratio τ_o/L^2. In terms of these dimensionless parameters, the lattices investigated in this work are among the smallest ever used. The "miniature lattice" used at the Brookhaven National Laboratory was actually a "large" assembly in terms of its scaled dimensions, since H_2O was used as its moderator.

An attempt to understand neutron behaviour in a small assembly led to the equations of sections 2.2 and 2.3. These general solutions of the exponential problem are not limited to small assemblies and are probably applicable over a wide range of subcritical systems. Different source conditions can also be treated within the same theoretical framework, since only the Fourier transform of the source condition need be known to solve the exponential problem presented here.

It is perhaps surprising that the theory gives good agreement with the flux curves, in view of the small size of the assemblies. The relatively large extrapolation distances required may indicate the lower limit of size at which simple boundary conditions can be used when age-diffusion theory is applied to a small assembly. It may be possible to extend the theory to even smaller assemblies, although it is likely that a more sophisticated treatment must then be used.

The fit of the theory to the experiments is encouraging and would seem to indicate that the reactor parameters measured have validity. However, since larger assemblies of this same enrichment, rod size, and spacing have not previously been investigated, the question of the significance of the results cannot yet be settled completely. Further measurements in much larger assemblies of this general type will be made in the near future at the M. I. T. Lattice Facility.

6. 1. 2 Corrections for Leakage and Source Effects in a Small Assembly

Correction methods have been developed for the leakage and source effects in small assemblies. The equations are given in sections 2. 5 through 2. 7. This part of the theory is not dependent on the previous treatment of the exponential problem. It can be applied by using any valid representation of the slowing down density and the thermal flux.

The treatment of the correction, to critical assembly values, of cadmium ratio measurements showed that measurements made in the asymptotic region of a subcritical assembly should give results identical with those made in a critical assembly. This theoretical prediction is not new. The correction for measurements made in a non-asymptotic region of a small assembly can be tested for consistency if two or more measurements are made in the same assembly. Application of this test to the ρ_{28} data showed good consistency in six of the eight lattices in which two measurements of ρ_{28} were made. This result is encouraging, and lends confidence to the method of correction as well to the use of the age-diffusion approximation in calculation of the slowing down densities and the thermal fluxes.

The theory for correction of the U^{238}/U^{235} fission ratio measurements can also be tested for consistency when measurements are made which differ only in the lattice spacing. This test was applied to the values of δ_{28} found for the three lattice spacings. The results again lend confidence to the method of correction. It

would seem that the correction for the flux shape is applicable to U^{238}/U^{235} fission ratio data measured in any exponential assembly, although the correction would be quite small in a large assembly.

It is recognized that consistency of these results among the small assemblies does not represent complete proof of the validity of the correction method. Further proof must await experimental measurements in larger lattices.

6. 1. 3 Position of Experiments in a Small Assembly

Three measures have been advanced for the evaluation of experimental position inside a subcritical assembly. The first is the determination of the extent of the asymptotic region, when it exists. If such a region is present, the cell measurements should be made inside it. By the use of the equations presented in sections 2. 2 or 2. 3, the extent of this region can be found in a proposed assembly. If such a region does not exist, as was the case in the lattices investigated for this report, the equations can be used to estimate the position where the flux variations will be smallest.

The second measure is the ratio of the lattice born and moderated neutron flux to the thermal neutron flux due to the source. The higher this ratio, the more representative the flux spectrum is of the lattice. The third measure is the magnitude of the thermal neutron flux in terms of the entering neutron current. Use of the equations of sections 2. 2 and 2. 3 provides a means of calculating values for these two measures and thus a way to evaluate a proposed experimental position.

In order to demonstrate the use of these measures, a table giving the above information for 128 possible lattices was prepared with only minor simplification of the theory. These results, listed with a sample problem in Appendix A, should be of considerable help in the future design of subcritical assemblies.

6. 1. 4 General Conclusions on the Use of Small Assemblies

The use of small assemblies is attractive owing to the ease of experimentation and the small amount of reactor materials used. Thus the present studies, carried out in part to determine whether or not there exists a lower limit to the useful size of a subcritical lattice, have a practical significance. If valid measurements of reactor parameters can be made in small subcritical assemblies it would be possible in the future to save both time and substantial sums of money in preliminary studies of new types of power reactors. The results obtained in this study indicate that an important potential for such economies exists in the use of small subcritical assemblies.

6. 2 THEORY OF A SMALL ASSEMBLY - RECOMMENDATIONS

It is important to make measurements in larger assemblies to further validate the data of this report and such measurements are strongly urged. Measurements of this nature, at least in the 99. 8 per cent D_2O range, are planned for the near future at the M. I. T. Lattice Facility.

It would be desirable to examine the boundary conditions used in the present theory. Among the problems which should be investigated are the size of the boundaries depending on the energy and the origin of the flux, and the effect of a non-isotropic source. Experimental investigation of these boundary conditions might be possible by the use of incident sources of varying neutron energy.

It also appears desirable to apply more rigorous theoretical methods, such as multigroup methods, to the problem of small assemblies.

6. 3 CALCULATIONS AND MEASUREMENTS IN LATTICES MODERATED BY H_2O AND D_2O

6. 3. 1 Conclusions

A summary of the calculated and measured quantities for lattices moderated by H_2O and D_2O is given in Table 5-10. These

values appear to be reasonably consistent with each other and were obtained in one of the smallest assemblies ever used for such purposes.

6. 3. 2 Recommendations

Measurements on assemblies with mixed moderators are interesting from a theoretical standpoint as well as for practical reasons, and more basic data are needed.

The measurement of ages to higher resonance energies than the indium resonance is of particular interest in the development and use of the theory of this report. These ages may also be calculated by using any of several machine codes. Among these are the Gam-1 code, (20), and the Corn Pone and the Chronos codes (12). It would be of interest to compare the results of machine calculations with the simple approximations used in this report for calculating ages.

It is important to resolve the discrepancies between the Thermos calculations and the measured intracell flux traverses. If the particular form of the scattering kernels of the D_2O and the HDO molecules are the cause of the discrepancy, a quantum mechanical approach probably will be necessary to obtain a better kernel. This problem is a difficult theoretical one, but work on it is under way at the Brookhaven National Laboratory.

Further measurements can be made with the present equipment and sets of rods. The measurements could be extended profitably in the direction of smaller lattice spacings and lower values of the D_2O content. Furthermore, the present assembly could be used for a study of the interaction effect in thin rods, over a much wider range of lattice spacing and moderator mixtures.

LITERATURE CITATIONS

In the following list of references, the proceedings of the first and second International Conferences on the Peaceful Uses of Atomic Energy, held at Geneva, are referred to as ICPUAE, (1955 and (1958).

(1) A. H. Barnes, et al, "The Exponential Experiments at Argonne National Laboratory", TID 5025. Also available in Reactor Science and Technology, Vol. 1, issues 1-3, pp. 131-46.

(2) G. Bell, Nuc. Sci. Eng., 5, 138 (1959).

(3) J. Bratten, Unpublished 22.42 course work, M. I. T. (1959).

(4) H. Brown and D. S. St. John, "Neutron Energy Spectrum in D_2O", DP-33 (1954).

(5) P. Brown, "Measurements of the Spatial and Energy Distribution of Thermal Neutrons in Heavy Water-Uranium Lattices", Ph. D. thesis, Nuclear Engineering Dept., M. I. T., to be completed in June, 1962, and published as an NYO report.

(6) F. E. Driggers and D. S. St. John, "Physics of Natural Uranium, Heavy Water Lattices", unpublished manuscript, Savannah River Laboratory.

(7) M. C. Edlund and G. K. Rhode, "Spectral Shift Control", Nucleonics, 16, No. 5, 80 (1958).

(8) E. Fermi and L. Marshall, "Spin Dependence of Slow Neutron Scattering by Deuterons", Phys. Rev., 75, 578 (1949).

(9) B. S. Finn and J. W. Wade, "Effect of the Contamination by Light Water on Lattices of Natural Uranium Rods in Heavy Water", Nuc. Sci. Eng., 7, 93 (1960).

(10) S. Glasstone and M. Edlund, The Elements of Nuclear Reactor Theory, D. Van Nostrand Co., Inc., Princeton, N. J., (1952), p. 263.

(11) H. Goldstein, P. Zweifel, and D. Foster, Jr., "The Slowing Down of Neutrons in Hydrogeneous Media-Status of Theory and Experiment", ICPUAE (1958), paper 2375.

(12) H. Goldstein et al., "Calculations of Neutron Age in H_2O and other Materials", ORNL-2639 (1961).

(13) E. Hellstrand, J. Appl. Phys., 28, 1493 (1957).

(14) H. C. Honeck, "The Distribution of Thermal Neutrons in Space and Energy in Reactor Lattices. Part I: Theory", Nuc. Sci. Eng., 8, 193 (1960).

(15) H. C. Honeck and I. Kaplan, "The Distribution of Thermal Neutrons in Space and Energy in Reactor Lattices. Part II: Comparision of Theory and Experiment", Nuc. Sci. Eng., 8, 203 (1960).

(16) H. C. Honeck, "Thermal Neutron Spectra in Slab Lattices", Trans. Am. Nuc. Soc., 3, No. 2, 489 (Dec. 1960).

(17) H. C. Honeck, "Thermos, a Thermalization Transport Theory Code for Reactor Lattice Calculations", BNL-5826 (1961).

(18) D. J. Hughes and J. A. Harvey, "Neutron Cross Sections", BNL-325 (1955).

(19) G. D. Joanou, A. J. Goodjohn, and N. F. Wikner, "Moments Calculations of the Fermi Age in Various Moderators", Trans. Am. Nuc. Soc., 4, No. 2, 24-1 (Nov. 1961).

(20) G. D. Joanou and J. S. Dudek, "GAM-1: A Consistent P_1 Multigroup Code for the Calculation of Fast Neutron Spectra and Multigroup Constants", GA-1850 (1961).

(21) I. Kirshenbaum, Physical Properties and Analysis of Heavy Water, McGraw-Hill Book Co., N. Y., (1951).

(22) H. Kouts, et al., "Exponential Experiments With Slightly Enriched Uranium Rods in Ordinary Water", ICPUAE (1955), paper 600.

(23) H. Kouts, et al., "Physics of Slightly Enriched, Normal Water Lattices; Theory and Experiment", ICPUAE (1958), paper 1841.

(24) H. Kouts and R. Sher, "Exponential Studies of Slightly Enriched Uranium Water Moderated Lattices; 0.600 Inch Diameter Rods". In Progress in Nuclear Energy, Series II, Vol. 2, Pergamon Press, London, (1961), pp. 285-335.

(25) R. B. Leachman, "The Fission Process-Mechanisms and Data" ICPUAE (1958), paper 2467.

(26) M. Nelkin, "Scattering of Slow Neutrons by Water", Phys. Rev., 119, 741 (1960).

(27) W. G. Pettus, "Neutron Age Measurements in Water and in Metal-Water Lattices", BAW-146 (1960).

(28) A. Radkowsky, "Temperature Dependence of Thermal Transport Mean Free Path", ANL-4476 (1950).

(29) The Reactor Handbook, Vol. 1, Physics, AECD-3645, (1945), p. 487.

(30) D. M. Roberts and W. G. Pettus, "Neutron Age in ThO_2-D_2O-H_2O Lattices", Trans. Am. Nuc. Soc., 4, No. 2, 24-2 Nov. 1961).

(31) T. Rockwell III (Ed.), Reactor Shielding Design Manual, D. Van Nostrand Co., Inc., Princeton, N. J., (1956), p. 408.

(32) J. B. Sampson and J. Chernick, "Resonance Escape Probability in Thermal Reactors". In Progress in Nuclear Energy, Series I, Vol. 2, Pergamon Press, London, (1961), p. 223.

(33) L. Silverman and W. Bradshaw, Anal. Chim. Acta., 10, 68 (1954).

(34) I. A. Sneddon, Fourier Transforms, McGraw-Hill Book Co., N. Y., (1951).

(35) N. L. Snidow, et al., "Critical Experiments on 4 per cent Enriched UO_2 Lattices Moderated by D_2O-H_2O Mixtures", Trans. Am. Nuc. Soc., 4, No. 2, 28-4, (Nov. 1961).

(36) J. W. Wade, "Neutron Age in Mixtures of D_2O and H_2O", Nuc. Sci. Eng., 4, 12 (1958).

(37) D. Wehmeyer, Personal communication. Dec., 1961.

(38) A. Weitzberg, I. Kaplan, and T. J. Thompson, "Measurements of Neutron Capture in U^{238} in Lattices of Uranium Rods in Heavy Water", NYO-9659 (1962).

(39) C. E. Wikdahl and F. Åkerhielm, "Measurements of Disadvantage Factors in a Small Mockup", ICPUAE (1958), paper 212.

(40) W. A. Wittkopf and K. E. Roach, "Nuclear Analysis of 4 per cent Enriched UO_2 Lattices Moderated by D_2O-H_2O Mixtures", Trans. Am. Nuc. Soc., 4, No. 2, 28-5, (Nov. 1961).

(41) J. Wolberg, I. Kaplan, and T. J. Thompson, "A Study of the Fast Fission Effect in Lattices of Uranium Rods in Heavy Water", NYO-9661 (1962).

NOMENCLATURE

SUPERSCRIPTS

^{e} denotes quantity pertaining to neutrons born and moderated in subcritical exponential lattice.

^{f} denotes quantity pertaining to fission energy neutrons.

^{i} denotes quantity pertaining to a theoretical infinite assembly.

^{s} denotes quantity pertaining to source neutrons.

* denotes quantity pertaining to a theoretical bare critical assembly (except in the case of v^{*}).

^{28} denotes a property of U^{238}.

^{25} denotes a property of U^{235}.

$^{-}$ operational notation indicating the Hankel or Sine transformation of the function over which the bar is written (except for $\bar{\mu}_i$ and the Thermos spectrum averaged quantities $\bar{D}$, $\bar{\lambda}_t$, $\bar{\Sigma}_a$).

$^{=}$ operational notation indicating the double transformation of the function over which the double bar is written.

SUBSCRIPTS

$_{L}$ denotes quantity pertaining to slightly enriched uranium in lattice assembly.

$_{D}$ denotes quantity pertaining to depleted uranium metal in foil.

$_{N}$ denotes quantity pertaining to natural uranium metal in foil.

Other subscripts are listed with the particular variables to which they pertain.

BRACKETS

[ ] Square brackets denote multiplication.

( ) Curved brackets denote the argument of a function.

SYMBOLS

A atomic mass (amu).

A_{eff} effective atomic mass (amu).

a radius in terms of the thermal diffusion length (R/L).

$B^2_{i,n}$ buckling of the i, n mode (cm^{-2}).

B^2_m material buckling (cm^{-2}).

C constant from integration (see equation (2. 2-35)).

D_e thermal diffusion constant for lattice born neutrons (cm).

D_s thermal diffusion constant for source neutrons (cm).

$\bar{D}$ Thermos spectrum averaged thermal diffusion constant (cm).

d_a axial extrapolation distance on one end (cm).

E energy (ev).

ERI effective resonance integral (barns).

E_{res} energy level of resonance (ev).

$F(r)$ incoming thermal neutron source current on end of assembly (neutrons/cm^2sec).

$F(\theta, \Sigma^f_s r_k)$ function defined by equation (2. 6-8).

$F_1(\theta, \Sigma^f_s r_k, \gamma/\Sigma^f_s)$ function defined by equation (2. 6-10).

f the thermal utilization (the fraction of thermal neutrons absorbed in the fuel).

f_j fractional contribution of the j^{th} resonance to the ERI.

G ratio of the thermal neutron absorptions in U^{238} to the total absorptions in the uranium.

H extrapolated height of a cylindrical assembly (cm).

I fission rate in the uranium rod (fissions/cm^3sec).

$J_o(\ )$ Bessel function of the first kind of order 0.

$J_1(\ )$ Bessel function of the first kind of order 1.

$K_p(\ )$ point kernel for the uncollided fast flux.

k_∞ infinite multiplication factor.

$k_{i,n}$ finite multiplication factor for the i, n mode.

L thermal neutron diffusion length (cm).

L_e thermal neutron diffusion length for lattice born neutrons (cm).

ℓ_1 non-leakage probability in the fast energy region.

ℓ_2 non-leakage probability in the epithermal energy region.

ℓ_3 non-leakage probability in the thermal energy region.

$M(E)$ Maxwellian neutron energy distribution.

N atomic concentration (atoms/cm^3 except in foils where it represents atoms/cm^2).

$N_n(\underline{r}, v)$ density of neutrons of speed v at radius $\underline{r}$ from a rod center (neutrons/cm^3).

n_i mole fraction of species i.

P geometric probability that a fast neutron will reach a foil.

$P(t)$ ratio of U^{235} fission product activity to U^{238} fission product activity per fission.

p_o resonance escape probability to thermal energies.

p_j resonance escape probability to the j^{th} resonance energy level.

$q(\tau, r, z)$ slowing down density in a system with no resonance absorption at the energy corresponding to age τ, (neutrons/cm^3sec).

R extrapolated radius of a cylindrical assembly (cm).

R_f cadmium ratio of a foil.

R_o cadmium ratio of an infinitely dilute gold foil

R_r radius of a fuel rod.

R_{28} cadmium ratio of U^{238} in a rod.

r radial coordinate in an exponential assembly (cm).

$\underline{r}$ radial coordinate from a rod center (cm).

r_f radial position of a foil (cm).

r_k radial distance from one rod to another rod (cm).

$S(\underline{r})$ relative thermal neutron density in a cell (normalized to 1.0 at the cell center).

T irradiation time (min).

t time delay from the end of the irradiation until count is made (min).

V volume (cm^3).

V_a volume of aluminum in cell (cm^3).

V_m volume of moderator in cell (cm^3).

V_u volume of uranium in cell (cm^3).

v thermal neutron speed in terms of 2200. m/sec.

v^* upper energy cutoff for thermos calculations.

W average difference in weights in D_2O determination (g).

X dummy variable representing θ.

Y dummy variable representing $\Sigma_s^f r_k$.

Z dummy variable representing γ/Σ_s^f.

z axial coordinate in an exponential assembly (cm).

z_f axial position of a foil (cm).

α_{28} ratio of captures to fissions for fast neutrons in U^{238}.

α experimental variable defined by equation (2.4-9).

β_i^2 quantity defined by equation (2.2-12) (cm^{-2}).

γ inverse thermal neutron relaxation length (cm^{-1}).

$\gamma(t)$ ratio of the fission product activity of a depleted foil to the fission product activity of a natural foil.

δ ratio of 1/v epicadmium capture to thermal capture in a U^{238} foil.

δ_{28} ratio of U^{238} fissions to U^{235} fissions in a rod.

δ_{28}^{sr} single rod value of δ_{28}.

ϵ fast fission factor (ratio of neutrons released from fast fission to neutrons released from thermal fission in a rod).

η number of neutrons released per thermal absorption in a rod.

θ angular variable.

λ radio-active decay constant (min^{-1}).

$\lambda_t(E)$ thermal neutron transport mean free path at energy E (cm).

$\bar{\lambda}_t$ Thermos spectrum averaged thermal neutron transport mean free path (cm).

μ_i roots of the equation $J_o(\mu_i) = 0$: (The first members of the series are 2.4048, 5.5201, 8.6537, . . .).

$\bar{\mu}_i$ average cosine of the scattering angle per collision.

ν_{25} average number of neutrons released per fission in U^{235}.

ν_{28} average number of neutrons released per fission in U^{238}.

ξ average neutron logarithmic energy decrement per collision.

π 3.14159 .

ρ distance from origin of fast neutron to foil (cm).

ρ_{28} ratio of epicadmium to subcadmium captures in U^{238}.

ρ_s density of sample in D_2O determination (g/cm^3).

ρ_{H_2O} density of H_2O in D_2O determination (g/cm^3).

ρ_{air} density of air in D_2O determination (g/cm^3).

σ_j contribution of resonance at the j^{th} energy level to the effective resonance integral (barns).

σ_o microscopic absorption cross section at 2200. m/sec (barns).

σ_{res} microscopic absorption cross section at a resonance energy level (barns).

σ_{epi} effective microscopic epicadmium absorption cross section (barns).

σ_{sub} effective microscopic subcadmium absorption cross section (barns).

$\sigma_{1/v}(E)$ 1/v absorption cross section in the 1/E slowing down energy region (barns).

Σ_a macroscopic thermal neutron absorption cross section including fission (cm^{-1}).

Σ_c macroscopic thermal neutron capture cross section (cm^{-1}).

Σ_f macroscopic thermal neutron fission cross section (cm^{-1}).

Σ_{total} macroscopic thermal neutron total cross section (cm^{-1}).

$\bar{\Sigma}_a$ Thermos spectrum averaged macroscopic thermal neutron absorption cross section including fission (cm^{-1}).

τ Fermi age of neutrons (cm^2).

τ_{in} Fermi age of neutrons to the indium resonance (cm^2).

τ_o Fermi age of neutrons to thermal energies (cm^2).

τ_r Fermi age of neutrons to a resonance energy (cm^2).

$\phi(E)$ neutron flux at energy E (neutrons/cm^2sec per ev).

ϕ_e thermal flux of lattice born and moderated neutrons (neutrons/cm^2sec).

ϕ_f fast neutron flux (neutrons/cm^2sec).

ϕ_s thermal flux of source neutrons (neutrons/cm^2sec).

ϕ_m average resonance flux in the moderator (neutrons/cm^2sec).

ϕ_u average resonance flux in the fuel (neutrons/cm^2sec).

ϕ_t total thermal flux (neutrons/cm^2sec).

ψ_i^2 radial buckling of the i^{th} mode (cm^{-2}).

χ counter efficiency.

∇^2 Laplacian operator.

APPENDIX A

QUALITY AND MAGNITUDE OF THE THERMAL FLUX IN EXPONENTIAL ASSEMBLIES

1. Description of the Tables

The following tables were obtained from equations (2.9-9), (2.9-10), (2.9-11), (2.9-12), and (2.9-13) with the aid of an IBM 709 computer. They apply to a cylindrical subcritical assembly with an extrapolated height equal to the extrapolated diameter. The lattice born slowing down and thermal fluxes were assumed to extrapolate to zero on all the boundaries. The thermal source flux was assumed to be caused by a plane current of F neutrons/cm^2 sec in the plane source case and a current of F $J_o(2.405r/R)$ neutrons/cm^2 sec in the J_o source case. The axial distance, z, was measured from the source end.

Two points are given for each lattice which is characterized by the parameters k_∞, τ_o/L^2, a particular source condition, and a scaled radius, R/L. The first point is the distance from the source end, along the central axis, where the asymptotic region begins. This region is defined to exist where a nuclide with a resonance energy whose age is $0.7\,\tau_o$ (about 5 to 25 ev) has a cadmium ratio within 1 per cent of what would be measured in a critical assembly. The second point is chosen along the central axis, about 30 per cent of the total length farther into the asymptotic region from the first point. Values of the fluxes at positions between the two points can be found by interpolation on a semi-log plot.

Two parameters are listed for each of the above two points. The first parameter is the ratio of lattice born and moderated thermal neutrons to thermal source neutrons. This dimensionless ratio is a measure of the quality of the thermal flux. The higher the ratio, the more nearly representative of a critical assembly the thermal flux is. The second parameter is the value of the dimensionless ratio, $[\phi_e/F][D/L]$. This ratio is a measure of the magnitude of the thermal flux available at the two points evaluated, in terms of the incoming

current at the source end. The normalizing factor (D/L) must be known in order to find the absolute value of the lattice born thermal flux in terms of the absolute value of the thermal current.

2. Sample Case

A sample case to illustrate the use of the tables follows: Consider a cylindrical subcritical assembly with the calculated homogeneous properties:

$k_\infty = 1.200$ (Infinite multiplication factor)

$\tau_o = 100.\ cm^2$ (Age to thermal energies)

$L^2 = 100.\ cm^2$ (Thermal diffusion area)

$R = 60.$ cm (Extrapolated radius)

$H = 120.$ cm (Extrapolated radius)

$F = 10^8$ neutrons/cm^2sec (Plane source)

$D = 1.0$ cm (Thermal diffusion constant)

By using the entering values:

$k_\infty = 1.200$

$\tau_o/L^2 = 1.0$

$R/L = 6.0$

the following quantities can be obtained from Table A-2:

	Asymptotic Point	Second Point
z/H	0.30	0.65
ϕ_e/ϕ_s	9.14	263.
$[\phi_e/F][D/L]$	0.234	0.0826
R_{crit}/L	9.39	

The following information can be obtained from these data:

1. The asymptotic region begins at
   $[0.30][120] = 36.$ cm
   from the extrapolated source end. At that point, the lattice

born thermal flux is

$$[0.234][10/1.0][10^8] = 2.34 \times 10^8 \text{ neutrons/cm}^2 \text{ sec;}$$

the thermal flux due to the source is

$$[2.34][10^8]/[9.14] = 0.256 \times 10^8 \text{ neutrons/cm}^2 \text{ sec;}$$

the ratio of the lattice born thermal flux to the total thermal flux is

$$9.14/[9.14 + 1.0] = 0.89, \text{ or } 89 \text{ per cent.}$$

2. In the asymptotic region, at

$$[0.65][120] = 78 \text{ cm}$$

from the extrapolated source end, the lattice born thermal flux is

$$0.0826[10/1.0][10^8] = 0.826 \times 10^8 \text{ neutrons/cm}^2 \text{ sec;}$$

the thermal flux due to the source is

$$[0.826 \times 10^8]/263 = 3.14 \times 10^5 \text{ neutrons/cm}^2 \text{ sec;}$$

the ratio of the lattice born flux to the total thermal flux is

$$263/[263 + 1] = .996, \text{ or } 99.6 \text{ per cent.}$$

3. The critical radius is

$$9.39[10] = 93.9 \text{ cm}$$

for a height of $2[93.9]$, or 187.8 cm.

Values of the various fluxes for positions between 36 cm and 78 cm can be obtained from the above data by using a semi-log interpolation.

Since the equations were solved for steps of 0.05 in the variable z/H, the asymptotic point for each lattice is given at the first step where the asymptotic condition holds true.

Table A-1. Quality and Magnitude of the Thermal Flux in Cylindrical Exponential Assemblies ($k_\infty = 1.100$).

$k_\infty = 1.100$ Plane Source

τ_o/L^2	R/L	Asymptotic Point			Second Point		
		z/H	ϕ_e/ϕ_s	Mag. ϕ_e	z/H	ϕ_e/ϕ_s	Mag. ϕ_e
0.25	5.0	0.15	1.53	0.327	0.70	112.	0.0658
	6.0	0.15	2.67	0.433	0.55	148.	0.166
	7.0	0.15	4.52	0.548	0.45	189.	0.319
	8.0	0.10	3.04	0.612	0.40	333.	0.532
	10.20	Crit.					
1.0	6.0	0.35	11.2	0.154	0.80	502.	0.0231
	8.0	0.25	15.6	0.282	0.60	1580.	0.0961
	10.0	0.20	23.6	0.432	0.50	5610.	0.247
	12.0	0.10	6.98	0.634	0.40	13,000.	0.874
	13.02	Crit.					
2.0	8.0	0.35	33.0	0.119	0.65	1400.	0.0376
	10.0	0.30	72.0	0.177	0.60	11,600.	0.0676
	12.0	0.25	107.	0.266	0.55	73,600.	0.134
	14.0	0.20	115.	0.427	0.50	401,000.	0.332
	16.00	Crit.					
3.0	10.0	0.35	109.	0.0986	0.75	72,700.	0.0203
	12.0	0.25	64.5	0.160	0.55	36,600.	0.0665
	14.0	0.25	225.	0.205	0.55	512,000.	0.105
	16.0	0.20	186.	0.309	0.45	449,000.	0.250
	18.50	Crit.					

$k_\infty = 1.100$ J_o-Shaped Source

τ_o/L^2	R/L	Asymptotic Point			Second Point		
		z/H	ϕ_e/ϕ_s	Mag. ϕ_e	z/H	ϕ_e/ϕ_s	Mag. ϕ_e
0.25	5.0	0.15	1.32	0.224	0.70	108.	0.0413
	6.0	0.15	2.26	0.302	0.55	138.	0.105
	7.0	0.15	3.76	0.386	0.45	168.	0.203
	8.0	0.10	2.47	0.446	0.40	283.	0.339
	10.20	Crit.					
1.0	6.0	0.35	9.95	0.100	0.80	487.	0.0145
	8.0	0.25	12.9	0.190	0.60	1430.	0.0605
	10.0	0.20	18.7	0.297	0.50	4700.	0.156
	12.0	0.10	5.30	0.450	0.40	10,100.	0.552
	13.02	Crit.					
2.0	8.0	0.35	28.0	0.0774	0.65	1280.	0.0236
	10.0	0.30	58.0	0.118	0.60	10,000.	0.0426
	12.0	0.25	82.9	0.179	0.55	60,300.	0.0841
	14.0	0.20	86.1	0.289	0.50	312,000.	0.209
	16.00	Crit.					
3.0	10.0	0.35	89.0	0.0646	0.75	65,400.	0.0127
	12.0	0.30	149.	0.0945	0.60	85,600.	0.0351
	14.0	0.25	171.	0.139	0.55	408,000.	0.0658
	16.0	0.20	138.	0.210	0.45	336,000.	0.157
	18.50	Crit.					

Table A-2. Quality and Magnitude of the Thermal Flux in Cylindrical Exponential Assemblies ($k_\infty = 1.200$).

$k_\infty = 1.200$ Plane Source

τ_o/L^2	R/L	Asymptotic Point			Second Point		
		z/H	ϕ_e/ϕ_s	Mag. ϕ_e	z/H	ϕ_e/ϕ_s	Mag. ϕ_e
0.25	3.0	0.25	0.934	0.153	0.85	11.1	0.0180
	4.0	0.20	1.60	0.285	0.75	46.8	0.0569
	5.0	0.15	2.00	0.426	0.60	106.	0.187
	6.0	0.15	4.14	0.670	0.50	244.	0.513
	7.29	Crit.					
1.0	5.0	0.40	8.73	0.134	0.75	104.	0.0354
	6.0	0.30	9.14	0.234	0.65	263.	0.0826
	7.0	0.25	11.8	0.349	0.55	468.	0.186
	8.0	0.15	5.28	0.477	0.50	1280.	0.399
	9.39	Crit.					
2.0	7.0	0.40	34.2	0.118	0.70	905.	0.0406
	8.0	0.35	48.4	0.174	0.65	2660.	0.0712
	9.0	0.30	57.2	0.256	0.60	6930.	0.131
	10.0	0.25	57.9	0.389	0.50	6790.	0.299
	11.57	Crit.					
3.0	9.0	0.35	70.1	0.127	0.65	6580.	0.0498
	10.0	0.30	71.4	0.176	0.60	14,400.	0.0842
	11.0	0.30	172.	0.233	0.60	74,200.	0.133
	12.0	0.25	146.	0.361	0.50	50,300.	0.305
	13.39	Crit.					

$k_\infty = 1.200$ J_o-Shaped Source

τ_o/L^2	R/L	Asymptotic Point			Second Point		
		z/H	ϕ_e/ϕ_s	Mag. ϕ_e	z/H	ϕ_e/ϕ_s	Mag. ϕ_e
0.25	3.0	0.25	0.860	0.0982	0.85	11.1	0.0113
	4.0	0.20	1.42	0.188	0.75	46.1	0.0356
	5.0	0.15	1.69	0.289	0.60	102.	0.117
	6.0	0.15	3.41	0.455	0.50	223.	0.322
	7.29	Crit.					
1.0	5.0	0.40	8.02	0.0854	0.75	102.	0.0222
	6.0	0.35	13.6	0.136	0.65	249.	0.0518
	7.0	0.30	19.2	0.214	0.60	425.	0.117
	8.0	0.15	4.14	0.324	0.50	1110.	0.251
	9.39	Crit.					
2.0	7.0	0.40	29.9	0.0759	0.70	850.	0.0254
	8.0	0.35	40.7	0.112	0.65	2420.	0.0446
	9.0	0.30	46.1	0.167	0.60	6100.	0.0824
	10.0	0.25	44.9	0.255	0.50	5660.	0.188
	11.57	Crit.					
3.0	9.0	0.35	57.6	0.0820	0.65	5880.	0.0313
	10.0	0.35	143.	0.104	0.60	12,500.	0.0528
	11.0	0.30	134.	0.152	0.60	62,800.	0.0831
	12.0	0.25	109.	0.236	0.50	40,400.	0.192
	13.39	Crit.					

Table A-3. Quality and Magnitude of the Thermal Flux in Cylindrical Exponential Assemblies (k_∞ = 1.300).

k_∞ = 1.300 Plane Source

τ_o/L^2	R/L	Asymptotic Point			Second Point		
		z/H	ϕ_e/ϕ_s	Mag. ϕ_e	z/H	ϕ_e/ϕ_s	Mag. ϕ_e
0.25	2.0	0.40	0.612	0.0494	0.85	2.18	0.00924
	3.0	0.25	1.08	0.176	0.75	10.9	0.0412
	4.0	0.20	1.98	0.352	0.60	32.4	0.159
	5.0	0.15	2.86	0.611	0.50	99.7	0.521
	6.01	Crit.					
1.0	4.0	0.55	8.79	0.0681	0.85	36.8	0.0168
	5.0	0.40	11.1	0.171	0.75	153.	0.0518
	6.0	0.30	12.9	0.331	0.65	481.	0.151
	7.0	0.20	10.4	0.624	0.55	1360.	0.542
	7.80	Crit.					
2.0	6.0	0.45	25.5	0.101	0.80	559.	0.0257
	7.0	0.40	48.0	0.166	0.75	2570.	0.0555
	8.0	0.30	37.8	0.305	0.65	5920.	0.159
	9.0	0.25	58.6	0.647	0.60	29,800.	0.565
	9.63	Crit.					
3.0	7.0	0.45	47.4	0.0800	0.75	1220.	0.0262
	8.0	0.40	77.8	0.124	0.70	4230.	0.0497
	9.0	0.35	110.	0.198	0.60	6190.	0.117
	10.0	0.30	143.	0.353	0.55	17,400.	0.279
	11.16	Crit.					

k_∞ = 1.300 J_o-Shaped Source

τ_o/L^2	R/L	Asymptotic Point			Second Point		
		z/H	ϕ_e/ϕ_s	Mag. ϕ_e	z/H	ϕ_e/ϕ_s	Mag. ϕ_e
0.25	2.0	0.40	0.593	0.0310	0.85	2.17	0.00577
	3.0	0.25	0.989	0.113	0.75	10.8	0.0258
	4.0	0.20	1.74	0.231	0.60	31.5	0.0997
	5.0	0.15	2.39	0.407	0.50	93.3	0.327
	6.01	Crit.					
1.0	4.0	0.55	8.48	0.0428	0.85	36.4	0.0105
	5.0	0.40	10.2	0.109	0.75	149.	0.0324
	6.0	0.30	11.1	0.214	0.65	455.	0.0946
	7.0	0.25	18.3	0.428	0.55	1230.	0.339
	7.80	Crit.					
2.0	6.0	0.50	37.9	0.0548	0.80	541.	0.0161
	7.0	0.40	41.8	0.106	0.75	2430.	0.0347
	8.0	0.35	67.0	0.185	0.65	5390.	0.0992
	9.0	0.25	45.3	0.415	0.60	26,200.	0.353
	9.63	Crit.					
3.0	7.0	0.50	75.2	0.0434	0.80	1870.	0.0127
	8.0	0.40	66.1	0.0793	0.70	3900.	0.0311
	9.0	0.35	89.2	0.127	0.60	5440.	0.0735
	10.0	0.30	111.	0.226	0.55	14,700.	0.175
	11.16	Crit.					

Table A-4. Quality and Magnitude of the Thermal Flux in Cylindrical Exponential Assemblies ($k_\infty = 1.400$).

$k_\infty = 1.400$ Plane Source

τ_o/L^2	R/L	Asymptotic Point			Second Point		
		z/H	ϕ_e/ϕ_s	Mag. ϕ_e	z/H	ϕ_e/ϕ_s	Mag. ϕ_e
0.25	2.0	0.40	0.675	0.0545	0.85	2.45	0.0104
	3.0	0.25	1.24	0.202	0.70	11.6	0.0650
	4.0	0.20	2.51	0.447	0.55	36.7	0.284
	5.0	0.15	6.49	1.39	0.50	391.	2.04
	5.25	Crit.					
1.0	-	-	-	-	-	-	-
	4.0	0.55	10.5	0.0817	0.85	46.4	0.0212
	5.0	0.40	14.6	0.223	0.75	230.	0.0781
	6.0	0.30	21.1	0.540	0.65	1060.	0.333
	6.86	Crit.					
2.0	5.0	0.55	20.1	0.0612	0.85	142.	0.0155
	6.0	0.45	32.9	0.130	0.80	817.	0.0376
	7.0	0.35	38.0	0.269	0.70	2810.	0.126
	8.0	0.30	90.6	0.731	0.60	10,500.	0.636
	8.49	Crit.					
3.0	6.0	0.55	46.9	0.0524	0.85	555.	0.0133
	7.0	0.45	61.3	0.104	0.80	2880.	0.0298
	8.0	0.40	115.	0.183	0.70	7530.	0.0884
	9.0	0.30	90.1	0.402	0.65	37,200.	0.282
	9.85	Crit.					

$k_\infty = 1.400$ J_o-Shaped Source

τ_o/L^2	R/L	Asymptotic Point			Second Point		
		z/H	ϕ_e/ϕ_s	Mag. ϕ_e	z/H	ϕ_e/ϕ_s	Mag. ϕ_e
0.25	2.0	0.40	0.654	0.0342	0.85	2.45	0.00650
	3.0	0.25	1.14	0.130	0.70	11.5	0.0406
	4.0	0.20	2.20	0.291	0.55	35.3	0.178
	5.0	0.15	5.24	0.893	0.50	364.	1.28
	5.25	Crit.					
1.0	-	-	-	-	-	-	-
	4.0	0.55	10.2	0.0513	0.85	45.9	0.0132
	5.0	0.40	13.3	0.142	0.75	224.	0.0488
	6.0	0.30	17.9	0.345	0.65	1000.	0.208
	6.86	Crit.					
2.0	5.0	0.60	28.0	0.0324	0.85	140.	0.00971
	6.0	0.45	29.7	0.0821	0.80	790.	0.0235
	7.0	0.40	63.1	0.160	0.70	2630.	0.0786
	8.0	0.30	72.7	0.463	0.60	9370.	0.398
	8.49	Crit.					
3.0	6.0	0.55	43.5	0.0330	0.85	540.	0.00829
	7.0	0.45	54.2	0.0655	0.80	2750.	0.0186
	8.0	0.40	97.0	0.116	0.70	6930.	0.0553
	9.0	0.35	180.	0.255	0.65	33,100.	0.176
	9.85	Crit.					

APPENDIX B

THE EFFECT OF AN EXPONENTIAL THERMAL FLUX DISTRIBUTION ON THE MEASUREMENT OF THE U^{238}/U^{235} FISSION RATIO

1. Single Rod Value

Consider a foil exposed in a rod at position $(0, z_f)$ in an exponential assembly with the coordinate system of Figure 2-1. The geometric probability, P, of a neutron reaching the foil if it is born at position (0, z) on the center line of the same rod is

$$P = \frac{2\pi\rho^2[1 - \text{Cos}\,\theta]}{4\pi\rho^2} \quad , \tag{B-1}$$

where

$$\rho^2 = [z-z_f]^2 + R_r^2 \quad ,$$

$$\theta = \arctan\,(R_r/[z-z_f]) \quad ,$$

and

$$R_r = \text{the radius of the rod} \quad .$$

If the neutron were born at a distance of three rod radii away from the foil, then

$$z - z_f = 3R_r \quad ,$$

$$\theta = \arctan\,(1/3) = 18.4° \quad ,$$

and

$$P = \frac{1.0 - 0.949}{2} = 0.025 \quad .$$

This value can be compared with the probability, P = 0.500, that a neutron born just next to the foil will reach the foil. It is evident that almost all of the neutrons which cause fast fission in the foil in a single rod measurement are born in the rod at positions within three rod radii of the foil. For a rod 1/4 inch in diameter, that distance is 0.375 inches, or 0.953 cms from the foil.

The birth rate density of fission energy neutrons in the rod is proportional to the thermal flux. In an exponential assembly with the coordinate system of Figure 2-1, the thermal flux can be assumed to have an exponential decay in the axial direction and a J_o-distribution in the radial direction. For the single rod value, the effect of the J_o-distribution may be neglected. The effect that the exponential distribution of the birth rate density has on the number of fast neutrons arriving at the foil will now be calculated. Consider the sum of fast neutrons born at three rod radii above and below the foil, in both an exponential assembly and in an infinite assembly. The ratio of the sums of the two birth rates is

$$\frac{\text{Birth rate density (infinite)}}{\text{Birth rate density (exponential)}} = \frac{1.0 + 1.0}{\exp(+3\gamma R_r) + \exp(-3\gamma R_r)} ,$$

where both the sums were normalized to a birth rate density of 1.0 at the foil position. In the Small Exponential Assembly a typical value of γ, the inverse thermal relaxation length, is

$$\gamma = 0.09 \text{ cm}^{-1} .$$

Substitution of this value, together with the radius of 0.318 cm for a 1/4 inch diameter rod, yields the value

$$\frac{\text{Birth rate density (infinite)}}{\text{Birth rate density (exponential)}} = 0.9963 .$$

Thus, the difference between a flat flux and an exponential flux in this case will change the sum of the birth rate densities at three rod radii from the foil by less than 0.4 per cent. Since the origin of nearly all the fast neutrons causing fast fission in the foil is closer than three rod radii, the effect of the exponential flux shape on the measured single rod value of the U^{238}/U^{235} fission ratio is negligible. This would not necessarily be true for thicker rods in the same thermal flux gradient.

2. The Interaction Effect

The variation in the interaction effect in an exponential assembly was considered in section 2.6 and a correction factor for the infinite

case was obtained as the right side of equation (2.6-7). Evaluation of the correction factor involves two integrals denoted by $F(\pi/2, \Sigma_s^f r_k)$ and $F_1(\theta, \Sigma_s^f r_k, \pm\gamma/\Sigma_s^f)$, which are defined in equations (2.6-8) and (2.6-10), respectively. It should be noted that the integral $F(\pi/2, \Sigma_s^f r_k)$ is merely the special case of $F_1(\pi/2, \Sigma_s^f r_k, \pm\gamma/\Sigma_s^f)$ when γ/Σ_s^f is equal to zero.

These integrals were evaluated on an IBM 7090 computer over the following range of parameters:

a. $\theta = \pi/2$

b. $\Sigma_s^f r_k = 0.5,\ 1.0,\ 1.5,\ 2.0,\ 2.5,\ 3.0,\ 4.0,\ 5.0,\ 6.0,\ 7.0$

c. $\gamma/\Sigma_s^f = 0.0,\ 0.1,\ 0.2,\ 0.3,\ 0.4,\ 0.5,\ 0.6,\ 0.7,\ 0.8,\ 0.9$

The values of F_1 for each combination of the above cases are given in Table B-1. The integrals were evaluated by means of a ten-point parabolic integration over the variable θ. A twenty-point integration performed for several of the cases was found to give the same results, within 0.2 per cent, as the ten-point integration.

In reading Table B-1, the dummy variables X, Y, and Z are used respectively for θ, $\Sigma_s^f r_k$, and γ/Σ_s^f. The table is for the variable $X = \pi/2$. Values of $F_1(\pi/2, Y, Z)$ for various values of Y are found in a column headed by the particular value of Z. The function $F(\pi/2, Y)$ is thus found under the column headed by $Z = 0$.

For any particular value of Y and Z, two values of the integral are listed in each column. The upper value refers to $F_1(\pi/2, Y, +Z)$, and the lower value refers to $F_1(\pi/2, Y, +Z)$, as denoted by the left side of the table. As indicated in equation (2.6-10), the correction factor normally would be evaluated by using the sum of the two values. It should be noted that the sum of the two values is always greater than twice the value of $F(\pi/2, Y)$. Thus, it can be seen from equation (2.6-7) that the exponential character of the thermal flux will always make the measured interaction effect in an exponential assembly greater than that which would theoretically be measured in an infinite assembly.

Table B-1

Tabulation of the Functions

$F_1(X, Y, +Z)$ and $F_1(X, Y, -Z)$

(X = 90 Degrees)

Values of Z	0.	0.10000	0.20000	0.30000	0.40000	0.50000	0.60000	0.70000	0.80000	0.90000
F1(X, 0.5, +)	0.64280	0.61598	0.59144	0.56886	0.54798	0.52859	0.51052	0.49363	0.47780	0.46292
F1(X, 0.5, -)	0.64280	0.67228	0.70494	0.74142	0.78256	0.82943	0.88348	0.94658	1.02123	1.11077
F1(X, 1.0, +)	0.32818	0.30762	0.28930	0.27289	0.25811	0.24473	0.23256	0.22145	0.21128	0.20194
F1(X, 1.0, -)	0.32818	0.35145	0.37801	0.40867	0.44460	0.48753	0.54015	0.60687	0.69508	0.81761
F1(X, 1.5, +)	0.17627	0.16231	0.15021	0.13962	0.13030	0.12203	0.11466	0.10805	0.10210	0.09671
F1(X, 1.5, -)	0.17627	0.19250	0.21158	0.23429	0.26174	0.29565	0.33878	0.39617	0.47781	0.60539
F1(X, 2.0, +)	0.09714	0.08814	0.08050	0.07394	0.06828	0.06333	0.05899	0.05514	0.05173	0.04867
F1(X, 2.0, -)	0.09714	0.10786	0.12081	0.13670	0.15654	0.18189	0.21533	0.26162	0.33116	0.45077
F1(X, 2.5, +)	0.05442	0.04875	0.04402	0.04003	0.03664	0.03371	0.03118	0.02896	0.02701	0.02528
F1(X, 2.5, -)	0.05442	0.06132	0.06986	0.08061	0.09446	0.11279	0.13789	0.17408	0.23108	0.33743
F1(X, 3.0, +)	0.03085	0.02731	0.02442	0.02201	0.01999	0.01827	0.01679	0.01551	0.01440	0.01342
F1(X, 3.0, -)	0.03085	0.03523	0.04076	0.04789	0.05735	0.07029	0.08871	0.11642	0.16215	0.25385
F1(X, 4.0, +)	0.01015	0.00880	0.00773	0.00687	0.00616	0.00556	0.00506	0.00464	0.00427	0.00396
F1(X, 4.0, -)	0.01015	0.01187	0.01413	0.01717	0.02142	0.02759	0.03706	0.05260	0.08091	0.14563
F1(X, 5.0, +)	0.00341	0.00291	0.00251	0.00221	0.00196	0.00175	0.00158	0.00144	0.00132	0.00122
F1(X, 5.0, -)	0.00341	0.00407	0.00498	0.00624	0.00809	0.01094	0.01561	0.02398	0.04091	0.08490
F1(X, 6.0, +)	0.00116	0.00097	0.00083	0.00072	0.00064	0.00056	0.00051	0.00046	0.00042	0.00038
F1(X, 6.0, -)	0.00116	0.00142	0.00177	0.00229	0.00308	0.00437	0.00662	0.01101	0.02089	0.05018
F1(X, 7.0, +)	0.00040	0.00033	0.00028	0.00024	0.00021	0.00019	0.00017	0.00015	0.00014	0.00012
F1(X, 7.0, -)	0.00040	0.00050	0.00064	0.00085	0.00118	0.00175	0.00282	0.00508	0.01075	0.03000

APPENDIX C

USE OF THE "THERMOS" CODE

1. General Description

The Thermos code for the IBM 704/709/7090 computer systems is particularly convenient for computing thermal parameters. The code calculates the scalar thermal neutron spectrum as a function of energy and position in a lattice cell by solving numerically the integral transport equation with isotropic scattering. A one-dimensional slab or cylindrical arrangement can be used. Thirty thermal velocity groups, twenty space points, and five mixtures of ten nuclides can be used in a calculation. Ten additional nuclides can be used for edit purposes. The theory of the code and some comparisons of the code calculations to experimental data have been published (14, 15, 16). This discussion is limited to the use of Thermos in obtaining homogenized cell parameters for use in the Exponential code. Input parameters used for these calculations are listed in Table C-1.

2. Calculation of η

The number of neutrons released per thermal absorption in the fuel, η, is defined by the equation

$$\eta = \frac{\nu_{25} \int^{\text{fuel}} \underline{r}\, d\underline{r} \int_0^{v^*} dv\, v\, \Sigma_f^{25}(\underline{r}, v)\, N_n(\underline{r}, v)}{\int^{\text{fuel}} \underline{r}\, d\underline{r} \int_0^{v^*} dv\, v \left[\Sigma_f^{25}(\underline{r}, v) + \Sigma_c^{25}(\underline{r}, v) + \Sigma_c^{28}(\underline{r}, v)\right] N_n(\underline{r}, v)} \qquad \text{(C-1)}$$

where

$\int d\underline{r}$ denotes integration over the spatial variable, $\underline{r}$;

$\int_0^{v^*} dv$ denotes integration over the velocity variable, v;

v^* is the upper velocity limit of the thermal group;

and

$N_n(\underline{r}, v)$ is the density of neutrons of speed v at position $\underline{r}$.

While η is primarily dependent upon the U^{235} concentration, it also depends on the thermal spectrum in the fuel. This variation with the neutron spectrum can be taken into account when the Thermos output is used for the calculation of η. The values of the integrals in equation (C-1) can be obtained in the output by using the fission cross section of U^{235} in the edit program and the total thermal absorption cross section including fission, of U^{235} and U^{238} in the primary code calculation.

3. Calculation of f

The fraction of thermal neutrons captured in the fuel, f, is defined by the equation

$$f = \frac{\int^{\text{fuel}} \underline{r}\, d\underline{r} \int_0^{v^*} dv\, v\, \Sigma_a^{\text{fuel}}(\underline{r}, v)\, N_n(\underline{r}, v)}{\sum_i \int^{\text{cell}} \underline{r}\, d\underline{r} \int_0^{v^*} dv\, v\, \Sigma_a^i(\underline{r}, v)\, N_n(\underline{r}, v)} . \qquad (C-2)$$

The denominator gives the total thermal absorption in the cell through summation of the absorption in each of the i nuclides.

The value of f can be obtained directly from the output of the Thermos code.

4. Calculation of $\bar{\Sigma}_a$

The average macroscopic thermal absorption cross section for the homogenized cell, $\bar{\Sigma}_a$, is defined by the equation

$$\bar{\Sigma}_a = \frac{\sum_i \int^{\text{cell}} \underline{r}\, d\underline{r} \int_0^{v^*} dv\, v\, \Sigma_a^i(\underline{r}, v)\, N_n(\underline{r}, v)}{\int^{\text{cell}} \underline{r}\, d\underline{r} \int_0^{v^*} dv\, v\, N_n(\underline{r}, v)} . \qquad (C-3)$$

The values of the integrals in equation C-3 can be obtained directly from the output of the Thermos code.

5. Calculation of f G

The fraction of thermal neutrons captured in U^{238}, fG, is defined by the equation

$$fG = \frac{\int^{\text{fuel}} \underline{r}\, d\underline{r} \int_0^{v^*} dv\, v\, \Sigma_c^{28}(\underline{r}, v)\, N_n(\underline{r}, v)}{\sum_i \int^{\text{cell}} \underline{r}\, d\underline{r} \int_0^{\text{cell}} dv\, v\, \Sigma_a^i(\underline{r}, v)\, N_n(\underline{r}, v)} \quad . \qquad \text{(C-4)}$$

The value of fG can be obtained directly from the output of the Thermos code.

6. Calculation of $\bar{D}$

The average diffusion coefficient for the homogenized cell, $\bar{D}$, is defined by the equations:

$$\lambda_t(v) = \frac{\int^{\text{cell}} \underline{r}\, d\underline{r}}{\sum_i \int^{\text{cell}} \underline{r}\, d\underline{r}\left[\Sigma^i_{\text{total}}(\underline{r}, v) - \Sigma^i_s(\underline{r}, v)\, \bar{\mu}_i\right]} \quad ; \qquad \text{(C-5)}$$

and

$$\bar{D} = \frac{\int^{\text{cell}} \underline{r}\, d\underline{r} \int_0^{v^*} dv\, v\, \lambda_t(v)\, N_n(\underline{r}, v)}{3 \int^{\text{cell}} \underline{r}\, d\underline{r} \int_0^{v^*} dv\, v\, N_n(\underline{r}, v)} \quad . \qquad \text{(C-6)}$$

In equations (C-5) and (C-6), little error is introduced, for these lattice spacings, if the contribution of the uranium and aluminum is ignored. Such an approximation also greatly simplified the preparation of the input data, since only one 30-point energy-dependent set of values for $\lambda_t(v)/3$ need then be calculated for each moderator mixture.

For the purposes of the calculations of $\lambda_t(v)/3$, the moderator was assumed to be a mixture of three atomic gases; hydrogen, deuterium, and oxygen, with atomic concentrations equal to the

actual atomic concentrations in the mixtures. Because of the variation of the scattering and transport properties of each of the three nuclides in the thermal region, a different approach was used in each case.

a. Oxygen

The following data for oxygen were used in equation (C-5):

$\sigma_{total} = \sigma_s = 3.58$ barns,

$\bar{\mu} = 2/3A$,

and

$A = 16.0$ (The atomic mass of oxygen).

b. Deuterium

The following data for deuterium were used in (C-5):

$\sigma_{total} = \sigma_s = 2.75 + 1.33 \exp[-0.148v^2]$ barns (4),

$\bar{\mu} = 2/[3A_{eff}]$,

and

$A_{eff} = 3.595$ (The Brown and St. John effective mass for bound deuterium) (4).

c. Hydrogen

The following data for hydrogen were used in (C-5):

$\sigma_{total} = \sigma_s = 22.7 + 26.2 \exp[-0.23\ v^2]$,

$\bar{\mu} = 2/[3A_{eff}(v)]$,

and

$$\frac{A_{eff}(v)}{1 + A_{eff}(v)} = \left[\frac{\sigma_s(v)}{80}\right]^{1/2}$$

(The Radkowsky approximation for bound hydrogen in H_2O) (28).

With the above equations and data, and by using the nuclide concentrations given in Table C-1, the value of $\lambda_t(v)/3$ was calculated for each of the thirty energy groups used in the Thermos code, and for each of the three moderator mixtures. The results are shown in Table C-2.

Table C-1. Input Used for Thermos Calculations

1. Nuclide concentrations:

	Nuclide	Concentration (barn cm)$^{-1}$
a. 1.143% rods	U^{235}	0.0005531
	U^{238}	0.04762
b. Aluminum tubes	Al^{27}	0.0602
c. 99.8% D_2O	D^2	0.06654
	H^1	0.000133
	O^{16}	0.03334
d. 90.27% D_2O	D^2	0.0602
	H^1	0.00649
	O^{16}	0.03334
e. 80.2% D_2O	D^2	0.05334
	H^1	0.01334
	O^{16}	0.03334

2. Slowing down source data:
   a. Spatially flat source throughout cell.
   b. High energy scattering cross sections:

Nuclide	Cross section (barns)
U^{238}	9.4
Al^{27}	1.5
D^2	7.0
H^1	19.

   c. All the reduced temperatures were taken as 1.0.

3. Arrangement (cylindrical):

	Space points	Region thickness (cm)
a. U rod	3	0.3175
b. Al tube	1	0.0864
c. Moderator (0.880 in.)	6	0.7697
Moderator (1.128 in.)	6	1.1004
Moderator (1.340 in.)	6	1.3826

4. All cross sections used in the thermal region are tabulated in BNL 5826 (17).
5. Brown and St. John free gas scattering kernels were used for deuterium and oxygen (4). The Nelkin kernel for bound hydrogen was used for hydrogen (28).

Table C-2

Values of $\lambda_t(v)/3$ in Mixtures of D_2O and H_2O for the Standard Thermos Velocity Mesh

Group	Velocity	$\lambda_t(v)/3$ 99.8% D_2O cm	$\lambda_t(v)/3$ 90.3% D_2O cm	$\lambda_t(v)/3$ 80.0% D_2O cm
1	0.1	0.979	0.5830	0.4060
2	0.2	0.981	0.5851	0.4076
3	0.3	0.982	0.5878	0.4100
4	0.4	0.985	0.5920	0.4145
5	0.5	0.987	0.5970	0.4187
6	0.6	0.991	0.6035	0.4249
7	0.7	0.995	0.6112	0.4314
8	0.8	1.000	0.6199	0.4395
9	0.9	1.004	0.6297	0.4492
10	1.0	1.011	0.6406	0.4591
11	1.1	1.017	0.6514	0.4688
12	1.2	1.026	0.6644	0.4823
13	1.3	1.031	0.6788	0.4960
14	1.4	1.038	0.6934	0.5104
15	1.5	1.048	0.7092	0.5260
16	1.605	1.055	0.7251	0.5422
17	1.72	1.065	0.7434	0.5614
18	1.845	1.076	0.7651	0.5837
19	1.98	1.089	0.7886	0.6075
20	2.1225	1.101	0.8136	0.6353
21	2.2775	1.115	0.8389	0.6626
22	2.455	1.130	0.8703	0.6963
23	2.66	1.147	0.9025	0.7342
24	2.8975	1.170	0.9407	0.7782
25	3.1725	1.186	0.9737	0.8169
26	3.49	1.205	1.006	0.8547
27	3.855	1.222	1.030	0.8975
28	4.2725	1.238	1.050	0.9025
29	4.7475	1.247	1.064	0.9182
30	5.285	1.256	1.072	0.9250

The velocities in the above table are in terms of the velocity at 1.0 kT. They must be multiplied by 2200. to obtain their value in meters/second.

The value of the integrals in equation (C-6), and the effect of leakage on the intracell flux traverses, can be found by introducing the leakage term, $D(v)B^2$, into the cell as an absorption term. This was done at the suggestion of H. C. Honeck, the author of Thermos, by calculating a value of B^2 for each lattice and using it in the input as a nuclide concentration whose microscopic absorption cross section was $\lambda_t(v)/3$. In order to preserve the correct dimensions, the values of $\lambda_t(v)/3$ were used in units of cm and those of the synthetic concentration in units of cm^{-2}.

The result of the introduction of a synthetic absorption term in the cell to represent the energy dependent leakage probability was a very slight change in the theoretical relative intracell flux traverses. The difference between the case with leakage and the case without leakage was never more than 0. 3 per cent in the theoretical traverses. For this reason, the theoretical curves for the infinite case were used throughout this report. However, the calculations did give values of the ratio

$$\frac{\int \underline{r}\, d\underline{r} \int_0^{v^*} dv\, v\, \lambda_t(v)\, B^2\, N_n(\underline{r}, v)}{3 \int \underline{r}\, d\underline{r} \int_0^{v^*} dv\, v\, N_n(\underline{r}, v)}$$

for each region of the cell. Division of the value of this ratio for the moderator region by the value of B^2 yields a spectrum averaged value of $\bar{D}$, as shown in equation (C-6). These values of $\bar{D}$ are given in Table 4-1.

APPENDIX D

DATA REDUCTION PROCEDURES

1. Axial and Radial Gold Flux Traverses

Each gold foil used in the axial and radial gold flux traverses was counted for a minimum of 9,000 counts. Routine data reduction procedures were then used to correct for the following conditions:

a. varying weight of the foils,
b. time delay before the counting,
c. counter dead time,
d. decay during count,
e. background of counter.

Since the bare and cadmium covered foils alternated on the foil stick, it was necessary to interpolate values of the cadmium-covered gold foil activation to find the cadmium ratio at the bare foil position. This was done by plotting the cadmium activation on two-cycle semi-log paper. The variation was smooth and the error from the procedure was within 2 per cent. Equation (2.4-7) was used to find the value of $p_o q/\phi_t \xi \Sigma_s$ for each bare foil position.

The thermal neutron flux values could then be determined from equations (2.4-9) and (2.4-10); in order to plot the flux to the scales used in Figure 4-1, however, a value of the current or flux at the source end was required. It was found in the course of these measurements that the flux at the center of the source end, multiplied by the counter efficiency, $(\chi\phi(0, 0))$ had a numerical value of $[3.0 \pm 0.2][10^7]$ neutrons/cm^{2}sec. The position used in the Gas Flow Geiger Counter was the one far from the detector. The value given above also includes the self-shielding of the 0.005 inch thick gold foils.

In the actual data handling for each lattice, the experimental thermal flux points were aligned with the theoretical curve, thus determining the value of a for the experiment. This value was then checked by calculating the value of $\chi\phi(0, 0)$ from it. This accounts

for the error quoted in the value of $\chi\phi(0, 0)$, since the value includes changes in the counter efficiency as well as errors in alignment.

The value of α, so determined, was then applied to the epicadmium data by using equation (2.4-11) and the appropriate value of $\xi\Sigma_s$ from Table 4-2. The values of ERI/σ_o given in Table 4-1 resulted from fitting the theoretical and experimental curves for the slowing down density.

2. Epicadmium to Subcadmium Absorption Ratio in U^{238}

The depleted U^{238} foils used in the determination of the cadmium ratio of U^{238} in the rods were carefully segregated from the other foils to prevent contamination with U^{235}. They were graded according to weight in order to minimize the small error caused by the self-shielding of the Np^{239} gamma rays during the counting procedure. Since the foils were reused, a delay of one month between uses was allowed to reduce the Np^{239} activity far below the natural background count of the foils.

Each pair of foils, consisting of a cadmium covered and a bare foil, was counted in the following order; cadmium covered, bare, bare, cadmium covered. Counts of the same foil were then added. Counting in this fashion removes the necessity for corrections for decay during counting if the count time is small compared with the half-life. Each count was from 30 to 45 minutes long in order to obtain better than 1 per cent counting statistics. The counts in the two channels of the system shown in Figure 3-5 were simply added after each count. Two or three counts normally were made on each pair of foils on successive days to improve the data and to check the half-life of the foils.

The data were corrected for varying weights of the foils and the background of the foil and counter by using routine data reduction. It was not necessary to make counter dead time corrections because of the relatively low count rates. The background of the foil was substantially greater than that of the counter. These backgrounds were determined in advance by counting the foils before they were irradiated.

The two or three measurements of the cadmium ratio of each pair of foils were averaged to find the final value. The spread in these values determined the error quoted for the quantity ρ_{28}; the normal statistical criteria for the deviation from the mean of two or three measurements were used. The value of ρ_{28} was then found from the formula

$$\rho_{28} = \frac{1}{R_{28} - 1} \quad .$$

3. U^{238}/U^{235} Fission Ratio

The quantity δ_{28} is defined by the relation

$$\delta_{28} = \frac{I_L^{28}}{I_L^{25}} \quad ,$$

where I^{28} and I^{25} are the fission rates of U^{238} and U^{235}, respectively, and where the subscript L indicates quantities pertaining to the lattice uranium.

If a depleted (D) and a natural (N) foil are irradiated in the rod, the ratio $\gamma(t)$ of their fission product gamma activity will be

$$\gamma(t) = \frac{I_D^{28} + I_D^{25} P(t)}{I_N^{28} + I_N^{25} P(t)} \quad .$$

The quantity P(t) is the ratio of U^{235} fission product activity to that of U^{238} per fission. P(t) may depend on the length of the irradiation and the counter bias, and also on the time delay between the end of the irradiation and the start of counting.

If the assumptions are made that:

$$I_N^{28} = \frac{N_N^{28}[I_D^{28}]}{N_D^{28}} \quad ,$$

$$I_D^{25} = \frac{N_D^{25}\left[I_N^{25}\right]}{N_N^{25}} ,$$

$$I_L^{25} = \frac{N_L^{25}\left[I_N^{25}\right]}{N_N^{25}} ,$$

and

$$I_L^{28} = \frac{N_L^{28}\left[I_D^{28}\right]}{N_D^{28}}$$

where N is the atomic concentration, then the following relationship can be found:

$$\delta_{28} = \left[\frac{\frac{N_L^{28}}{N_L^{25}}\frac{N_N^{25}}{N_D^{28}}\left[\gamma(t) - \frac{N_D^{25}}{N_N^{25}}\right]}{1 - \frac{N_N^{28}}{N_D^{28}}\gamma(t)}\right] P(t) \quad . \qquad \text{(D-1)}$$

Equation (D-1) is the relationship between the experimentally measured value of $\gamma(t)$ and the desired quantity, δ_{28}, when the measurement is made in a slightly enriched fuel rod with natural and depleted foils. Use of the values;

$N_L^{25}/N_L^{28} = 0.01172$ for the 1.143% (by weight) enriched U,

$N_D^{25}/N_D^{28} = 18. \times 10^{-6}$ for the depleted foil metal,

$N_N^{25}/N_N^{28} = 0.00719$ for the natural foil metal,

as well as the relationship,

$$N_N^{28} + N_N^{25} = N_D^{28} + N_D^{25} = N_L^{28} + N_L^{25} ,$$

reduces equation (D-1) to

$$\delta_{28} = \left[\frac{0.6088\gamma(t) - 0.00151}{1.0 - 0.993\gamma(t)}\right] P(t) \quad .$$

P(t) must be separately determined. In these experiments, the same counter bias and irradiation time was used throughout. The value of P(t) was determined by Wolberg (41) who used the same equipment and bias setting for the counter. A graph of P(t) is shown in Figure D-1. The solid line is the determination by Wolberg. The dotted line shows where the graph was extended backward in time by using a relative measurement. The value of P(t) shows no change, within the experimental error, over this time interval.

In a typical experiment, the depleted and natural foils were irradiated back to back in a split fuel rod. They were protected from fission product pickup by very thin aluminum foils. The foils were not counted until two hours after the end of the irradiation to allow the activity associated with the 23-minute half-life decay of U^{239} to decay. The depleted and the natural foils were alternated in the counter. Ten-minute counts were made of the depleted activity and three-minute counts were made of the natural activity. The usual background and weight corrections were made on the fission product activity curves obtained.

In order to compare the activity of the depleted and the natural foils at the same time after the end of the irradiation, the activity of one of the foils must be interpolated. The midtime of each count can be taken accurately as the time at which the activity was measured. The natural activity was chosen for interpolation because it always gave a smooth, slowly changing curve on a semi-log plot. The formula

$$A_i = A_2\left[\frac{A_1}{A_2}\right]^{[t_i - t_2]/[t_1 - t_2]}$$

was used for interpolation; A_1 and A_2 are the activities associated

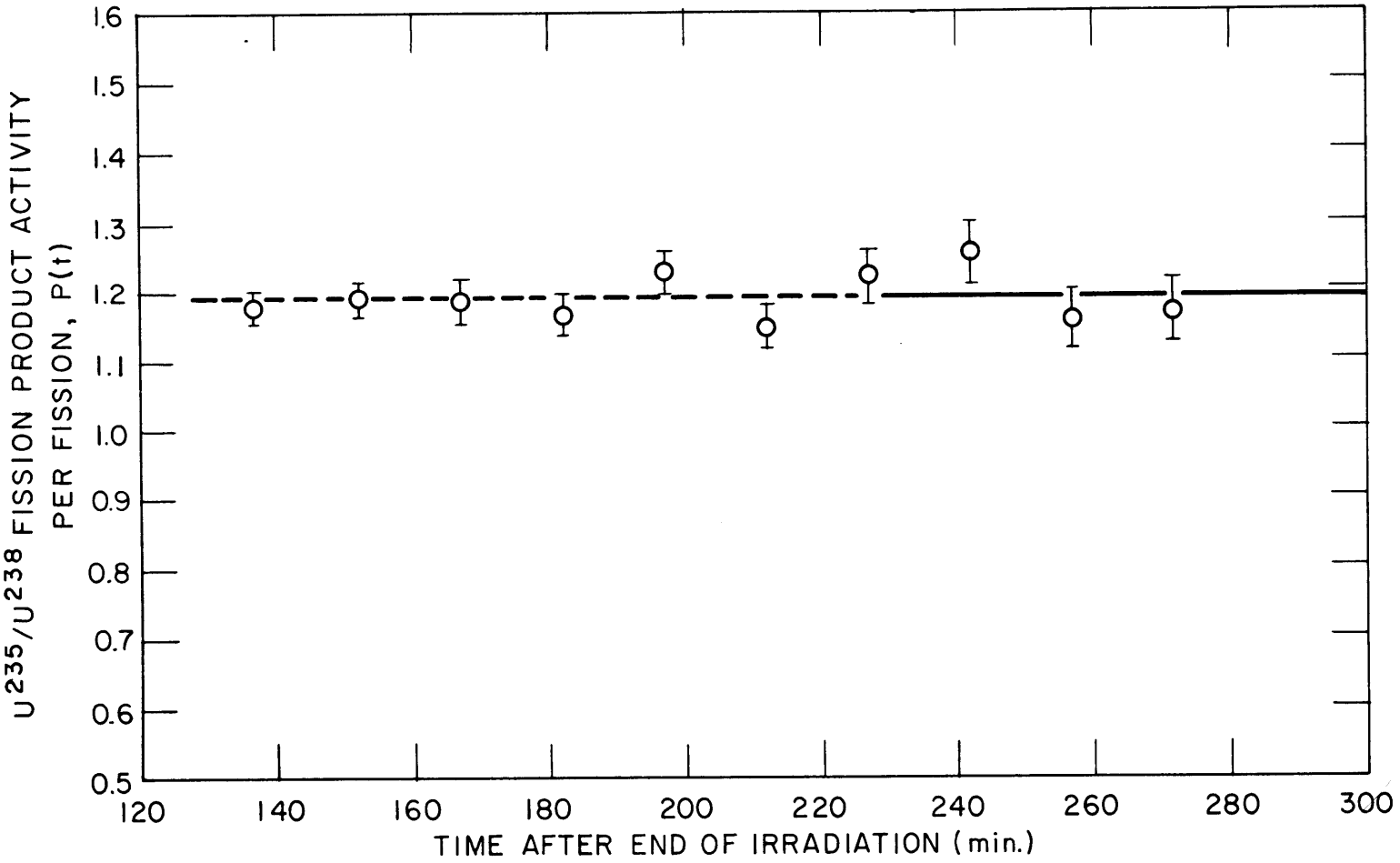

FIG. D-1 P(t) FOR FISSION PRODUCT ACTIVITY ABOVE 0.72 Mev

with times t_1 and t_2; A_i is the activity at a time t_i between t_1 and t_2. The formula is the equivalent of making a linear interpolation on a semi-log plot.

The activities of the two foils were usually counted for a period of about two hours. Each pair of measurements made during that time constituted one measurement of $\gamma(t)$. After reduction to δ_{28}, the group of measurements was treated in a normal statistical manner to obtain the quoted errors.

4. Intracell Gold Flux Traverses

The small foils and the cadmium covers used for these traverses are tedious to handle. Careful attention to the smallest experimental details is necessary to make traverses across small cells.

Each gold foil used in these traverses was counted for a minimum of 10,000 counts in the case of the bare foils, and at least 5,000 counts in the case of the cadmium covered foils. Routine data reduction procedures were then used to correct for the following conditions:

a. varying weights of the foils,
b. time delay before the counting began,
c. decay during counting,
d. background of the counter,
e. a J_o correction for the flux shape.

The counting rates invariably were too low to require a dead time correction for the gamma-ray spectrometer. Because of the design of the foil holder, shown in Figure 3-5, two sets of measurements were made along each of the two traverse directions in the cell. Since the two sets of measurements for each traverse were in opposite directions from the center of the cell, they compensated for any small amount the foil holder might have been out of level, and they also improved the data. The two sets of data were averaged for each traverse.

The reduction of the bare and epicadmium activities was carried out at first by using equations (2.4-10), (2.4-11), and (2.4-7), as was done in the case of the axial and radial gold flux traverses. In the case of the intracell flux traverse, it was found that the use of these equations, which correct the subcadmium, epithermal activation of the bare foil, was not necessary. The difference in the result between using these equations, and simply subtracting the epithermal activation from the bare activation was less than 1 per cent in the most extreme case. Since this is within the experimental error in the intracell flux traverses, the simpler method of just subtracting the epithermal from the bare activation to find the subcadmium activation was used for all of the intracell traverses. The reason for so small a difference is that the cadmium ratio from the center of the cell to the outer edge of the cell does not vary by more than about 12 per cent in the most extreme case.

To avoid reflecting small errors from the epicadmium curves into the subcadmium curves during the subtraction of the epicadmium activities from the bare activities, an average value of the epicadmium activity for all points of 0.445 inches, or farther, from the center of the rod was used. All the epicadmium activations at 0.445 inches, or farther, from the center of the rod were averaged to obtain that mean value for each lattice. The epicadmium activation was invariably flat, within the experimental error, at this distance from the center of the rod.

The data were compared with the theoretical flux traverses by normalizing the two curves at the center of the rod.

APPENDIX E

THE EXPONENTIAL AND CRITICAL CODES

1. The Exponential Code

The Exponential code numerically evaluates equations (2.9-9), (2.9-10), and (2.9-12). The restriction that the height of the assembly is equal to the diameter was not incorporated in the code, and the computation can be made with any ratio of height to diameter.

The Exponential code includes an approximate check for a critical condition, and also computes two critical quantities listed in the output description. These critical quantities are only approximations for comparision purposes and should not be used for other calculations, as in equations (2.5-4) and (2.5-7). Critical quantities for these equations should be computed using the Critical code in the second section of this appendix.

Fifteen terms are allowed in the J_0 - expansion and twenty terms are allowed in the sine expansion. Values of the three equations will be computed for as many as twenty equally spaced points along the central axis of the assembly.

The computation requires about 0.2 minutes per case using the IBM 7090 computer and about 1.0 minutes per case using the IBM 709 computer.

All input numbers are dimensionless. The first column in the input card listing, which follows, is the card number. The second column is the FORMAT as it appears in the code. The third column is the LIST of the input statement in the code, and the fourth column is a description of each item. The carriage of the printer is assumed to operate under program control.

The input cards are as follows:

1.2. 3.4.	(8F9.4)	U1	The first fifteen roots of the equation $J_o(\mu_i)=0$ (i.e. 2.4048, 5.5201, 8.6537, 11.7915.....) followed by
		B1	the first fifteen values of $J_1(\mu_i)$ (i.e. 0.5191, -0.3403, 0.2715, -0.2325.....). Two blank fields will be left on the fourth card.
5.	(2F10.4,	A	The ratio of the extrapolated radius to the thermal diffusion length (R/L).
		Y	The ratio of the extrapolated height to the extrapolated radius (H/R).
	6I5)	JOBNO	An identification number.
		ITOP	Number of terms to be used in the J_o-expansion, ($\leq$ 15).
		NTOP	Number of terms to be used in the sine expansion, ($\leq$ 20).
		KTOP	Number of evenly spaced points on the central axis (not counting z=0), at which the equations are to be evaluated, ($\leq$ 20).
		INST1	The code will print intermediate results if INST1 = 2. The code will not print intermediate results if INST1 = 1.
		INST2	Same as INST1.
6.	(9F8.5)	XKIN	Values of k_∞ to be used, (>1.0). No more than nine values may be listed.
7.	(9F8.4)	TAUO	Values of the ratio τ_o/L^2. No more than nine values may be listed.
8.	(9F8.4)	TAU1	Values of the ratio τ/L^2. No more than nine values may be listed.

A case will be computed for each combination of a value of k_∞ and τ_o/L^2. The value of τ/L^2 used in each case will be taken from the corresponding field on card 8 as the value of τ_o/L^2 on card 7.

The printed output will be about 5300 lines for each case if both INST1 and INST2 have a value of 2. If the two items have the value of 1, the final output will be 30 lines for each case.

The output is labeled and largely self explanatory. The column headings have the following meaning:

K	edit point along the central axis.
SUMFS	$[\phi_s/F][D/L]$
SUMF1	$[\phi_e/F][D/L]$
SUMQ	$[p_o q/F][L]$
(F1/FS)	ϕ_e/ϕ_s
(F1+FS)/Q	$\Sigma_a\phi/p_o q$

A "P" following each of the above, (e.g. SUMFSP) indicates that the value is for a plane source. A "J" following each of the above indicates that the value is for a J_o- source.

The two values, CRIT ABS RATE/PQ and CRIT RADIUS, are only approximations for comparision purposes and should not be used for calculations. These two quantities can be accurately calculated using the Critical code. Otherwise, the numbers listed by the Exponential code should be accurate evaluations of the equations to at least 0.1 per cent.

2. The Critical Code

The Critical code finds the value of the quantity, B^2L^2, from the equation

$$\frac{k_\infty \exp(-B^2\tau_o)}{1+L^2B^2} = 1 \ .$$

The value is then used to numerically evaluate equation (2.9-13) for an assembly with a height equal to the diameter.

A simple iteration technique is used to solve the transcendental equation. The technique could undoubtedly be improved by using an extrapolation procedure. Up to 50 iterations are allowed before the iteration is terminated.

This code was used to find the values of the scaled critical radius listed in Appendix A and the values of the critical ratios used in equations (2.5-4) and (2.5-7). The asymptotic regions listed in Appendix A were found by comparing the values of $\Sigma_a\phi^*/p_oq^*$ computed by the Critical code with the values of the same quantity computed by the Exponential code.

The computation requires about 0.05 minutes per case using an IBM 709 computer. All numbers on the input cards are dimensionless. The input cards are as follows:

1.	(72H--)		Hollerith identification.
2.	(E10.5,	DEL	Iteration criterion. The critical equation is iterated until the difference between the right and left sides of the equation is less than DEL.
	3I5)	NKI	Number of values of k_∞ to be used, (≤ 7).
		NTAU	Number of values of τ_o/L^2 to be used, (≤ 7).
		NTAU1	Number of values of τ/L^2 to be used, (≤ 7).
3.	(7F10.6)	XKI	Values of k_∞.
4.	(7F10.6)	TAU	Values of τ_o/L^2.
5.	7F10.6)	XTAU	Values of τ/τ_o.

A scaled critical radius,(R^*/L), will be computed for each combination of a value of k_∞ and τ_o/L^2. The value of $\Sigma_a\phi^*/p_oq^*$ will then be computed for each value of τ/τ_o listed in the input.

The printed output will be two lines for each critical case. The value of $\Sigma_a\phi^*/p_oq^*$ will be printed directly under the value of XTAU. The number of iterations required will be under IT.

Fortran Listing of the Exponential Code

```
      DIMENSION TAUO(9), TAU1(9), XKIN(9), U1(15), B1(15), B(15),
       C(15), D(15), E(15,20), F(15,20), G(15,20), H(15,20), FSSINH
       (15,20), FSP(15,20), SUMFSP(20), F1P(15,20,20), F1SIN(20,20),
      SUMF1P(20), GP(15,20,20), SUMGP(20), FSJ(20), SUMF1J(20),
       SUMGJ(20), KROW(20), F1XFSP(20), F1XFSJ(20), FXGP(20), X(15)
1     FORMAT(2F10.4, 6I5/9F8.5/(9F8.4))
2     FORMAT(8F9.4)
4     HSINEF(X,Y)=EXPF(X*(1.0-Y))/2.0-1.0/(2.0*EXPF(X*(1.0-Y)))
6     HTANF(X)=(1.0-1.0/EXPF(2.0*X))/(1.0+1.0/EXPF(2.0*X))
      READINPUTTAPE 4,2,U1,B1
7     READINPUTTAPE 4,1,A,Y,JOBNO,ITOP,NTOP,KTOP,INST1,
       INST2,XKIN,TAUO,TAU1
      PI=3.1415927
      ZERO=0.0
      IZERO=0
      FSPO=ZERO
8     DO 14 I=1,ITOP
      B(I)=2.0*(SQRTF(A**2+U1(I)**2))
      X(I)=Y*B(I)/2.0
      IF(X(I)-20.0)9,11,11
9     C(I)=(A*HTANF(X(I)))/(U1(I)*B1(I)*B(I))
      D(I)=1.0/HSINEF(X(I),ZERO)
      GO TO 13
11    C(I)=A/(U1(I)*B1(I)*B(I))
      D(I)=ZERO
13    FSPO=FSPO+4.0*C(I)
10    DO 12 N=1,NTOP
      TEMPN=FLOATF(N)
      E(I,N)=(8.0*TEMPN*PI)/(TEMPN**2*PI**2+Y*Y*(A**2+
        U1(I)**2))
      F(I,N)=(U1(I)/A)**2+(TEMPN*PI/(Y*A))**2
12    CONTINUE
14    CONTINUE
      XNORM=U1(1)*B1(1)/2.0
      FSJO=2.0*U1(1)*B1(1)*C(1)
      FLKTOP=FLOATF(KTOP)
16    FORMAT(15H1JOHN PEAK NO.I10,9H,RADIUS=F8.4,7H,ITOP
        =I2,7H, NTOP=I2,7H, KTOP=I2,/11H K INFINIT=9F8.5,/11H
      TAU ZERO=9F8.4,/11H TAU ONE=9F8.4,/15F8.4/15F8.4)
      WRITEOUTPUTTAPE2,16,JOBNO,A,ITOP,NTOP,KTOP,XKIN,
        TAUO,TAU1,U1,B1
165   FORMAT(23H RATIO OF HT TO RADIUS=F7.4)
      WRITEOUTPUTTAPE2,165,Y
      GOTO(20,17),INST1
17    WRITEOUTPUTTAPE 2,18,NTOP
```

```
18    FORMAT(107H0VALUE OF B(I), C(I), D(I), (I ACROSS) AND
        E(I,N), F(I,N), (I ACROSS, N DOWN) WHERE TOP VALUES
        ARE I=15, N=I2)
19    FORMAT(8E15.5/E16.5,6E15.5)
      WRITEOUTPUTTAPE 2,19,B,C,D,((E(I,N),I=1,15),N=1,NTOP
        ),((F(I,N),I=1,15),N=1,NTOP)
20    DO 90 L=1,9
      IF(XKIN(L)-0.0)92,92,22
22    DO 88 J=1,9
      IF (TAUO(J)-0.0)88,88,24
24    XKFIN=XKIN(L)/((1.0+F(1,1))*EXPF(TAUO(J)*F(1,1)))
      ACRIT=SQRTF(8.2514*(1.0+TAUO(J))(1.0/(XKIN(L)-1.0)))
      IF(XKFIN-1.0)25,84,84
25    DO 26 K=1,KTOP
      SUMFSP(K)=ZERO
      SUMF1P(K)=ZERO
      SUMQP(K)=ZERO
      SUMF1J(K)=ZERO
      SUMQJ(K)=ZERO
26    CONTINUE
      DO 42 I=1,ITOP
      DO 38 N=1,NTOP
      G(I,N)=TAUO(J)*F(I,N)
      IF(G(I,N)-20.0)30,30,28
28    G(I,N)=ZERO
      GOTO 32
30    G(I,N)=1.0/EXPF(G(I,N))
32    H(I,N)=TAU1(J)*F(I,N)
      IF(H(I,N)-20.0)36,36,34
34    H(I,N)=ZERO
      GOTO 38
36    H(I,N)=1.0/EXPF(H(I,N))
38    CONTINUE
      DO 40 K=1,KTOP
      TEMPK=FLOATF(K)
      IF(X(I)-20.0)39,41,41
39    FSSINH(I,K)=HSINEF(X(I),TEMPK/FLKTOP)*D(I)
      GOTO 47
41    BXKXKT=X(I)*TEMPK/FLKTOP
      IF(BXKXKT-20.0)43,45,45
43    FSSINH(I,K)=1.0/EXPF(BXKXKT)
      GOTO 47
45    FSSINH(I,K)=ZERO
47    FSP(I,K)=4.0*C(I)*FSSINH(I,K)
      SUMFSP(K)=SUMFSP(K)+FSP(I,K)
40    CONTINUE
42    CONTINUE
      DO 60 K=1,KTOP
      TEMPK=FLOATF(K)
      DO 58 N=1,NTOP
```

```
      TEMPN=FLOATF(N)
      F1SIN(N,K)=SINF(TEMPN*PI*TEMPK/FLKTOP)
      DO 56 I=1,ITOP
      IF(G(I,N))44,44,46
44    F1P(I,N,K)=ZERO
      GOTO 48
46    F1P(I,N,K)=E(I,N)*C(I)*F1SIN(N,K)/((F(I,N)+1.0)/(XKIN(L)*
        G(I,N))-1.0)
48    SUMF1P(K)=SUMF1P(K)+F1P(I,N,K)
      IF(H(I,N))50,50,52
50    QP(I,N,K)=ZERO
      GOTO 54
52    QP(I,N,K)=E(I,N)*C(I)*F1SIN(N,K)*H(I,N)/(1.0/XKIN(L)-
        G(I,N)/(1.0+F(I,N)))
54    SUMQP(K)=SUMQP(K)+QP(I,N,K)
56    CONTINUE
      SUMF1J(K)=SUMF1J(K)+XNORM*F1P(1,N,K)
      SUMQJ(K)=SUMQJ(K)+XNORM*QP(1,N,K)
58    CONTINUE
      KROW(K)=K
      FSJ(K)=XNORM*FSP(1,K)
60    CONTINUE
      KDIM=KTOP-1
      DO 62  K=1,KDIM
      F1XFSP(K)=SUMF1P(K)/SUMFSP(K)
      F1XFSJ(K)=SUMF1J(K)/FSJ(K)
      FXQP(K)=(SUMF1P(K)+SUMFSP(K))/SUMQP(K)
      FXQJ(K)=(SUMF1J(K)+FSJ(K))/SUMQP(K)
62    CONTINUE
      FXQC=EXPF(TAU1(J)*(XKIN(L)-1.0)/(1.0+TAUO(J)))/XKIN(L)
      XMUL=1.0/(1.0-XKFIN)
      GOTO (74,66),INST2
66    WRITEOUTPUTTAPE 2,64,XKIN(L),TAUO(J),TAU1(J),A,
        NTOP,KTOP
64    FORMAT(10H0K INFIN= F8.5,12H, TAUO/L**2=F8.4,12H,
        TAU1/L**2=F8.4,4H, A=F8.4,/104H0VALUE OF G(I,N),
        H(I,N), FSSINH(I,K), FSP(I,K), (I ACROSS, N OR K DOWN),
        THEN F1P(I,N,K) AND QP(I,N,K),/98H(I ACROSS, N DOWN,
        FOR EACH K), THEN F1SIN(N,K), (N ACROSS, K DOWN),
        WHERE TOP VALUES ARE I=15, N=I2,4H, K=I2)
      WRITEOUTPUTTAPE 2,19,((G(I,N),I=1,15),N=1,NTOP),
        ((H(I,N),I=1,15),N=1,NTOP),((FSSINH(I,K),I=1,15),K=1,KTOP
        ),((FSP(I,K),I=1,15),K=1,KTOP),(((F1P(I,N,K),I=1,15),N=
        1,NTOP),K=1,KTOP),(((QP(I,N,K),I=1,15),N=1,NTOP),
        K=1,KTOP)
72    FORMAT(10E12.4/E13.4,8E12.4,E10.3)
      WRITEOUTPUTTAPE 2,72,((F1SIN(N,K),N=1,20),K=1,KTOP)
74    WRITEOUTPUTTAPE 2,75,XKIN(L),TAUO(J),TAU1(J),A,Y
75    FORMAT(10H1K INFIN=F8.5,12H, TAUO/L**2=F8.4,12H,TA
      U1/L**2= F8.4,4H, A=F8.4,24H, RATIO OF HT TO RADIUS
        =F7.4)
```

```
76    FORMAT(9H0K FINIT=F9.5,7H, MULT=E11.5,19H, CRIT
        ABS RATE/PQ=E11.5,14H, CRIT RADIUS=E11.5)
      WRITE OUTPUTTAPE 2,76,XKFIN,XMUL,FXQC,ACRIT
78    FORMAT(120H0 K    SUMFSP    SUMF1P      SUMQP
        (F1/FS)P  (F1+FS)/QP      FSJ     SUMF1J      SUMQJ
        (F1/FS)J  (F1+FS)/QJ)
      WRITEOUTPUTTAPE 2,78
80    FORMAT(1H012,E11.4,E58.4/(1H0I2,2E11.4,3E12.5,E11.4,
        4E12.5))
82    FORMAT(1H0I2,2E11.4,E12.5,E35.4,2E12.5)
      WRITEOUTPUTTAPE 2,80,IZERO,FSPO,FSJO,(KROW(K),
        SUMFSP(K),SUMF1P(K),SUMQP(K),F1XFSP(K),FXQP(K),
        FSJ(K),SUMF1J(K),SUMQJ(K),F1XFSJ(K),FXQJ(K),K=1,
        KDIM)
      WRITEOUTPUTTAPE 2,82,KTOP,SUMFSP(KTOP),SUMF1P
        (KTOP),SUMQP(KTOP),FSJ(KTOP),SUMF1J(KTOP),
        SUMQJ(KTOP)
      GOTO 88
84    WRITEOUTPUTTAPE 2,75,XKIN(L),TAUO(J),TAU1(J),A
86    FORMAT(37H0THE CASE IS OVER CRITICAL, K FINITE=
        F9.5,14H, CRIT RADIUS=E11.5)
      WRITEOUTPUTTAPE 2,86 XKFIN,ACRIT
88    CONTINUE
90    CONTINUE
92    WRITEOUTPUTTAPE 2,94,JOBNO
94    FORMAT(22H0JOHN PEAK, END OF NO.I10)
      CALL EXIT
      END(1,1,0,0,0,0,0,0,0,0,0,0,0,0,0)
```

Fortran Listing of the Critical Code

```
      DIMENSION XKI(7), TAU(7), XTAU(7), NIT(7, 7), A(7, 7),
        CHECK(7, 7), TAU1(7, 7, 7), ANS(7, 7, 7)
1     FORMAT(E10.5, 3I5)
2     FORMAT(7F10.6)
4     FORMAT(72H
                                  )
5     READINPUTTAPE 4, 4
      READINPUTTAPE 4, 1, DEL, NKI, NTAU, NTAU1
      READINPUTTAPE 4, 2, XKI, TAU, XTAU
      DO 18 I=1, NKI
      DO 16 J=1, NTAU
      BL2=(XKI(I)-1.0)/(TAU(J)+1.0)
      DO 10 K=1, 50
      BL2X=XKI(I)/(EXPF(BL2*TAU(J))*(1.0+BL2))
      IF(ABSF(1.0-BL2X)-DEL)6, 6, 8
6     BL2=BL2X*BL2
      NIT(I, J)=K
8     BL2=BL2X*BL2
      NIT(I, J)=K
10    CONTINUE
12    A(I, J)=SQRTF(8.2514/BL2)
      CHECK(I, J)=XKI(I)/(EXPF(BL2*TAU(J))*(1.0+BL2))
      DO 14 L=1, NTAU1
      TAU1(I, J, L)=XTAU(L)*TAU(J)
      ANS(I, J, L)=EXPF(BL2*TAU1(I, J, L))/XKI(I)
14    CONTINUE
16    CONTINUE
18    CONTINUE
      WRITEOUTPUTTAPE 2, 4
      WRITEOUTPUTTAPE 2, 20, (XTAU(L), L=1, NTAU1)
20    FORMAT(50H0KINFINITE  TAUTHERM  IT  K FINITE
        CRIT RADIUS7F10.6)
22    FORMAT(1H0F9.6, F10.6, I5, F12.7, E13.5, 7F10.6)
      DO 26 I=1, NKI
      DO 24 J=1, NTAU
      WRITEOUTPUTTAPE 2, 22, XKI(I), TAU(J), NIT(I, J), CHECK
        (I, J), A(I, J), (ANS(I, J, L), L=1, NTAU1)
24    CONTINUE
26    CONTINUE
      CALL EXIT
      END(1, 1, 0, 0, 0, 0, 0, 0, 0, 0, 0, 0, 0, 0, 0)
```